c. 3

# LA-8626-MS (ENDF-304)

IS-4 REPORT SECTION

**REPRODUCTION COPY**

# Evaluated Neutron-Induced Cross Sections for $^{54,56}$Fe to 40 MeV



LOS ALAMOS SCIENTIFIC LABORATORY
Post Office Box 1663 Los Alamos, New Mexico 87545

This report was not edited by the Technical Information staff.

This work was supported by the US Department of Energy, Fusion Materials Irradiation Test Facility Project, Office of Fusion Energy and Office of Basic Energy Sciences.



**UNITED STATES**
**DEPARTMENT OF ENERGY**
**CONTRACT W-7405-ENG. 36**

LA-8626-MS (ENDF-304)
UC-34c
Issued: December 1980

# Evaluated Neutron-Induced Cross Sections for $^{54,56}$Fe to 40 MeV

E. D. Arthur
P. G. Young


# EVALUATED NEUTRON-INDUCED CROSS SECTIONS FOR $^{54,56}$Fe TO 40 MeV

by

E. D. Arthur and P. G. Young

ABSTRACT

Cross sections for neutron-induced reactions on $^{54,56}$Fe were calculated employing several nuclear models--optical, Hauser-Feshbach, preequilibrium, and DWBA--in the energy range between 3 and 40 MeV. As a prelude to the calculations, the necessary input parameters were determined or verified through analysis of a large body of experimental data both for neutron- and proton-induced reactions in this mass and energy region. Calculated cross sections as well as neutron and gamma-ray emission spectra were incorporated into an ENDF/B-formatted evaluation suitable for use to 40 MeV. Details of both the calculations and the final evaluated data files are described in this report, and extensive comparisons to experimental data are given.

## I. INTRODUCTION

Nuclear data needs for the Fusion Materials Irradiation Test Facility (FMIT) require evaluated neutron cross sections up to energies around 40 MeV.[1] Since natural iron constitutes one of the most important materials for which such data is needed, we have performed a comprehensive set of nuclear model calculations for neutron reactions on $^{54,56}$Fe between 3 and 40 MeV. Calculated results expressed in ENDF format were joined to the latest ENDF/B-V evaluation[2] at 3 MeV to produce a new evaluation applicable to 40 MeV. Not only does the present evaluation extend the Version V data to higher energies, but certain energy balance problems occurring below 20 MeV are also corrected.

Since generally little neutron experimental data, with the exception of total cross sections, exist above 20 MeV, the majority of the evaluation by

necessity depended upon results determined from nuclear-model calculations. In this energy range, the reaction mechanisms governing most neutron-induced reactions on medium-mass nuclei can be described by means of the Hauser-Feshbach statistical model,[3] along with corrections for preequilibrium and direct-reaction effects. In order to use such models properly, suitable input parameters (e.g., optical model sets, gamma-ray strength functions, etc.) must be determined that are valid for use in both the mass and energy range of interest in the calculation. Our efforts to determine and verify the choice of input parameters through use of and comparison to several independent data types are described in Sec. II. In Sec. III we describe briefly the nuclear model codes used and present comparisons of calculated cross sections to available experimental data, both for neutron and proton-induced reactions. Since our efforts to express calculated cross sections, spectra, and angular distributions in ENDF/B format resulted in the adoption of some nonstandard representations, we describe in Sec. IV some of the formats used and present several examples of the evaluated data at higher energies.

## II. PARAMETER DETERMINATION

### A. Neutron Optical Potential

The spherical optical model was used to calculate total cross sections and elastic scattering angular distributions as well as particle transmission coefficients for the Hauser-Feshbach portion of the calculations. For neutrons, the optical parameters used to generate such transmission coefficients must be constrained to produce agreement with higher-energy data (total cross sections, elastic angular distributions, reaction cross sections) while reproducing lower energy information (average resonance quantities). By doing so, the double criteria of realistic compound nucleus formation cross sections (important at all incident energies) and reasonable behavior of the low-energy transmission coefficients [important in processes such as (n,2n) where low-energy neutrons are emitted] can be met. To determine such parameters, we followed the approach of Lagrange and co-workers[4] in which low-energy resonance data are used to simultaneously supplement and constrain parameters determined from fits to data at higher energies. We chose a standard representation for the neutron optical potential, that is, a real potential of the Woods-Saxon form, and an imaginary potential consisting of a surface Woods-Saxon derivative form plus a Woods-Saxon volume portion and a Thomas spin-orbit term. (For more detail on the optical

potential, see Ref. 5.) In our determination of parameters, we included the following data: (1) total cross sections between 2 and 40 MeV; (2) s- and p-wave strength functions $S_0$, $S_1$, along with values for the potential scattering radius R'; (3) elastic scattering angular distributions between 6 and 14 MeV; and (4) reaction cross sections between 5 and 30 MeV.

The resulting neutron parameters determined from fits to these data types appear in Table I. Figure 1 illustrates the total cross sections calculated with these parameters compared to data available for natural iron.[6-19] Below 2 MeV it was difficult to obtain reasonable fits to the data, primarily because of resonance structure that persists in the total cross section up to energies around 3-4 MeV. Optical parameters have been obtained[20] that fit these data at lower energies without unphysical parameter values but these are applicable only up to 20 MeV. Since our fits covered a much larger energy range, the lower energy portion was compromised somewhat to achieve reasonable agreement over the entire energy range. The effect of this discrepancy is minimized to some extent since it occurs at the lower end of the energy range covered in the calculations. Since reasonable agreement was obtained for s- and p-wave strength values, this helps ensure the proper behavior of lower-order transmission coefficients used in the Hauser-Feshbach calculations.

Examples of elastic cross sections calculated with these parameters are compared to data[21-36] between 4.6 and 25 MeV in Figs. 2-6. In Fig. 7, comparisons are made to nonelastic cross sections[37-53] below 40 MeV. Our predicted

TABLE I

NEUTRON OPTICAL MODEL PARAMETERS

| | r(fm) | a(fm) |
|---|---|---|
| $V(MeV) = 49.747 - 0.4295E - 0.0003E^2$ | 1.287 | 0.56 |
| $W_{vol}(MeV) = -0.207 + 0.253E$ | 1.345 | 0.47 |
| $V_{SO}(MeV) = 6.2$ | 1.12 | 0.47 |
| $W_{SD}(MeV) = 6.053 + 0.074E$ | 1.345 | 0.47 |
| Above 6 MeV | | |
| $W_{SD}(MeV) = 6.497 - 0.325(E-6)$ | | |

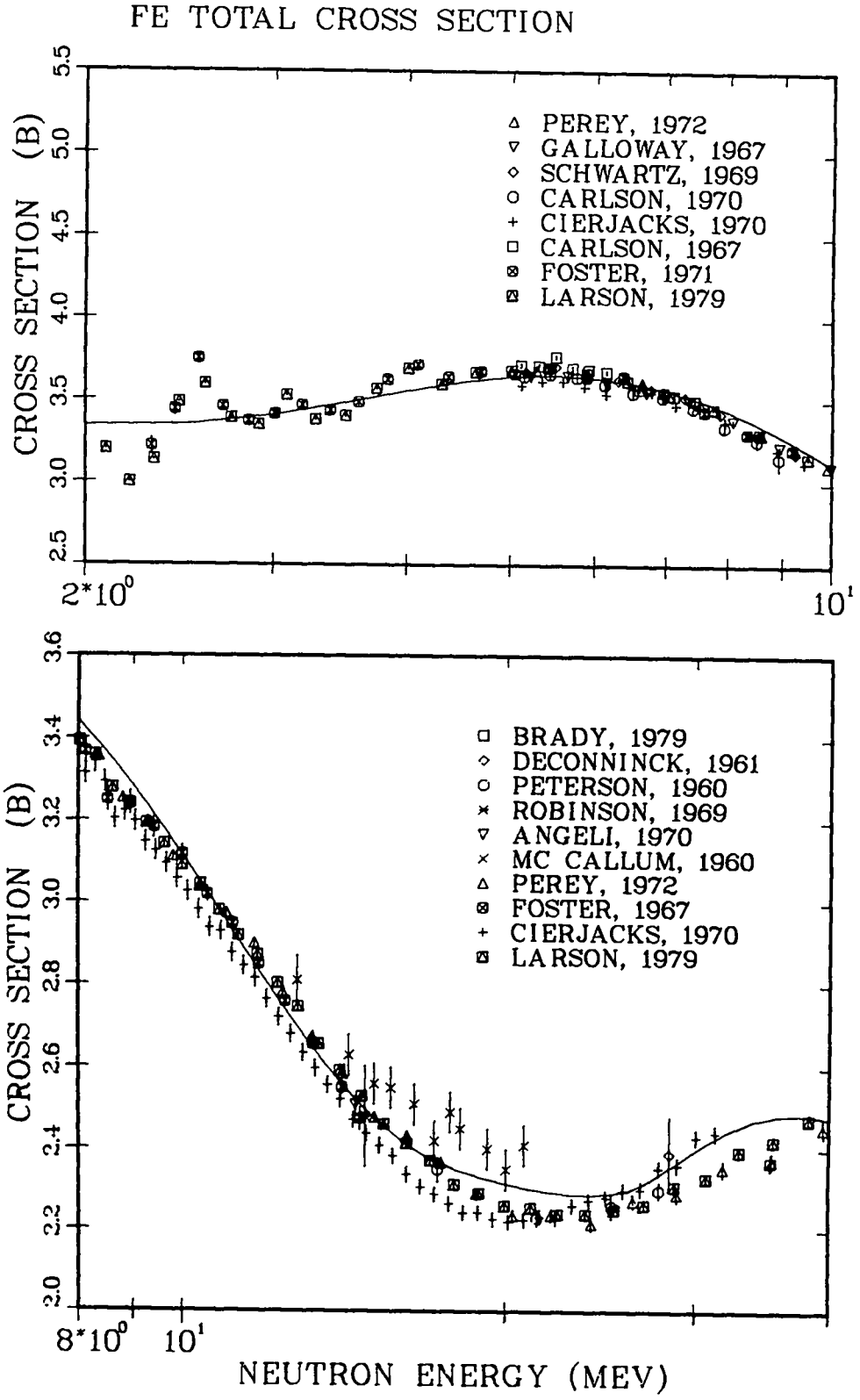


Fig. 1.
Measured and calculated total cross section for iron.
Experimental data are from Refs. 6-19.

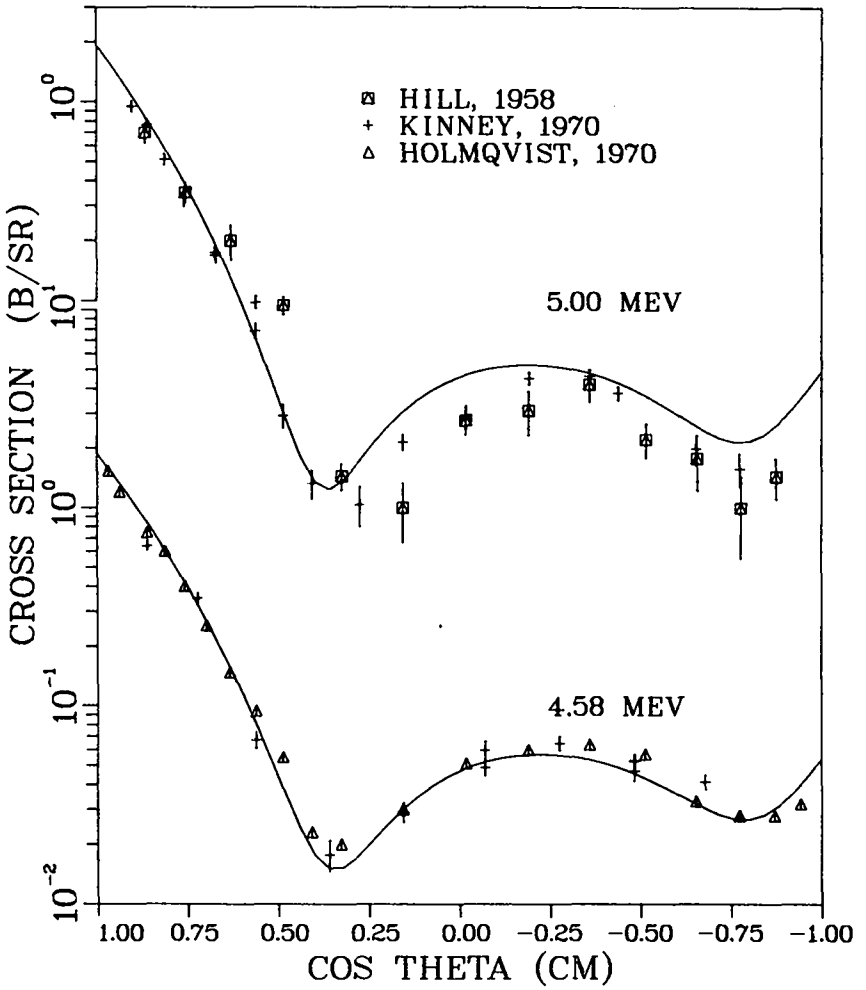


Fig. 2.
Measured and calculated elastic angular distributions for iron. Experimental data are from Refs. 21-23.

nonelastic cross section over-estimates new results[37] available at 40 MeV that were not available for inclusion in our fit. In addition, trends in the older nonelastic data indicated a somewhat higher value when extrapolated to 40 MeV. This over-prediction in the calculated reaction cross section at 40 MeV led us to renormalize downward our calculated Hauser-Feshbach cross sections in this energy range by about 10%.

## B. Charged-Particle Optical Parameters

Proton and alpha particle transmission coefficients were calculated from optical parameters based on published sets obtained from experimental data fits in the mass and energy range of interest to our calculations. We adjusted the

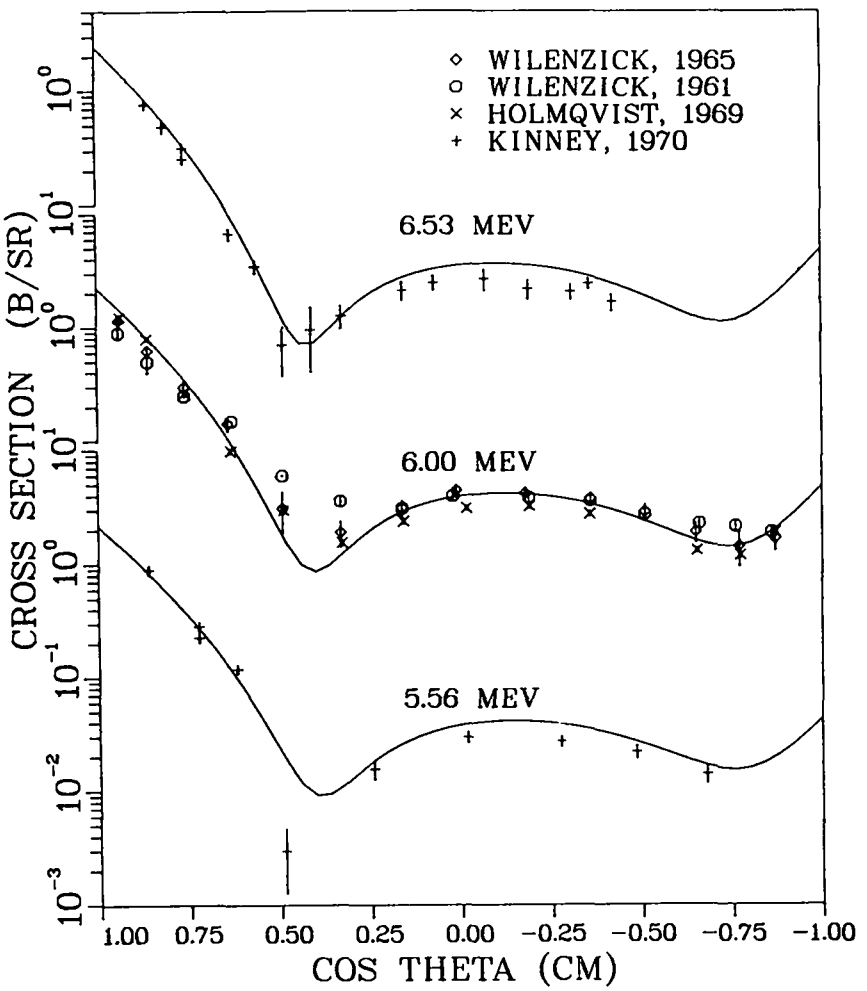


Fig. 3.
Measured and calculated elastic angular distributions for iron. Experimental data are from Refs. 23-26.

parameters to better fit various experimental data types available at low and high energies. For protons, we began with the Perey[54] proton optical parameter set. We compared the reaction cross sections calculated using these parameters to data[55,56] for p + $^{56}$Fe and found an over-prediction above 30 MeV as shown by the solid curve in Fig. 8. We then added an energy dependence to the imaginary potential to produce the short-dash curve in Fig. 8, which is in better agreement with the data.

We were also interested to determine how well these parameters reproduced low-energy proton data. Recently there has been interest in the behavior of reaction cross sections for cases where sub-Coulomb barrier protons are concerned.[57] In the calculation of the $^{54}$Fe(n,np) cross section, the binding

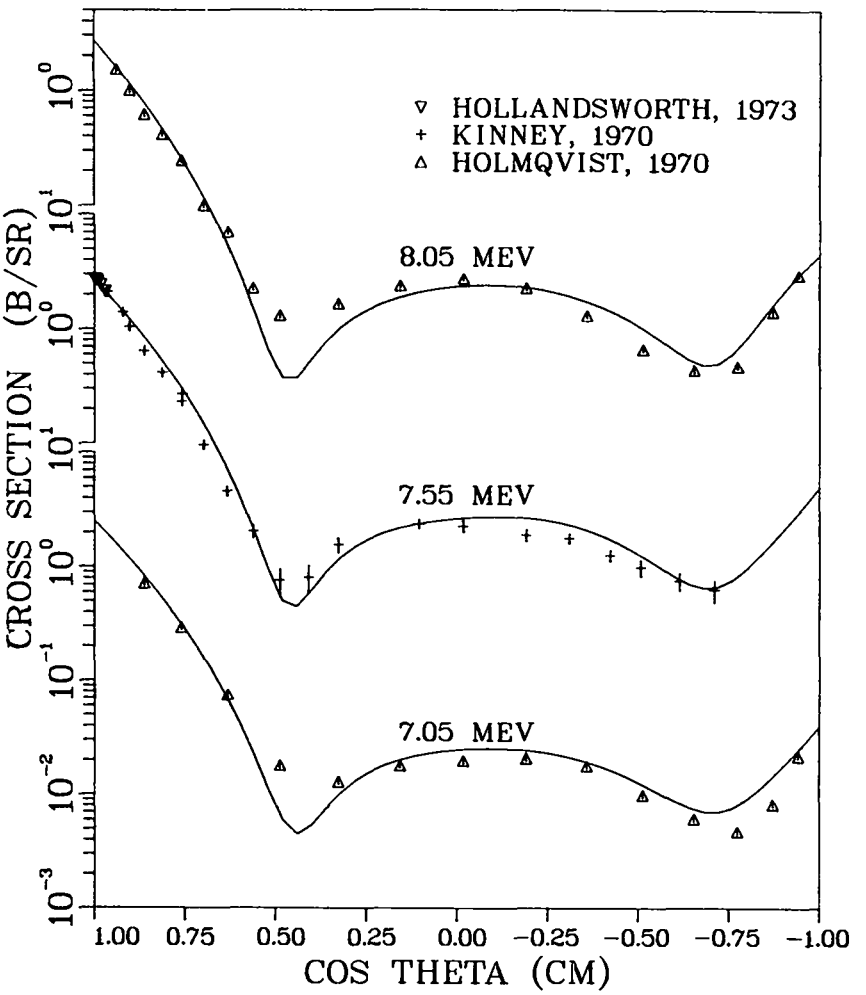


Fig. 4.
Measured and calculated elastic angular distributions for iron. Experimental data are from Refs. 22, 23, and 27.

energy of the proton in the $^{54}Fe$ compound nucleus is 4.5 MeV less than that of the neutron, leading to an incident energy range where only proton and gamma-ray emission compete. To test the low-energy behavior of these parameters, we calculated the $^{55}Mn(p,n)$ cross section and determined that low-energy proton cross sections[58,59] were reasonably described, as shown in Fig. 9. Table II lists the modified form of the Perey proton parameters that we obtained.

We followed a similar approach to determine alpha-particle optical parameters for use in our calculations. The Lemos set[60] determined from the analysis of 20 to 30 MeV alpha scattering in this mass region formed the basis for

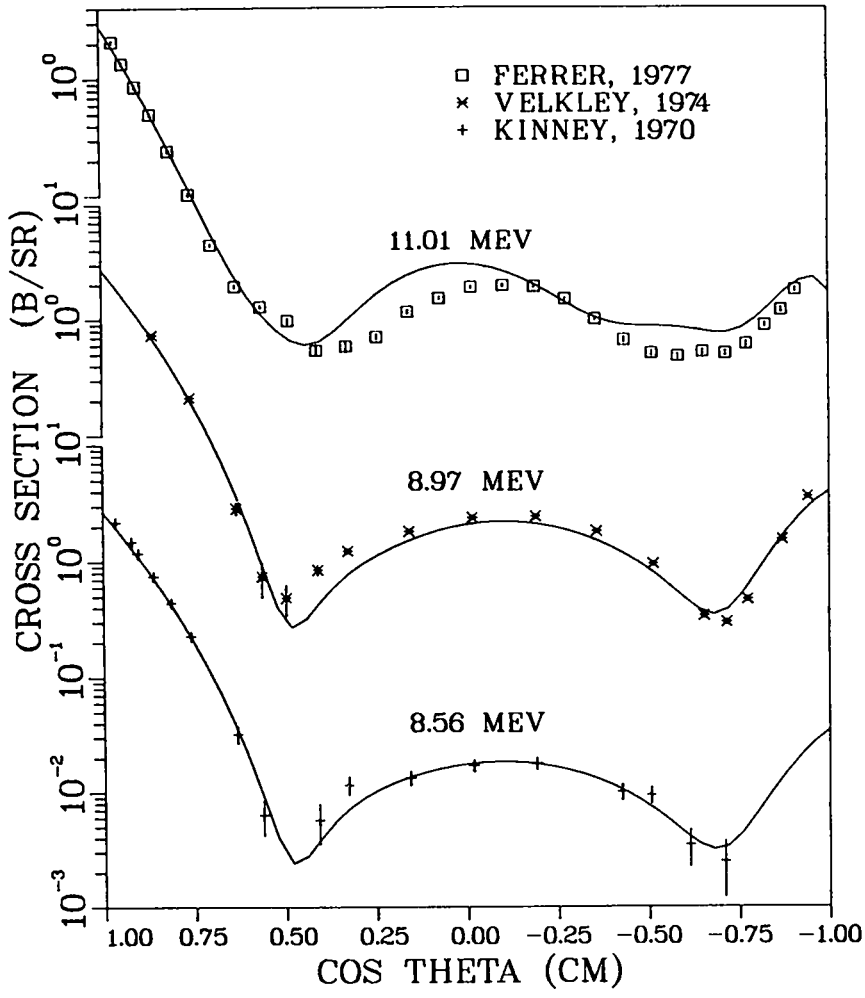


Fig. 5
Measured and calculated elastic angular distributions for iron. Experimental data are from Refs. 23, 28, and 29.

TABLE II

PROTON OPTICAL MODEL PARAMETERS

| | r(fm) | a(fm) |
|---|---|---|
| V(MeV) = 58.384 - 0.55E | 1.25 | 0.65 |
| $W_{SD}$(MeV) = 13.5 - 0.15E | 1.25 | 0.47 |
| $V_{SO}$(MeV) = 7.5 | 1.25 | 0.47 |
| $r_c$(fm) = 1.25 | | |

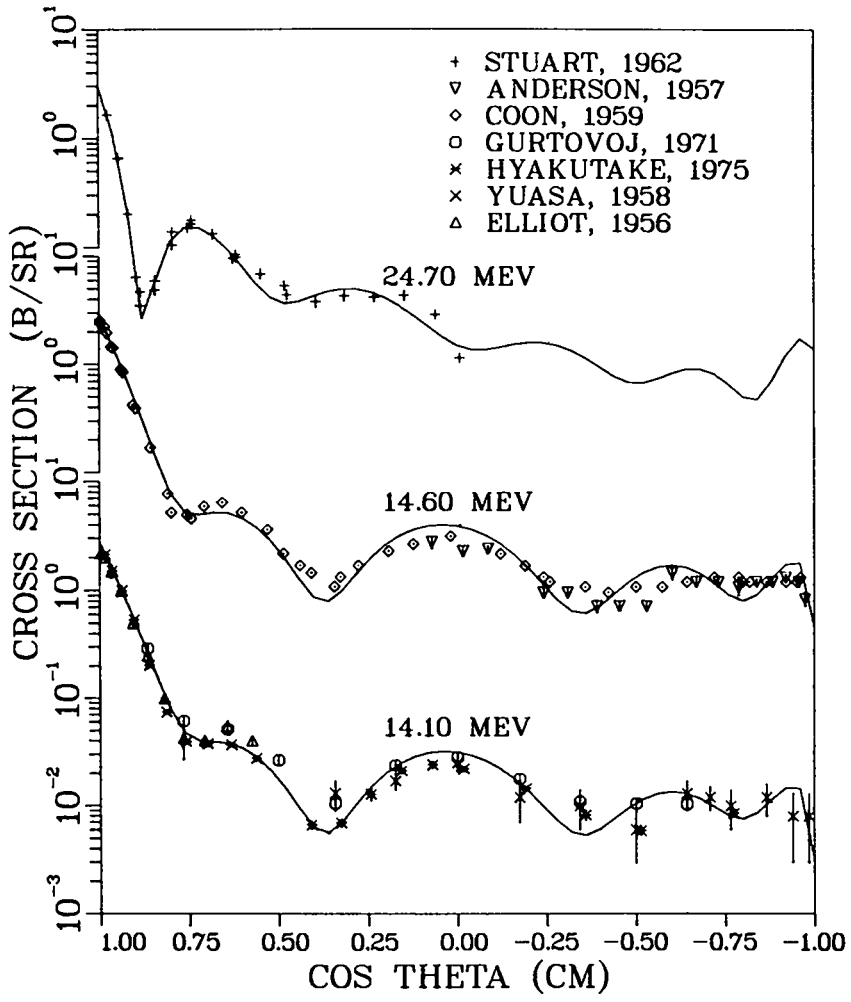


Fig. 6
Measured and calculated elastic angular distributions for iron. Experimental data are from Refs. 30-36.

our parameters. Energy dependences for both the real and imaginary potential were determined by approximate fits to trends in the potential depths given by Lemos at several incident energies. Further guidance was obtained from measurements made at higher energies in which such energy dependences were determined. We checked the applicability of the resulting optical parameters by calculation of $^{51}V(\alpha,n)$ and $^{55}Mn(\alpha,n)$ cross sections[61,62] using the neutron parameters of Table I. The results appear in Fig. 10. We did not attempt to make further tests at higher energies since in the calculations the emission of higher energy alpha particles is influenced strongly by nonstatistical effects that have a decreased sensitivity to the transmission coefficients used. The final adopted alpha-particle optical parameters are given in Table III.

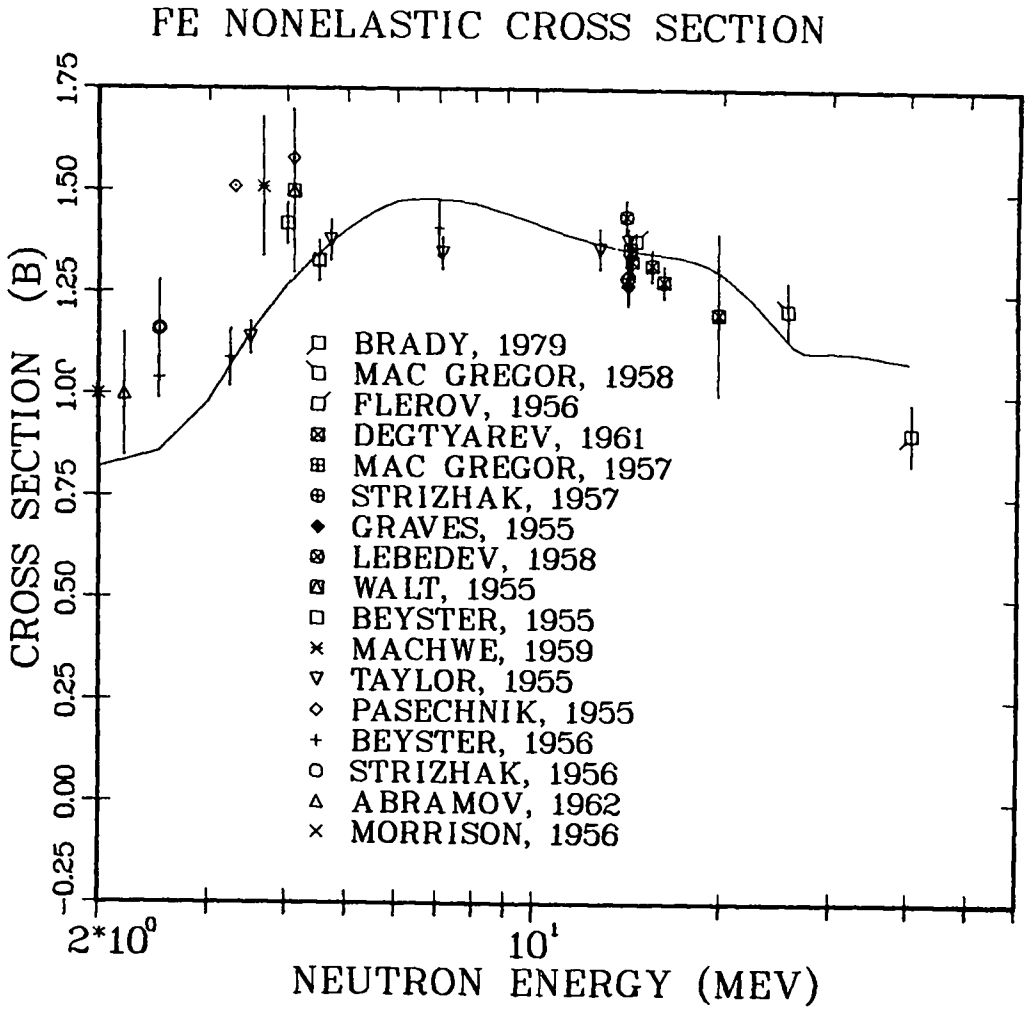


Fig. 7.
Measured and calculated nonelastic cross sections for iron. Experimental data are from Refs. 37-53.

TABLE III

ALPHA OPTICAL MODEL PARAMETERS

| | r(fm) | a(fm) |
|---|---|---|
| V(MeV) = 193 - 0.15E | 1.37 | 0.56 |
| $W_{vol}$(MeV) = 21 + 0.25E | 1.37 | 0.56 |
| $r_c$(fm) = 1.4 | | |

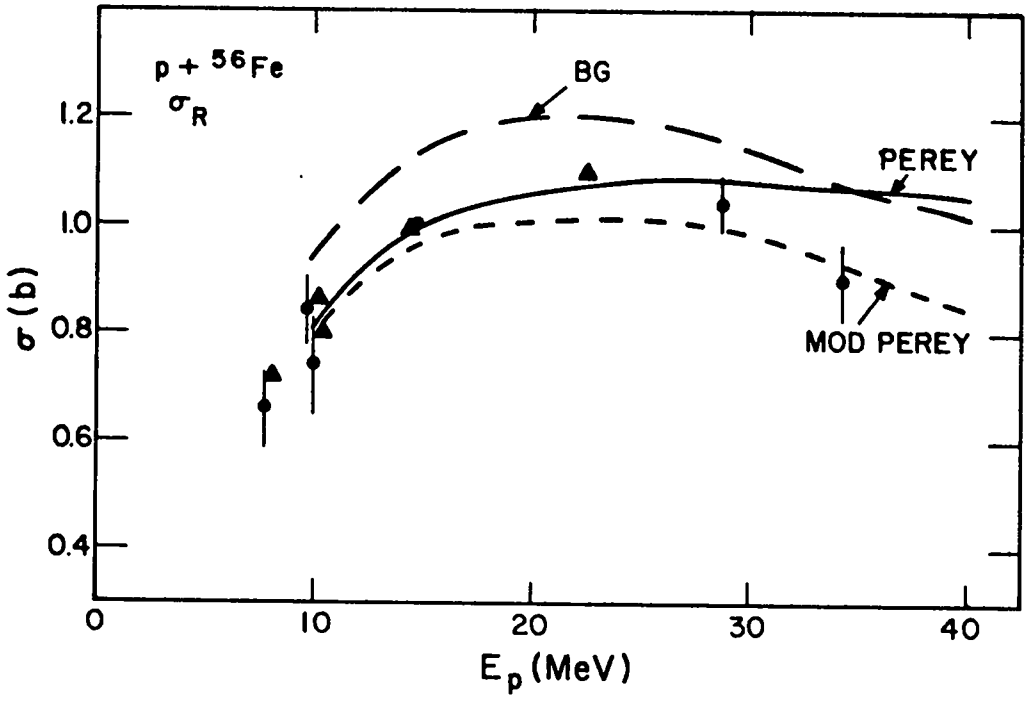


Fig. 8.
Calculated p + $^{56}$Fe reaction cross sections compared to experimental data (Refs. 55 and 56). The solid curve results from the parameters of Perey,[54] the long-dashed curve from the parameters of Becchetti,[168] and the short-dashed curve from our parameters.

## C. Gamma-Ray Strength Functions and Transmission Coefficients

Gamma-ray emission can be an important competitor to particle emission, particularly around reaction thresholds. We chose to calculate gamma-ray transmission coefficients through use of gamma-ray strength functions determined from fits to neutron capture cross sections.[63] This method avoids many of the problems that occur when the normalization of gamma-ray transmission coefficients is determined directly from the ratio of the average gamma width, $\langle\Gamma_\gamma\rangle$, and the s-wave resonance spacing, $\langle D\rangle$, as is often done in these types of calculations. Such $\langle\Gamma_\gamma\rangle$ and $\langle D\rangle$ values are not always reliable, especially in the present case where information needed for compound systems away from the line of stability must be inferred from the systematic behavior of such quantities. Gamma-ray strength functions should be more reliable since their behavior is expected to vary slowly between nearby nuclei.[64] For this problem, we determined gamma-ray strength functions through fits to $^{54}$Fe and $^{56}$Fe capture

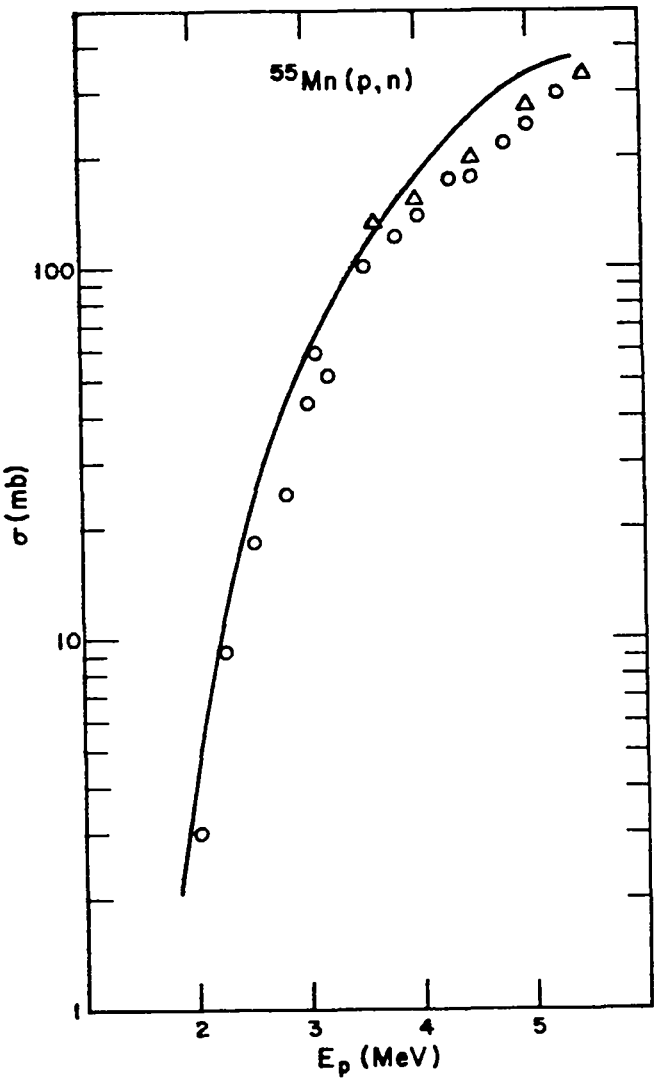


Fig. 9.
Measured and calculated cross sections for the $^{55}Mn(p,n)$ reaction. Experimental data are from Refs. 58 and 59.

data[65,66] below 1 MeV. A giant dipole resonance shape was used along with parameters determined from photonuclear data. Only E1 transitions were considered. Some of our preliminary Hauser-Feshbach calculations of photon production spectra indicated an improvement in the agreement of the calculated spectra to the experimental results if a 45% reduction in the tail of the Lorentz curve used to represent the giant dipole resonance was made below $\varepsilon_\gamma$ = 9 MeV. This alteration was also included in the form assumed in the determination of the

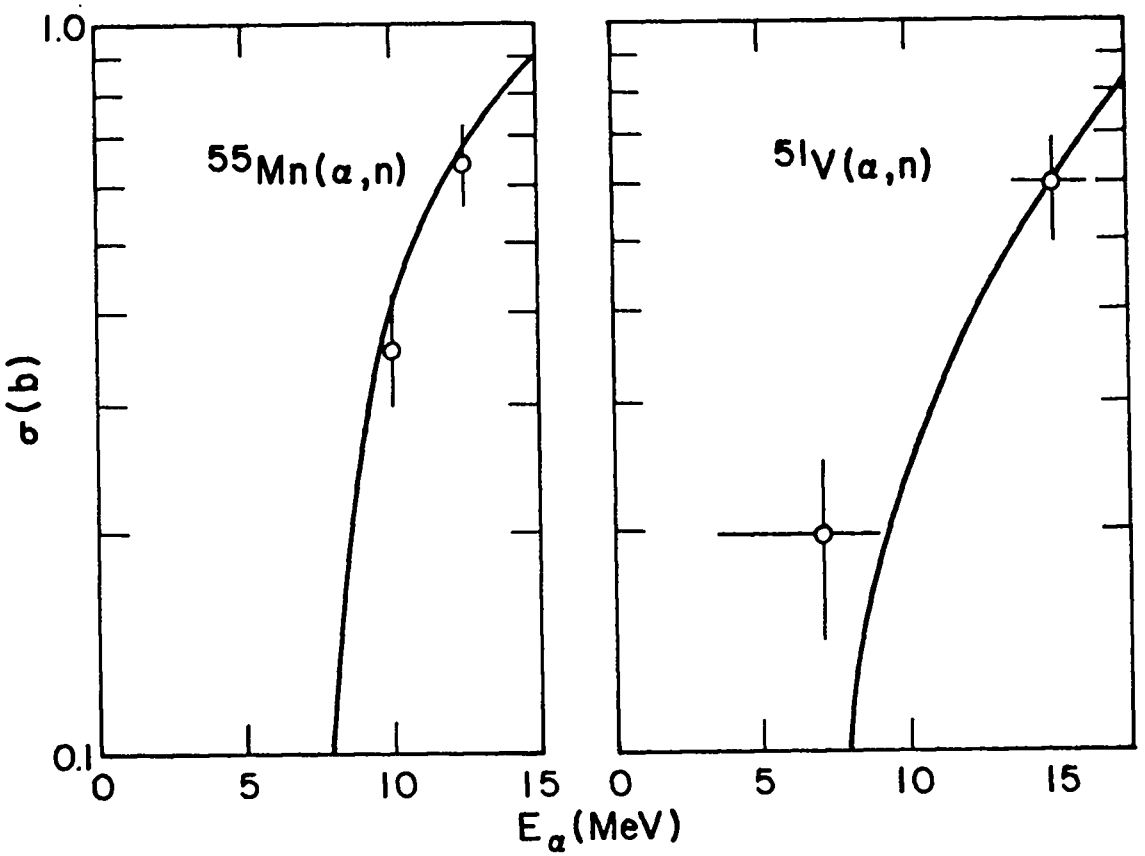


Fig. 10.
Measured and calculated cross sections for the $^{55}Mn(\alpha,n)$ and $^{51}V(\alpha,n)$ reactions. Experimental data for the two reactions are from Refs. 61 and 62, respectively.

strength function. The normalizing constants obtained for the strength functions through fits to $^{54}Fe(n,\gamma)$ and $^{56}Fe(n,\gamma)$ data were essentially identical, differing only by about 5% even though the $^{54}Fe$ capture cross section is about 50% higher than that of $^{56}Fe$.

Since gamma-ray production spectra were of interest along with cross sections for the production of isomeric states, we employed a detailed gamma-ray cascade model in our Hauser-Feshbach calculations. In addition to E1 transitions, we allowed gamma-ray emission by M1 and E2 transitions, which were normalized to the E1 component through use of the Weisskopf estimate. A giant dipole resonance form was also assumed for these transitions.

## D. Discrete Levels and Level-Density Parameters

The inclusion of a large number of discrete levels (where reliable experimental data exist) is advantageous in these calculations since such level information results in more reliable cross sections, particularly around reaction thresholds. Such level data also provide constraints to ensure a reasonable behavior of level-density parameters at lower-excitation energies. We took level information--energies, spins, parities, and gamma-ray branching ratios--from the compilation of Lederer and Shirley.[67] A listing of the discrete levels used appears in Appendix A.

To represent the continuum excitation energy region occurring above the last discrete level, we used the Gilbert-Cameron[68] level-density model consisting of Fermi-gas and constant temperature portions. For the Fermi-gas part, we generally used the level-density parameters, a, and pairing energies, $\Delta$, given by Cook.[69] The constant temperature parameters were adjusted to produce agreement with the cumulative number of available discrete levels while joining smoothly to the Fermi-gas expression at an excitation energy, $U_x$. Both Fermi-gas and constant temperature parameters appear in Table IV.

## E. Preequilibrium Model and Parameters

Reaction mechanisms other than those described by the Hauser-Feshbach statistical model begin to have important effects on neutron cross sections and spectra at higher energies. As part of the corrections to the statistical model results, we applied the preequilbrium model based on the master equations method of Kalbach.[70] In this model, rates involving transitions between particles and holes are directly proportional to the square of the absolute value of the matrix element describing two-body residual interactions. The form for the square of the matrix element has been recently parameterized by Kalbach[71] from fits to higher energy nucleon-induced reaction data as

$$M^2 = \frac{kf(\varepsilon)}{A^3\varepsilon} \quad . \tag{1}$$

Here $\varepsilon$ is the excitation energy available per exciton, E/n, and $f(\varepsilon)$ represents a function valid for different ranges of $\varepsilon$. We used a normalization constant of $k = 160$ MeV$^3$ and the single-particle state densities were taken to be equal to $A_i/13$ where $A_i$ is the mass of the ith residual nucleus. We also included pairing effects in the calculation of excitation energies that may account for

TABLE IV

LEVEL DENSITY PARAMETERS

| Nucleus | a ($MeV^{-1}$) | Δ (MeV) | $E_o$ (MeV) | T (MeV) | $U_x$ (MeV) |
|---|---|---|---|---|---|
| $^{48}Cr$ | 6.587 | 2.79 | -1.379 | 1.255 | 5.297 |
| $^{49}Cr$ | 6.563 | 1.35 | -0.354 | 1.239 | 7.104 |
| $^{50}Cr$ | 6.545 | 2.89 | 0.217 | 1.367 | 10.472 |
| $^{51}Cr$ | 6.442 | 1.35 | -1.098 | 1.358 | 8.585 |
| $^{52}Cr$ | 6.154 | 2.65 | 1.069 | 1.29 | 8.368 |
| $^{53}Cr$ | 6.501 | 1.35 | -0.491 | 1.272 | 7.456 |
| $^{51}Mn$ | 6.293 | 1.54 | -0.91 | 1.383 | 8.844 |
| $^{52}Mn$ | 6.178 | 0.0 | -1.379 | 1.255 | 5.297 |
| $^{53}Mn$ | 5.874 | 1.3 | -1.154 | 1.463 | 8.846 |
| $^{54}Mn$ | 5.85 | 0.0 | -2.173 | 1.432 | 7.047 |
| $^{55}Mn$ | 6.665 | 1.27 | -0.82 | 1.282 | 7.813 |
| $^{56}Mn$ | 7.233 | 0.0 | -2.176 | 1.214 | 6.505 |
| $^{51}Fe$ | 6.054 | 1.54 | 1.273 | 2.226 | 2.028 |
| $^{52}Fe$ | 6.015 | 3.08 | 1.142 | 1.366 | 9.563 |
| $^{53}Fe$ | 5.888 | 1.54 | -0.357 | 1.385 | 8.019 |
| $^{54}Fe$ | 5.568 | 2.84 | 0.322 | 1.535 | 10.686 |
| $^{55}Fe$ | 5.909 | 1.54 | -1.574 | 1.538 | 10.297 |
| $^{56}Fe$ | 6.355 | 2.81 | -0.224 | 1.447 | 11.712 |
| $^{57}Fe$ | 6.923 | 1.54 | -1.587 | 1.366 | 9.862 |

The quantities above are defined as:

a = Level density parameter of the Fermi-gas level density expression.

Δ = Pairing energy.

$E_o$ and T = Constant temperature level density parameters.

$U_x$ = Matching energy at which constant temperature and Fermi-gas expressions are joined.

the slight difference in our value for k over that recommended by Kalbach, namely, $k = 135\ MeV^3$.

In addition to preequilibrium effects, we also included for $(n,\alpha)$ reactions contributions from pickup and knockout processes as described in a series of phenomenological expressions derived by Kalbach.[70] These contributions, in fact, produce most of the cross sections for the $(n,\alpha)$ reaction and allow alpha-particle emission to be calculated without use of quantities such as alpha-particle preformation constants.

The prequilibrium model as it is generally used does not include angular momentum effects so we assumed that the spin distribution of the preequilibrium components would be the same as that obtained from the equilibrium Hauser-Feshbach calculations. This approximation becomes worse as one goes to higher incident energies where preequilibrium effects dominate in the emission of particles from the first compound nucleus. However, since parameters for the preequilibrium model have in general been determined through the analysis of charged-particle experimental data measured at energies of tens of MeV, the potential effect of such problems may have been lessened through the phenomenological parameter values obtained.

In addition to providing corrections to calculated spectra and cross sections, calculated preequilibrium fractions were also used in conjunction with phenomenological expressions for secondary particle angular distributions determined from fits by Kalbach and Mann[72] to particle-induced reaction data. Their analysis led to the following expression for the doubly differential cross section:

$$\frac{d^2\sigma}{d\varepsilon d\Omega} = a_0(\mathrm{MSD}) \sum_{\ell=0}^{8} b_\ell P_\ell(\cos\theta) + a_0(\mathrm{MSC}) \sum_{\substack{\ell=0 \\ \Delta\ell=2}}^{8} b_\ell P_\ell(\cos\theta) \quad . \tag{2}$$

Here $a_0(\mathrm{MSD})$ and $a_0(\mathrm{MSC})$ refer to fractions of the preequilibrium cross section resulting from multistep direct (MSD) and multistep compound (MSC) contributions. In our calculations, the multistep direct fraction could be approximated through use of the total preequilibrium cross section, and the multistep compound was approximated by using the evaporation portion of the cross section. The Legendre coefficients, $b_\ell$, appearing in Eq. (2) were found

in Ref. 72 to be essentially dependent only on the energy of the emitted particle,

$$b_\ell = \frac{2\ell + 1}{1 + \exp\ [A_\ell(B_\ell - \varepsilon)]} \quad , \tag{3}$$

where $A_\ell$ and $B_\ell$ depend only on $\ell$.

## F. The Direct Reaction Model and Parameters

The preequilibrium and Hauser-Feshbach statistical models are not adequate to fully describe the excitation of low-lying collective states in $^{54,56}Fe$ through neutron inelastic scattering since strong direct reaction processes are involved. The lower-order terms involving a small number of particle-hole pairs in the preequilibrium model can approximate in a crude manner the direct reaction process and for this reason the exciton or geometry-dependent hybrid models have sometimes been used to account for such direct effects in particle emission spectra. We chose, however, to perform Distorted Wave Born Approximation (DWBA) calculations to describe the excitation of collective states through the direct reaction mechanism. We used the DWBA program DWUCK[73] along with the neutron optical parameters of Table I. Observed differential cross sections can be related to ones obtained from the DWBA calculation by

$$\frac{d\sigma}{d\Omega}_\ell = \left| \langle J_A\ k0 | J_B k\rangle \right|^2 \beta_\ell^2\ \sigma_{DW}^\ell(\theta) \quad , \tag{4}$$

where $\langle J_A k0 | J_B k\rangle$ is the Clebsch-Gordon coefficient (in this case) for scattering on a spin zero target nucleus. The deformation parameters $\beta_\ell$ were taken from values determined by Mani[74] from analysis of proton inelastic scattering on $^{54}Fe$ and $^{56}Fe$. Table V lists the states for which DWBA calculations were made along with the $\beta_\ell$ parameters used.

The direct cross sections obtained for the levels appearing in Table V were combined with Hauser-Feshbach calculations after the total compound nucleus formation cross section was renormalized to account for the direct reaction contributions. Because of the ambiguity as to the amount of the direct reaction process accounted for in the preequilibrium model, preequilibrium corrections were not applied to states having calculated DWBA cross sections. In these cases, only the DWBA and compound nucleus contributions were combined to produce a total cross section for such a state.

TABLE V

DWBA PARAMETERS USED TO CALCULATE DIRECT INELASTIC SCATTERING FROM $^{54,56}$Fe Levels

| $^{54}$Fe | $E_x$(MeV) | $J^\pi$ | $\beta_\ell$ |
|---|---|---|---|
| | 1.408 | 2+ | 0.18 |
| | 2.538 | 4+ | 0.05 |
| | 2.950 | 6+ | 0.02 |
| | 2.959 | 2+ | 0.098 |
| | 3.166 | 2+ | 0.052 |
| | 3.295 | 4+ | 0.033 |
| | 3.834 | 4+ | 0.052 |
| | 4.048 | 4+ | 0.024 |
| | 4.265 | 4+ | 0.045 |
| | 4.579 | 2+ | 0.026 |
| $^{56}$Fe | | | |
| | 0.846 | 2+ | 0.22 |
| | 2.085 | 4+ | 0.03 |
| | 2.658 | 2+ | 0.06 |
| | 2.960 | 2+ | 0.02 |
| | 3.123 | 4+ | 0.087 |
| | 3.370 | 2+ | 0.06 |
| | 3.388 | 6+ | 0.037 |
| | 3.602 | 2+ | 0.05 |
| | 3.755 | 6+ | 0.04 |
| | 3.832 | 2+ | 0.03 |
| | 4.120 | 4+ | 0.045 |
| | 4.298 | 4+ | 0.04 |
| | 4.401 | 2+ | 0.05 |
| | 4.510 | 3− | 0.1 |
| | 4.612 | 2+ | 0.055 |
| | 4.740 | 2+ | 0.05 |
| | 4.880 | 2+ | 0.05 |

## III. CALCULATED RESULTS AND DATA COMPARISONS

### A. Nuclear Models and Codes

The cross sections presented here result from application of the basic models discussed earlier--optical, direct reaction, preequilibrium, and Hauser-Feshbach. To generate total cross sections, shape elastic angular distributions, and particle transmission coefficients, we used the spherical optical code SCAT2[75] with the parameters of Tables I, II, and III. As mentioned in Sec. II F, the DWBA code DWUCK[73] was used to calculate direct reaction cross sections for inelastic scattering from collective levels in $^{54}Fe$ and $^{56}Fe$. For the Hauser-Feshbach portion of the calculations, we relied on the COMNUC[76] and GNASH[77] codes, both of which include angular momentum and parity conservation explicitly. The COMNUC code was generally used for neutron energies below 4-5 MeV, since it contains a complete treatment of width-fluctuation corrections needed for accurate cross-section calculations at low energies where only a few channels are open. At higher energies, the GNASH multistep Hauser-Feshbach code was used since it includes preequilibrium corrections and can handle complex decay chains involving up to eight compound nuclei. Figure 11 illustrates a decay chain used for cross section calculations at higher incident neutron energies. Such detail is required since it is necessary to follow the production and decay of compound nuclei formed not only by successive neutron emission but also by multiple proton emission.

A summary of the important reaction cross sections obtained from the calculations is given in Fig. 12. That it is important to follow the decay of proton emission products is clearly shown. For example, Fig. 12 illustrates that processes involving complex chains such as (n,2np) (sum of n,p2n + n,npn + n,2np) become important and actually begin to dominate when compared to reactions involving only neutron emission. This occurs because these cross sections are produced by sequences involving several paths and also because the compound systems produced at higher energies tend to become more proton rich. Gamma-ray production cross sections and spectra were required at all incident neutron energies, which meant that the decay sequences also had to include gamma-ray deexcitation of nuclei populated in all major reactions.

### B. Inelastic Scattering and Neutron Emission

Comparison to data available for inelastic scattering to discrete final states presents an opportunity to check several aspects of the calculations.

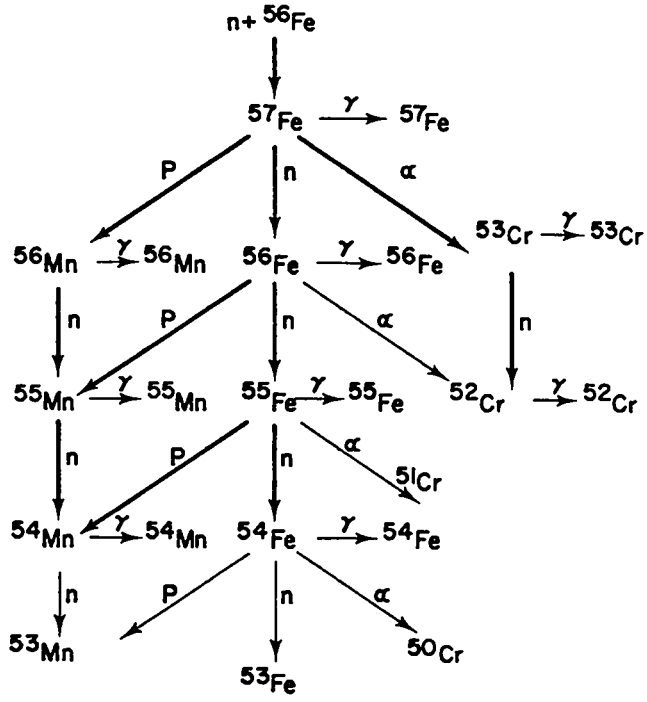


Fig. 11.
Schematic diagram of the reaction chains for n + $^{56}Fe$ that was included in the calculation.

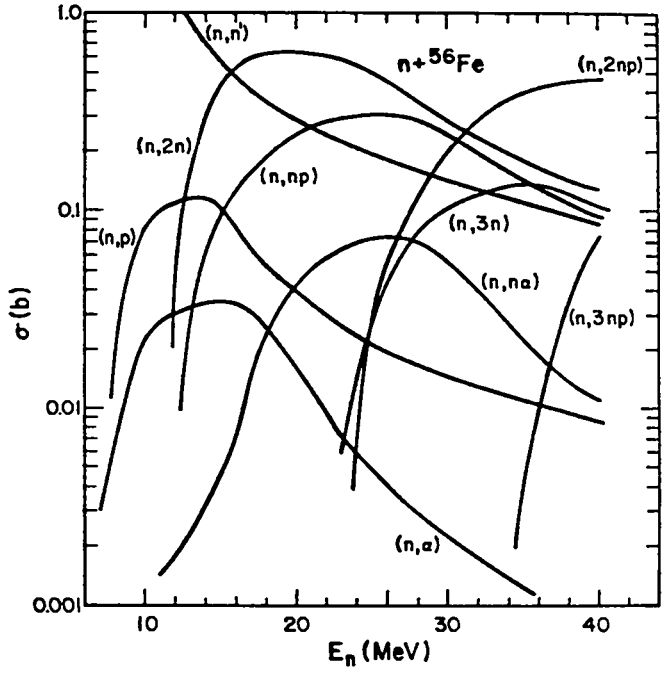


Fig. 12.
Composite of n + $^{56}Fe$ cross sections that resulted from the calculations.

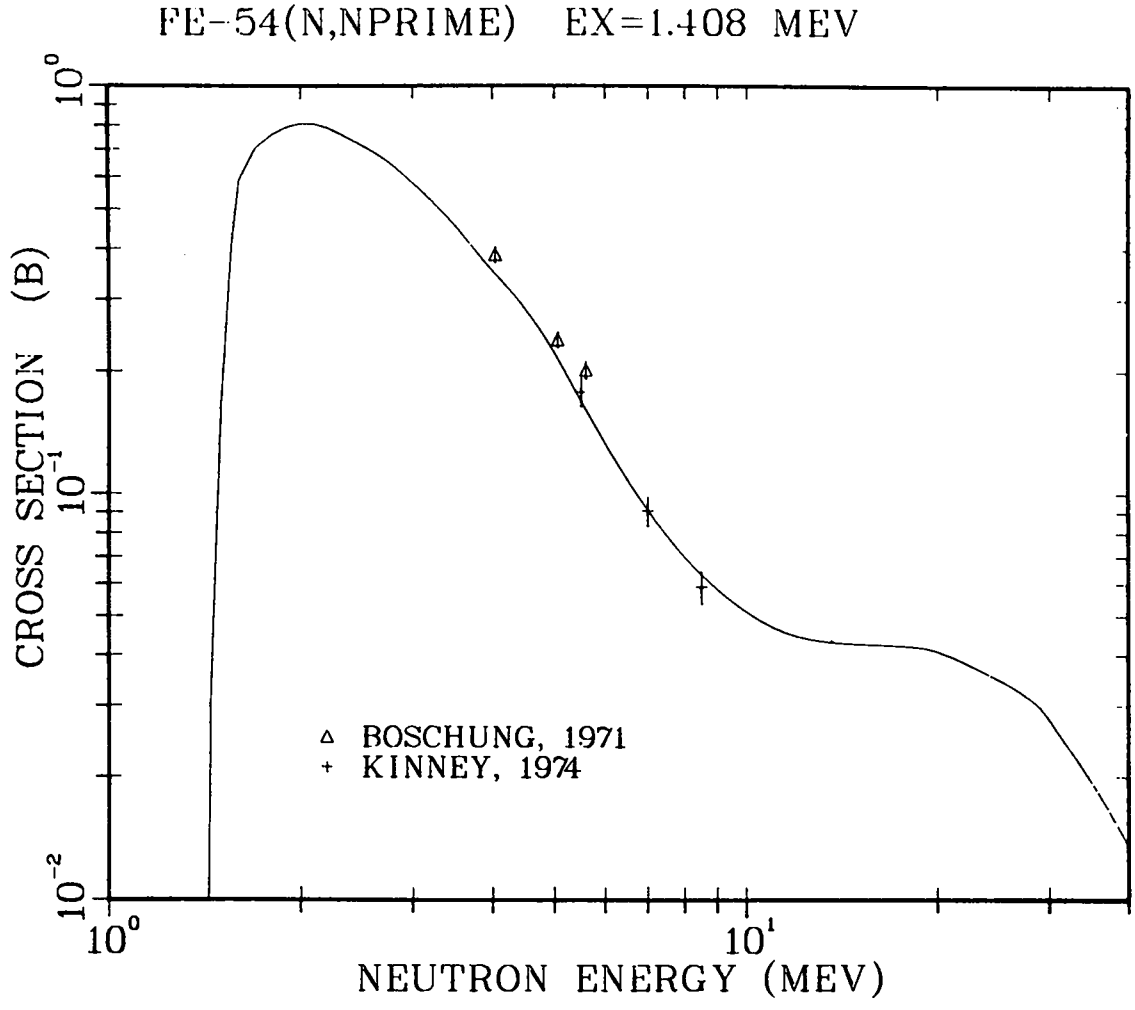


Fig. 13.
Calculated and measured excitation functions for the $^{54}Fe(n,n')$ reaction to the 1.408-MeV level in $^{54}Fe$. Experimental data are from Refs. 78 and 79.

For low energies the calculated cross sections depend on the suitability of the neutron optical parameters used to provide transmission coefficients for the Hauser-Feshbach model, the width-fluctuation corrections and, where applicable, the results of DWBA calculations. We compare in Figs. 13 and 14 calculated excitation functions for inelastic scattering to discrete states of $^{54}Fe$ measured[78,79] between 3 and 10 MeV. Similar results[23,79-89] are shown in Figs. 15-18 for discrete states in $^{56}Fe$. The agreement indicates a proper choice of neutron optical parameters both for use in the compound nucleus calculation and also within the DWBA calculation of direct contributions. Further tests of the calculated direct cross section appear in Fig. 19 where comparisons are made to

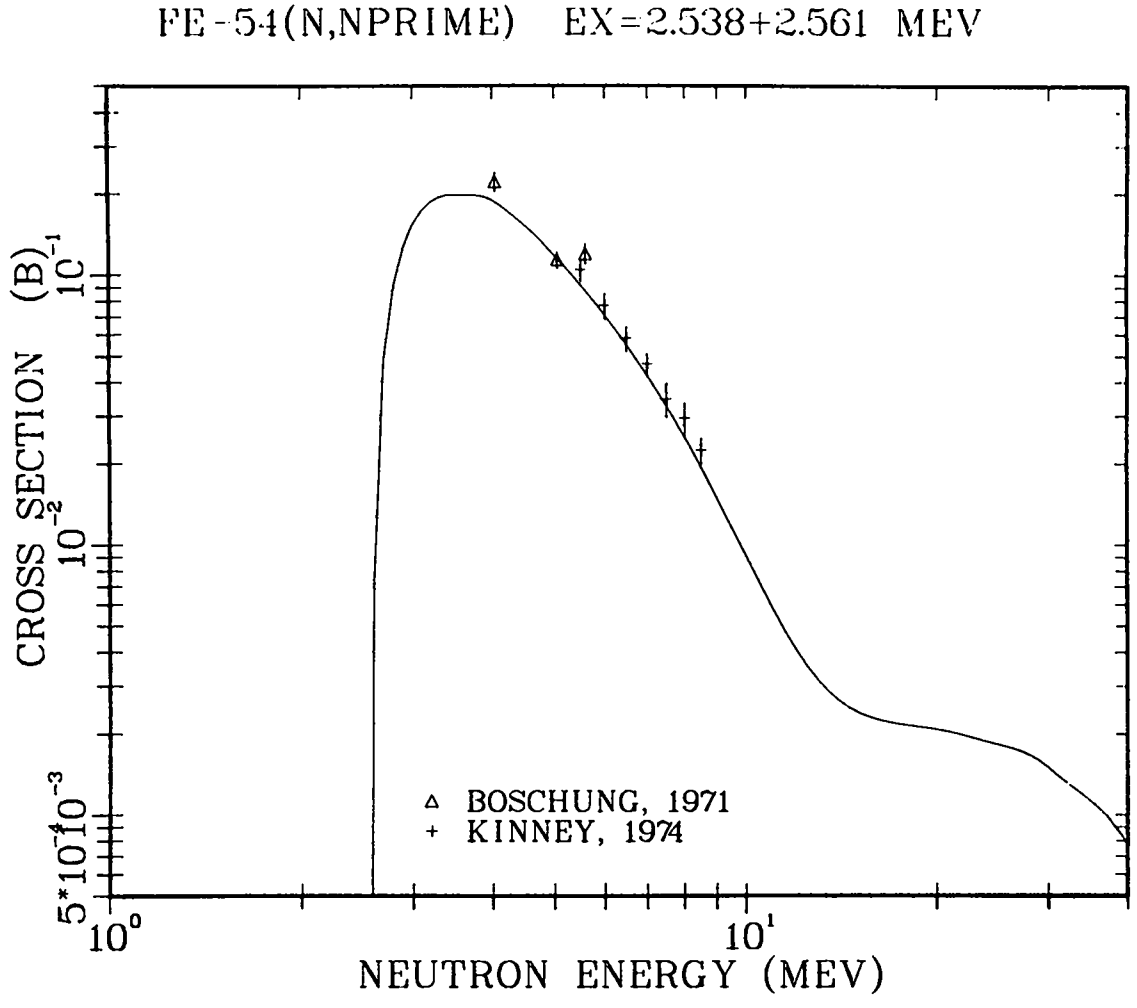


Fig. 14.
Calculated and measured composite excitation functions for the $^{54}Fe(n,n')$ reactions to the 2.538- and 2.561-MeV levels in $^{54}Fe$. Experimental data are from Refs. 78 and 79.

angular distributions[34,90] measured for excitation of the 0.846-MeV, $J^{\pi} = 2^{+}$ state in $^{56}Fe$ by 14.1-MeV neutrons. Here compound nucleus contributions are minimal with the neutron optical parameters as used in the DWBA calculation providing the major effect.

In this energy range there exist several measurements of the neutron emission spectrum, and these are compared to our calculated results in Figs. 20-22. In Fig. 20, the angle-averaged results of Hermsdorf,[91] Lukyanov,[92] and Vonach[93] and the 90-degree measurement of Clayeux[94] are compared to the calculated spectrum at 90 degrees. In Figs. 21 and 22, measurements at 4 angles between 35 and 145 degrees by Kammerdiener[95] are compared to the calculations.

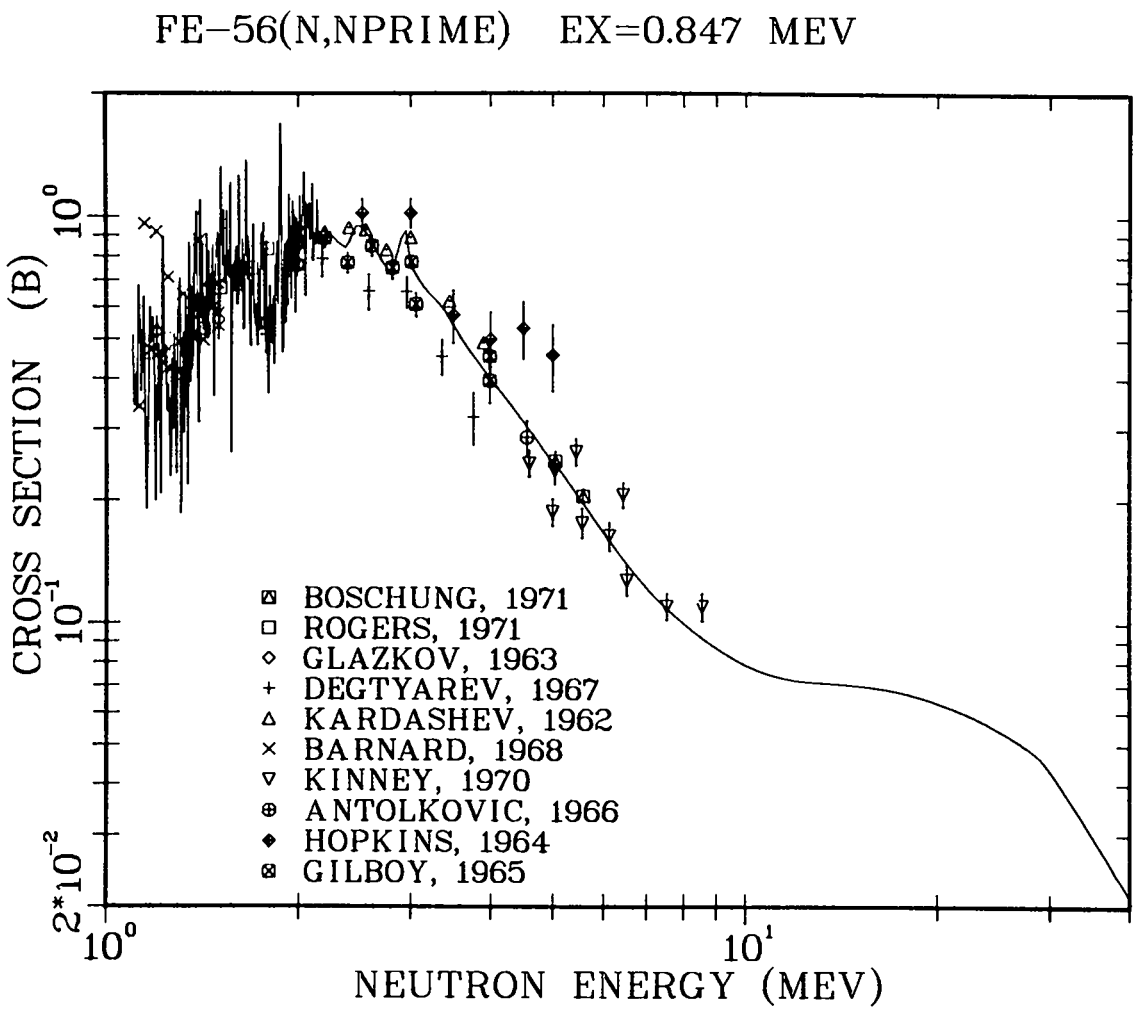


Fig. 15.
Calculated (above 3 MeV) and measured excitation functions for the $^{56}Fe(n,n')$ reaction to the 0.847-MeV level in $^{56}Fe$. Experimental data are from Refs. 23, 79-87.

These comparisons illustrate the importance of preequilibrium effects on the spectrum and confirm the choice of the preequilibrium parameters used.

In Sec. II. E, we described a set of phenomenological expressions[72] for the angular distributions of particles populating a continuum of secondary energies. These expressions were derived generally from fits to higher energy particle-induced data and have not been tested at lower energies of interest to many neutron applications. At 14.1 MeV, the secondary neutron angular distributions measured by Hermsdorf[91] provide data for such a test and are compared in Fig. 23 for a series of secondary energy ranges. While some discrepancies

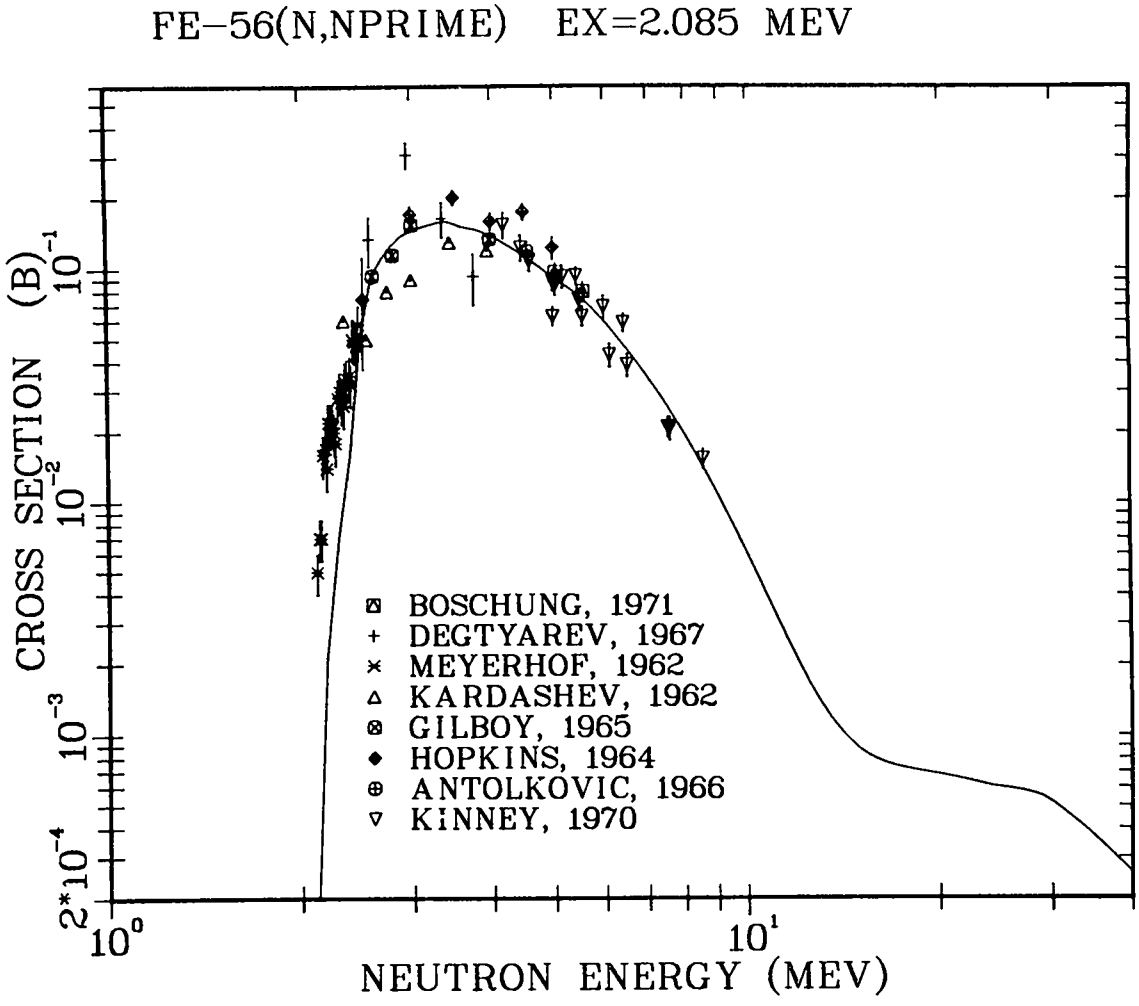


Fig. 16.
Calculated and measured excitation functions for the $^{56}Fe(n,n')$ reaction to the 2.085-MeV level in $^{56}Fe$. Experimental data are from Refs. 23, 79, 82, 83, and 85-88.

exist, the over all agreement is reasonable. Since these parameters were determined principally from higher energy data, their applicability should increase at the higher incident energies of this calculation.

## C. (n,2n) Cross Sections

The comparison to (n,2n) data provides the opportunity to evaluate the behavior of the low energy neutron transmission coefficients as well as to test, indirectly, effects from competing reactions involving mainly proton and gamma-ray emission. Furthermore, the calculated cross section from threshold to several MeV above threshold results principally from transitions to discrete final

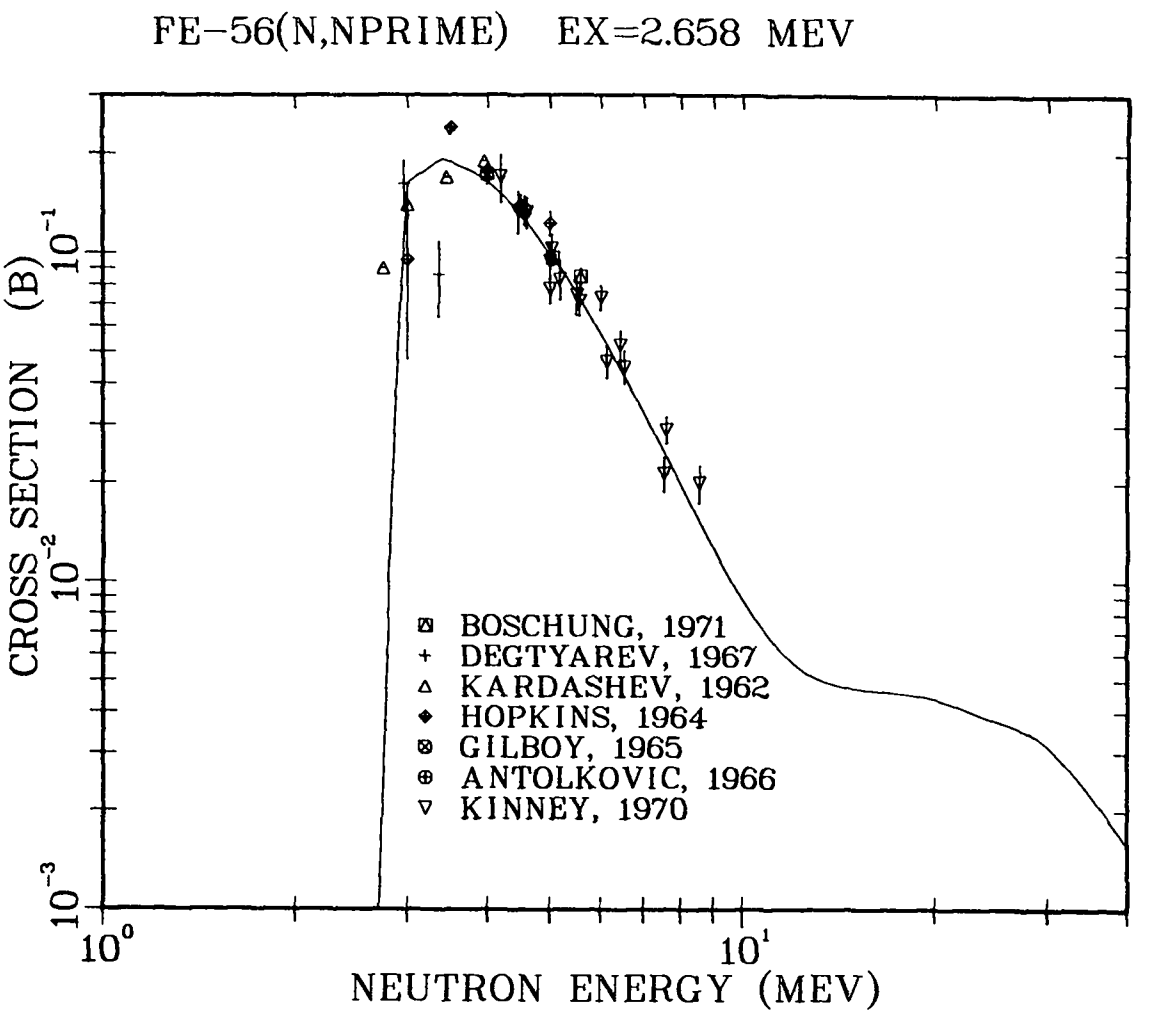


Fig. 17.
Calculated and measured excitation functions for the $^{56}$Fe(n,n') reaction to the 2.658-MeV level in $^{56}$Fe. Experimental data are from Refs. 23, 79, 82, 83, and 85-87.

states in the residual nucleus. Thus, neutron transmission coefficients can be tested without complications from level-density effects.

Two types of iron (n,2n) data exist--the first from scintillator tank measurements on natural iron and the second from activation measurements of the $^{54}$Fe(n,2n) cross section. The tank measurements on natural iron provide data mainly about the $^{56}$Fe(n,2n) reaction where, in the case of the $^{56}$Fe compound nucleus, neutron and proton separation energies are essentially equivalent and neutron emission dominates. In this case, calculations are sensitive to the neutron transmission coefficients and, around threshold, to the amount of gamma-ray competition included. As described in Sec. II C., we used the gamma-

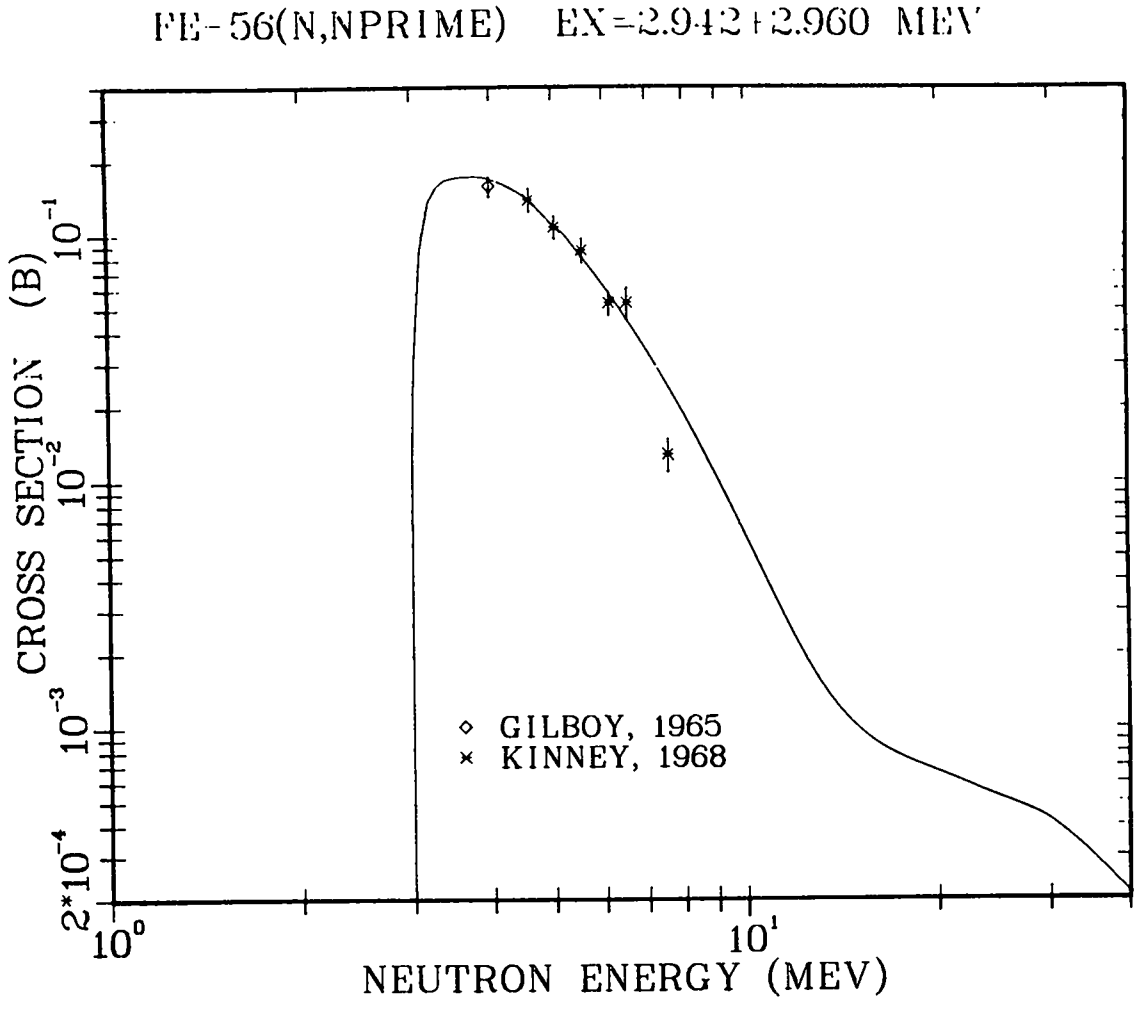


Fig. 18.
Calculated and measured composite excitation functions for the $^{56}Fe(n,n')$ reactions to the 2.942- and 2.960-MeV levels in $^{56}Fe$. Experimental data are from Refs. 87 and 89.

ray strength function method to provide the normalization for the gamma-ray transmission coefficients occurring in the problem. In the case of the $^{56}Fe$ compound system, values of the s-wave resonance parameters $\langle\Gamma_\gamma\rangle$ and $\langle D\rangle$ are not available experimentally and would have to be determined from systematics if gamma-ray transmission coefficients were normalized to the $2\pi\langle\Gamma_\gamma / D\rangle$ ratio, which would lead to an increased probability for error. The use of gamma-ray strength functions should alleviate such problems, and the (n,2n) cross section around threshold provides data to test this assumption. Figure 24 compares the calculated (n,2n) cross section for natural iron to measurements by Frehaut[96]

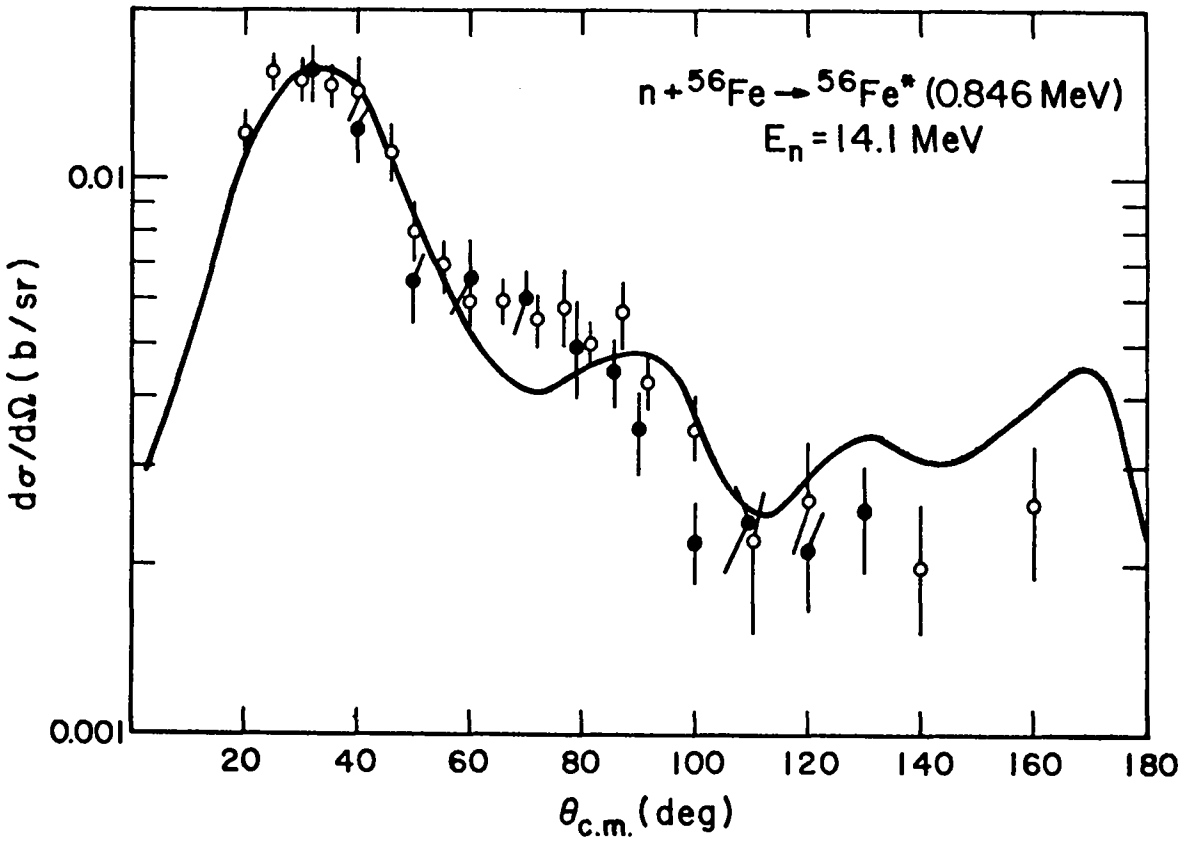


Fig. 19.
Calculated and measured angular distributions for the $^{56}Fe(n,n')$ reaction to the 0.846-MeV level for 14.1-MeV incident neutrons. Experimental data are from Refs. 34 and 90.

and Veeser[97]. The threshold agreement confirms both the gamma-ray transmission coefficient normalization as well as the neutron transmission coefficient behavior. Some disagreement occurs with the Veeser data at higher energies, but this is generally less than 8%.

A quite different situation exists for the $^{54}Fe(n,2n)$ reaction. In the $^{54}Fe$ compound system, the binding energy of the proton is about 4.5 MeV less than that of the neutron so that the probability of neutron emission is decreased and the effect of the competing (n,np) reaction becomes more important. Figure 25 compares our calculation to several measurements[98-109] of this cross section. The fact that reasonable agreement is obtained for this cross section, which represents less than 10% of the total reaction cross section, indicates the suitability of the parameters used to describe the competing reactions that dominate.

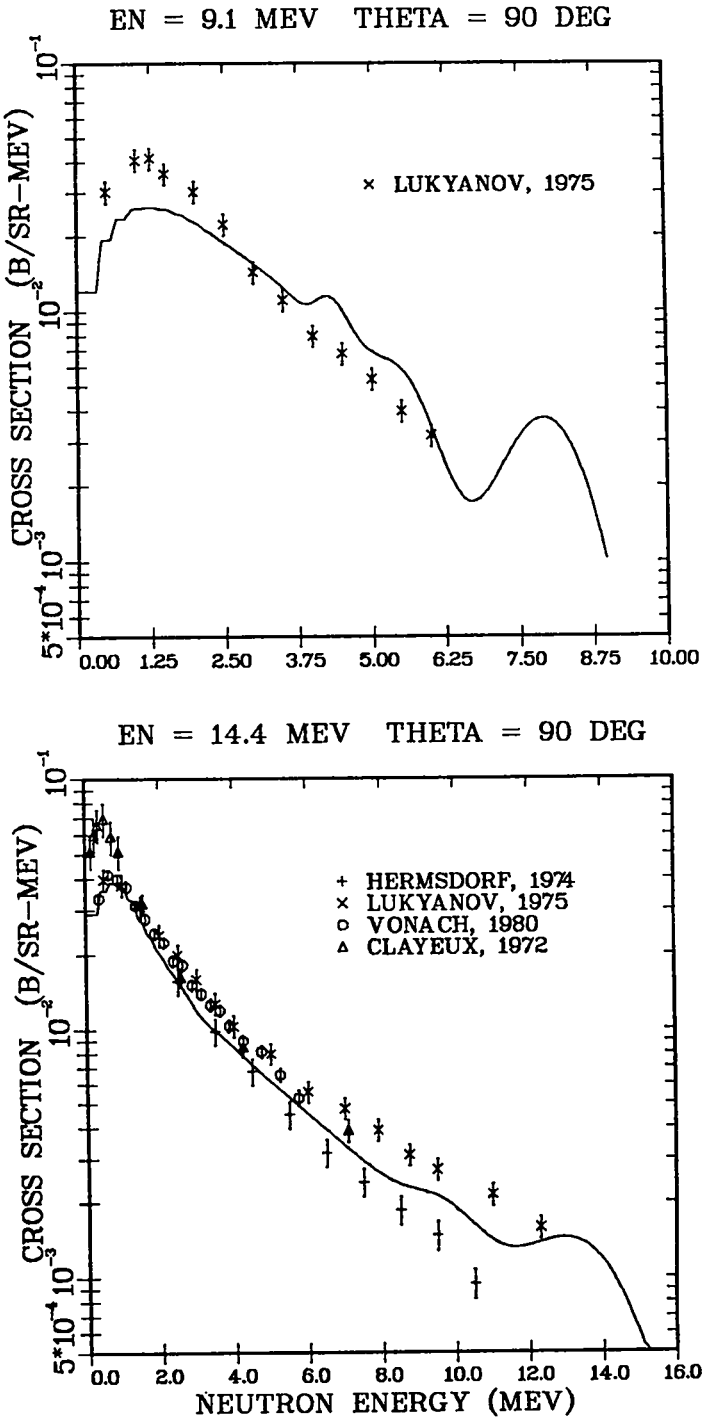


Fig. 20.
Calculated neutron emission spectra at 90 degrees for 9.1- and 14.4-MeV neutrons incident on iron compared to the measurements of Refs. 91-94. The data shown for Hermsdorf,[91] Lukyanov,[92] and Vonach[93] have been averaged over several angles.

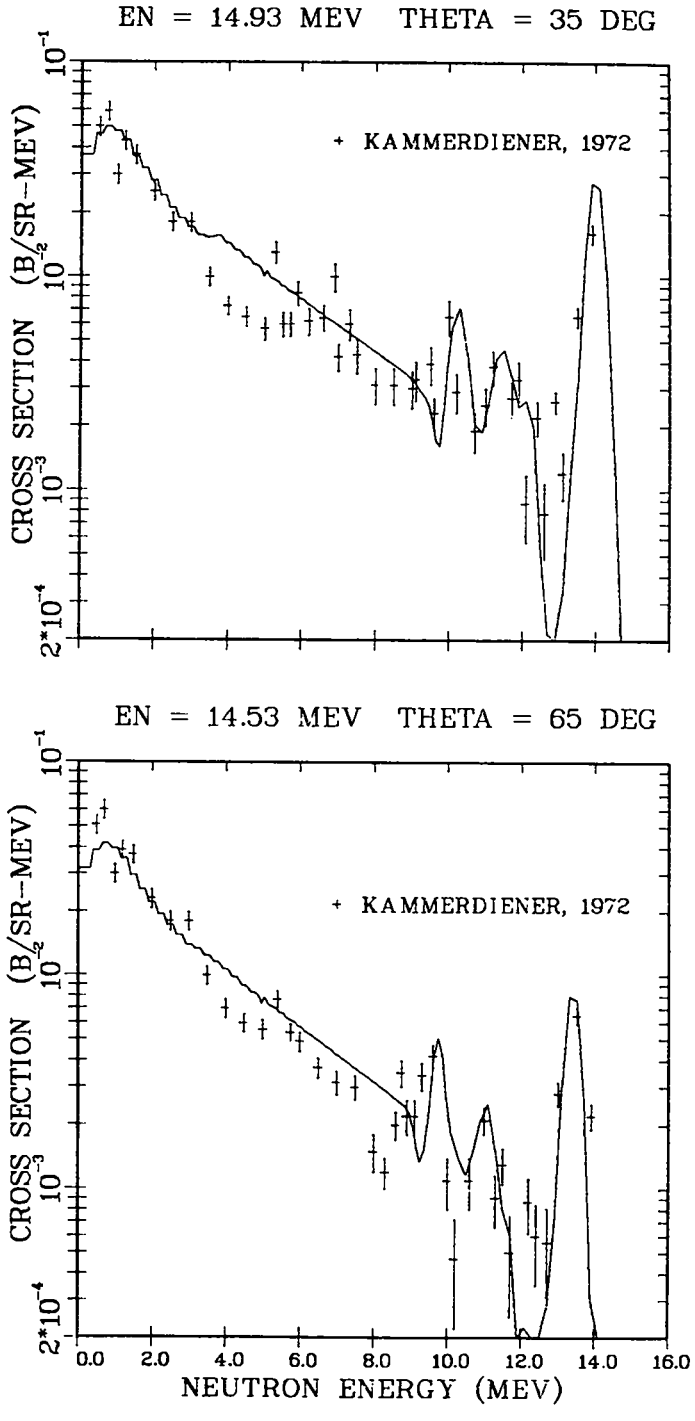


Fig. 21.
Calculated neutron emission spectra at 35 and 65 degrees compared to Kammerdiener's[95] iron measurements near 14 MeV.

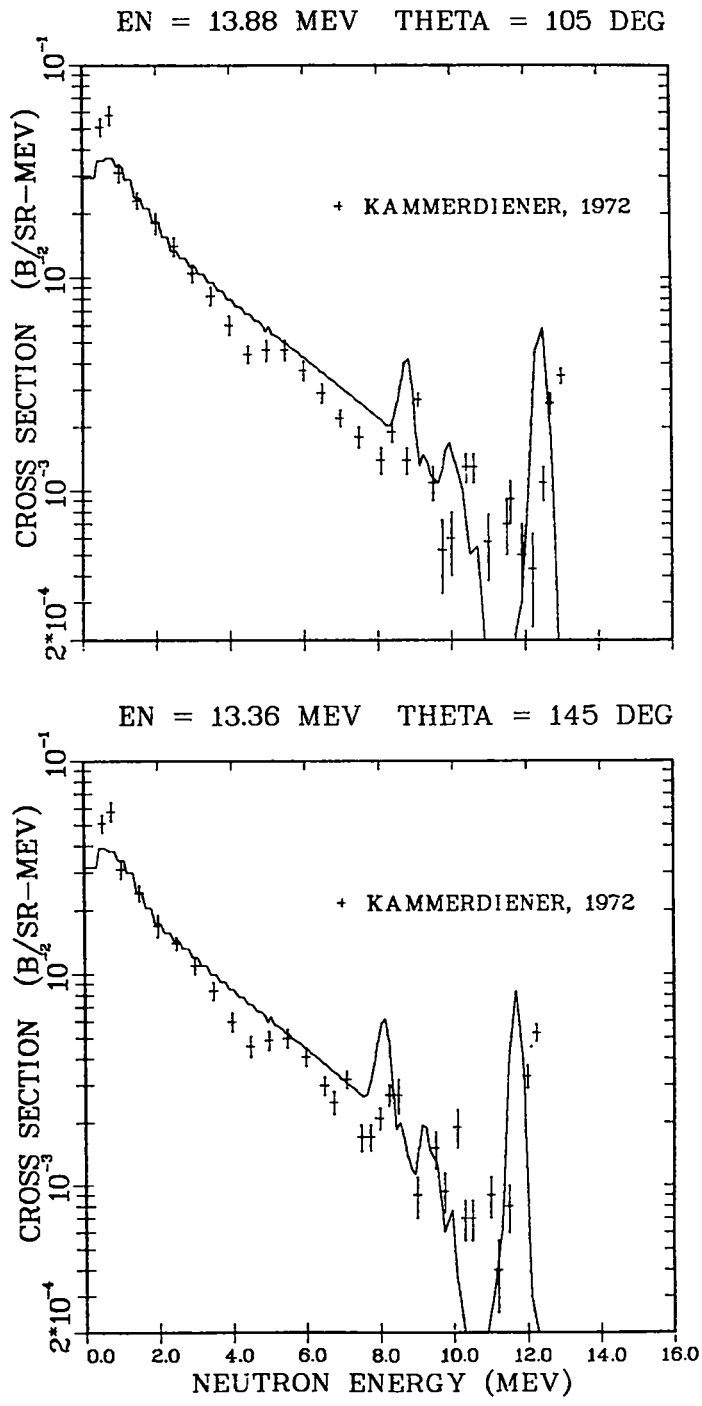


Fig. 22.
Calculated neutron emission spectra at 105 and 145 degrees compared to Kammerdiener's[75] iron measurements near 14 MeV.

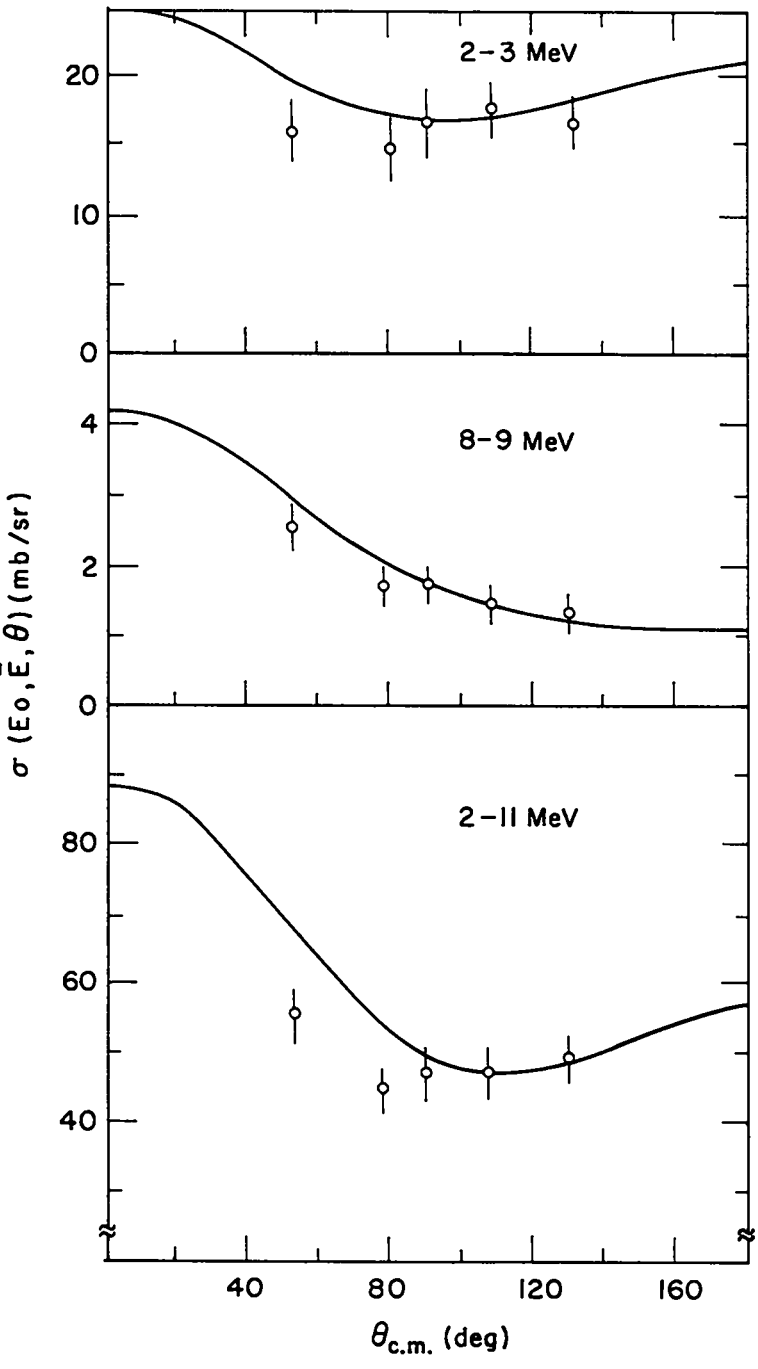


Fig. 23.
Calculated angular distributions of emission neutrons from 14.6-MeV neutron interactions with iron compared to Hermsdorf's measurements[91] for several secondary energy ranges.

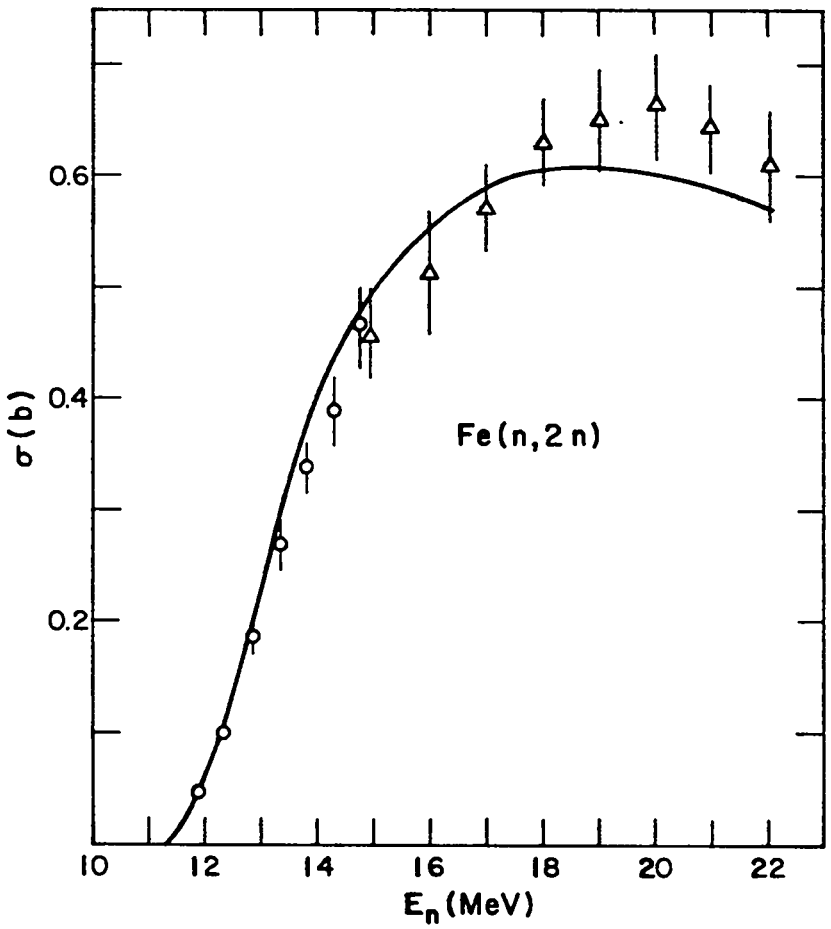


Fig. 24.
Comparison of calculated iron (n,2n) cross sections with the scintillation tank measurements of Frehaut[96] (circles) and Veeser[97] (triangles).

D. (n,p) Reactions and Proton Emission

Several data types exist involving proton emission from iron isotopes that provide opportunities to test proton transmission coefficients calculated with the parameters of Table II. Figures 26 and 27 compare calculated (n,p) cross sections for $^{54}Fe$ and $^{56}Fe$ to data[102,106,107,110-137] measured for these reactions. The $^{54}Fe(n,p)$ theoretical curve of Fig. 26 was obtained after a 4% reduction was made in the Fermi-gas level-density parameter, a, over that normally obtained from the Cook systematics.[69] However, this reduction made little difference in the calculation below 10 MeV as more than 90% of the cross section was obtained from transitions to discrete levels in $^{54}Mn$ or to the region of the continuum described by the constant temperature level-density expression. Both sets of calculations for the $^{54}Fe$ and $^{56}Fe(n,p)$ reactions

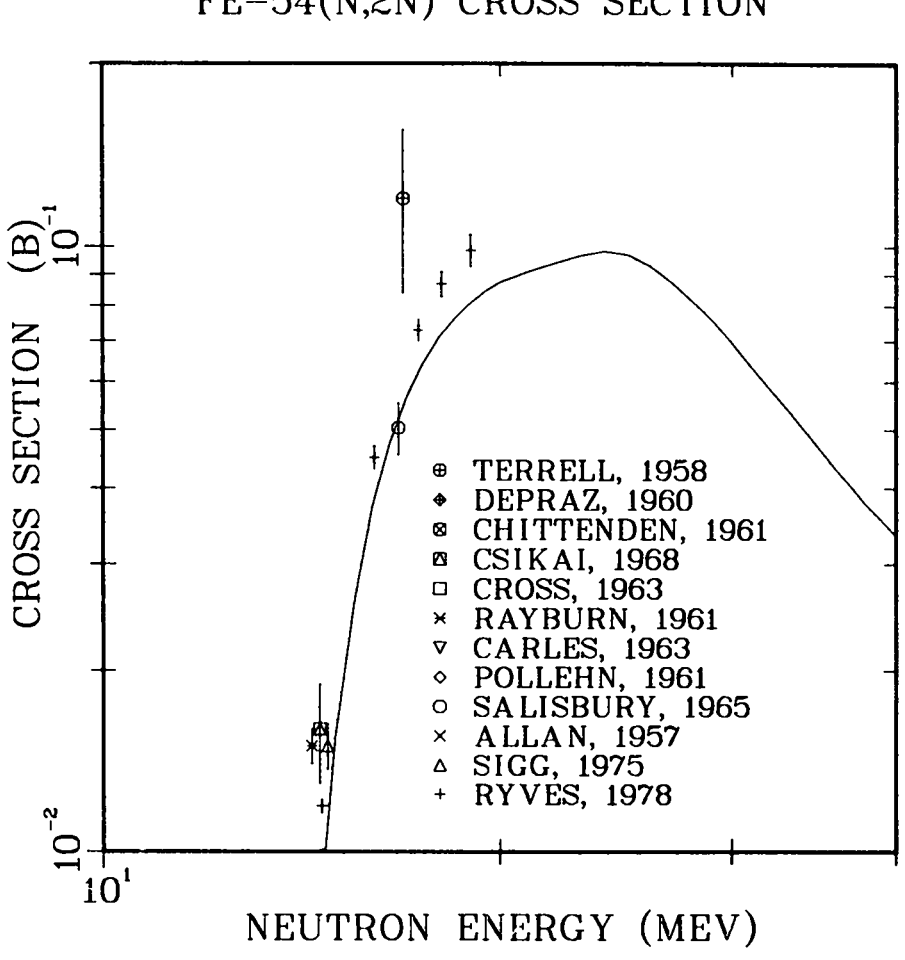


Fig. 25.
Calculated and measured $^{54}Fe(n,2n)$ cross sections.
The experimental results are from Refs. 98-109.

agree reasonably well with the data, although perhaps better agreement could be obtained if some adjustment was made in the proton optical parameters to reduce slightly the amount of lower-energy proton emission. This adjustment was not attempted because of the possible effects on the higher-energy behavior of the proton transmission coefficients, which were checked by calculations of higher energy proton reaction data (see Sec. III B).

Recently new data for the total proton-production cross section induced by 15-MeV neutrons have been obtained by measurements of the spectrum and angular distribution of the emitted protons.[138] At 15 MeV this total measured spectrum is a sum of contributions of (n,p), (n,pn), and (n,np) reactions, thus providing a further test of the behavior of proton transmission coefficients.

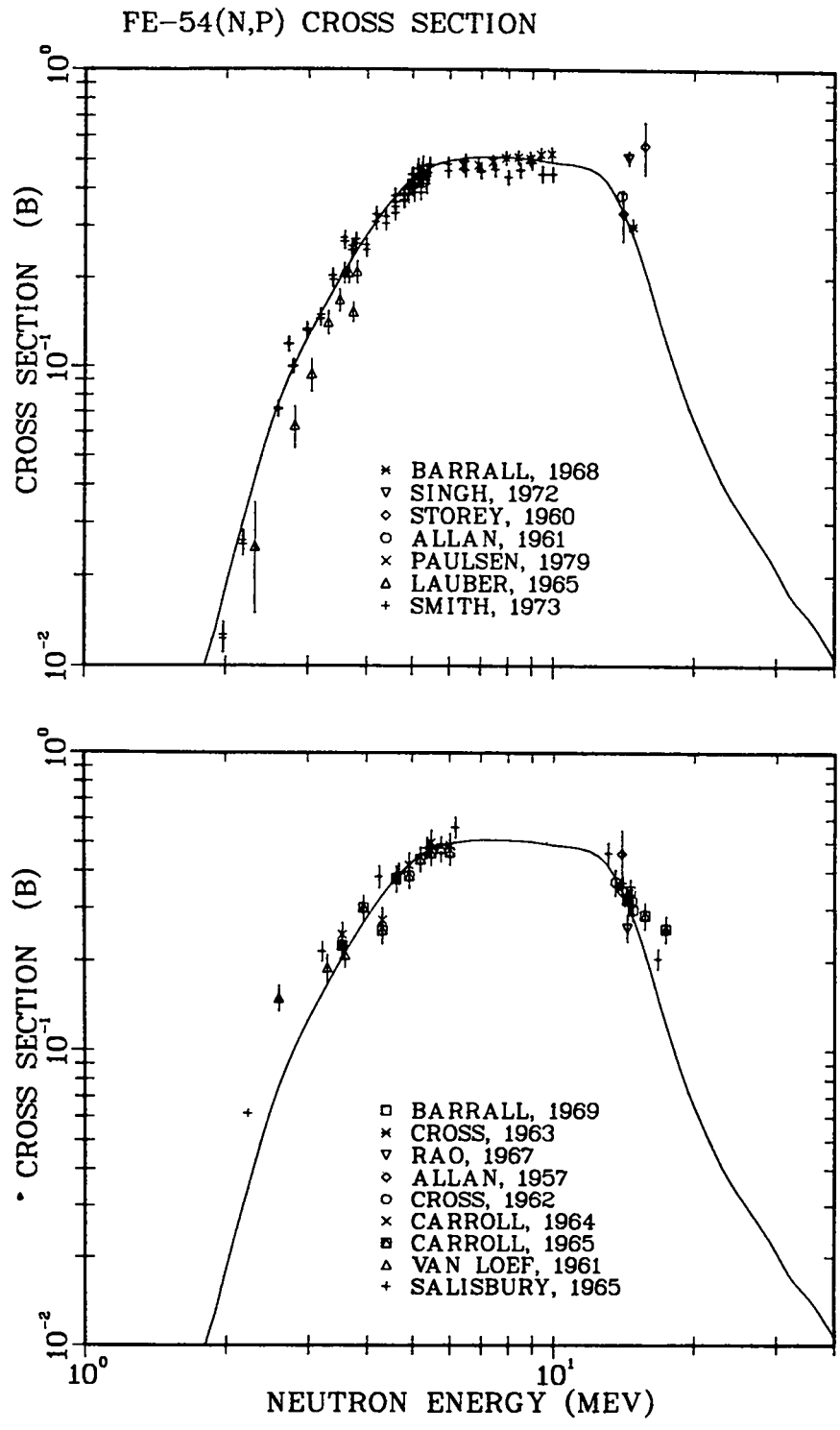


Fig. 26.
Calculated and measured $^{54}Fe(n,p)$ cross sections. The experimental data are from Refs. 102, 106, 107, 110-122.

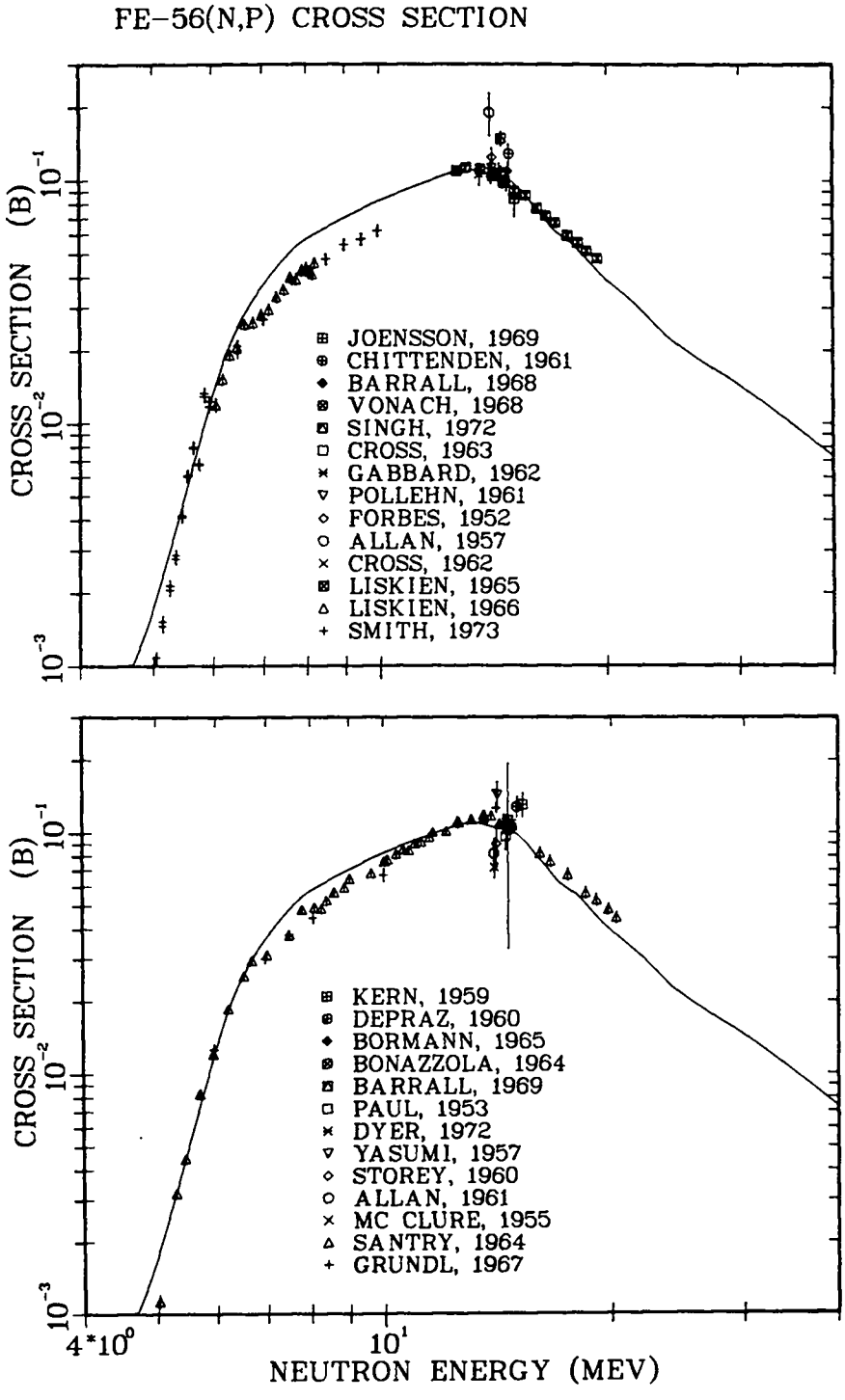


Fig. 27.
Calculated and measured $^{56}Fe(n,p)$ cross sections. The experimental results are from Refs. 99, 100, 102, 105, 107, 110-114, 117, 122-137.

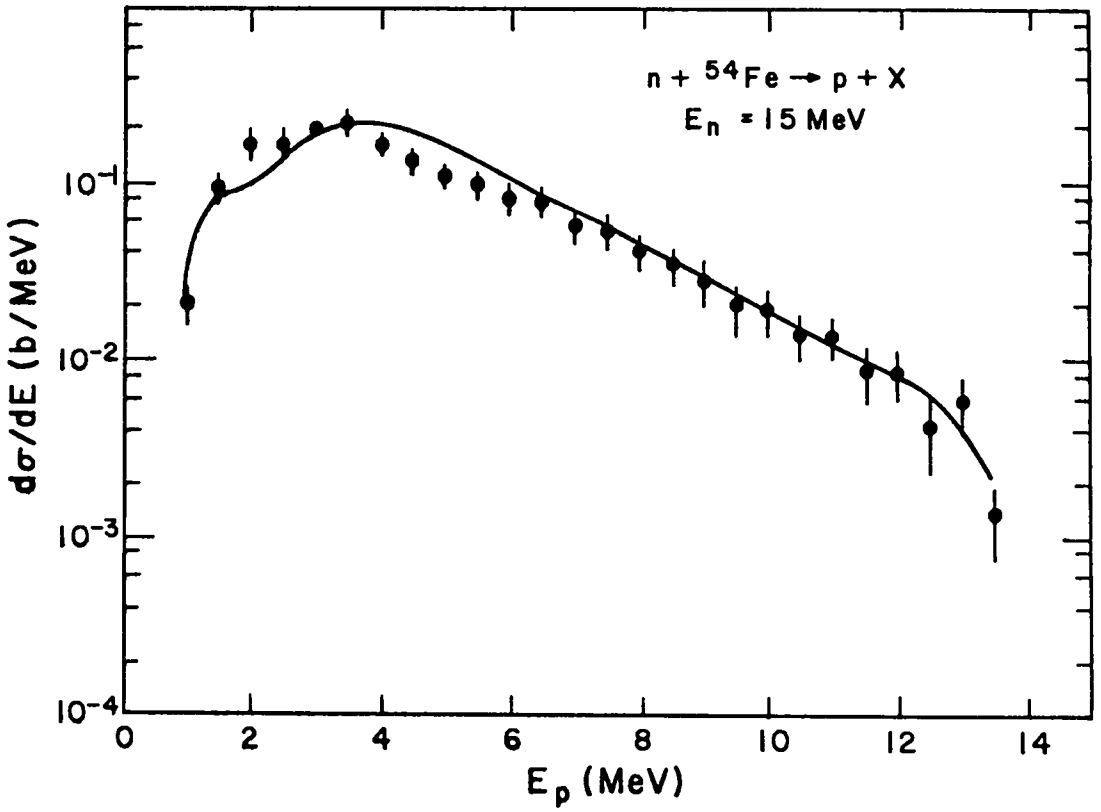


Fig. 28.
Calculated and measured[138] proton emission spectra from 15-MeV neutron interactions with $^{54}Fe$.

Effects resulting from the relative preequilibrium correction applied to the emission of protons can also be tested, since for the (n,p) and (n,pn) reactions at higher energies a large portion of these cross sections originates from the preequilibrium mechanism.

Figures 28 and 29 show the calculated proton emission spectra produced by 15-MeV neutron interactions with $^{54}Fe$ and $^{56}Fe$ along with the measurements of Grimes et al.[138] The low energy portion of the $^{56}Fe$ emission spectrum is in good agreement with the data and arises from the emission of low-energy protons from the (n,np) reaction. The agreement at the higher energy portion of the spectrum illustrates the validity of the preequilibrium corrections. For $^{54}Fe$ there is an even larger contribution from the (n,np) process; however, the large size of the (n,p) contribution to the emission spectrum prevents the occurrence of an explicit dip in either the measured or calculated spectrum.

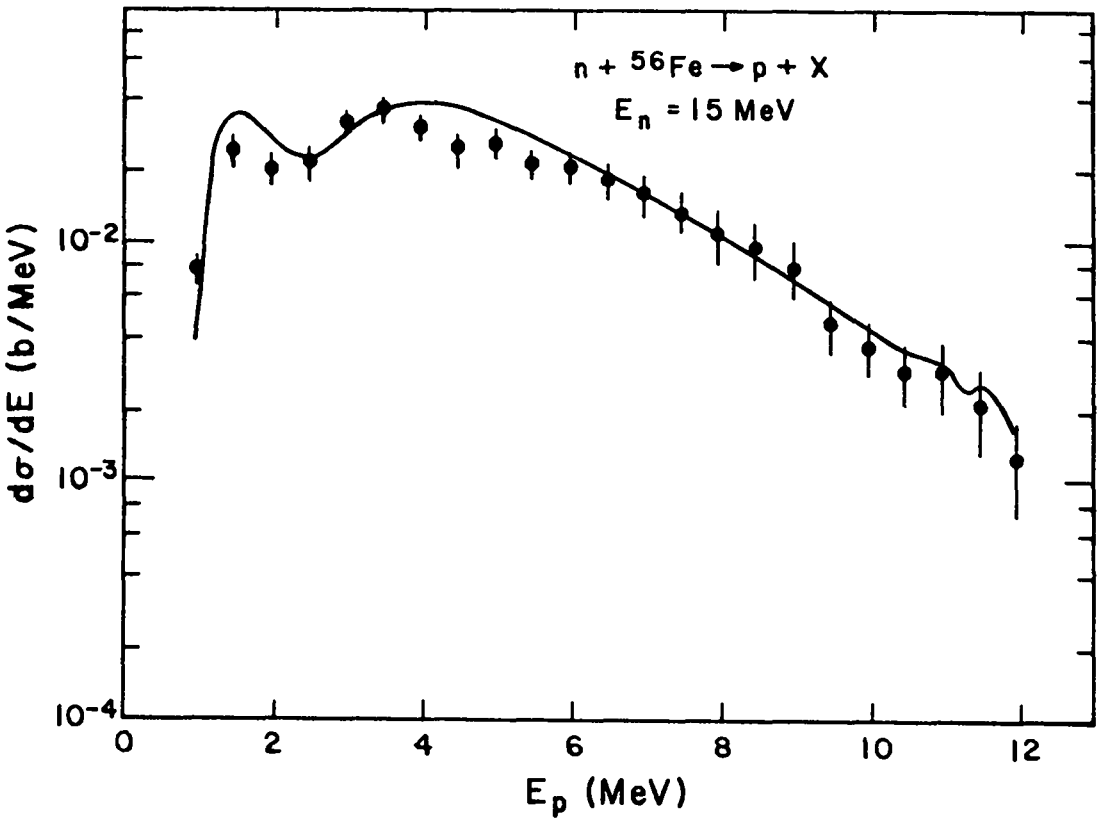


Fig. 29.
Calculated and measured[138] proton emission spectra from 15-MeV neutron interactions with $^{56}Fe$.

E. (n,α) Reactions and Alpha-Particle Emission

Alpha-production data for iron isotopes include measurements of the $^{54}Fe(n,\alpha)$ cross sections below 19 MeV, which are supplemented by recent measurements of secondary alpha-particle spectra induced by 15-MeV neutrons on $^{54}Fe$ and $^{56}Fe$. Theoretical calculations for comparison to such data present some difficulties in that there exists much less information concerning alpha-particle optical parameters needed to produce transmission coefficients applicable at lower energies. Furthermore, the mechanism for (n,α) reactions at higher energies seems not to be well described by either the statistical or preequilibrium models unless, for the latter case, assumptions are made concerning alpha-preformation constants or phenomenological descriptions of other reaction mechanisms are included. For these calculations we used, in addition to the Hauser-Feshbach and preequilibrium models, empirical expressions developed by Kalbach[70] to describe pickup and knockout contributions to the (n,α) cross

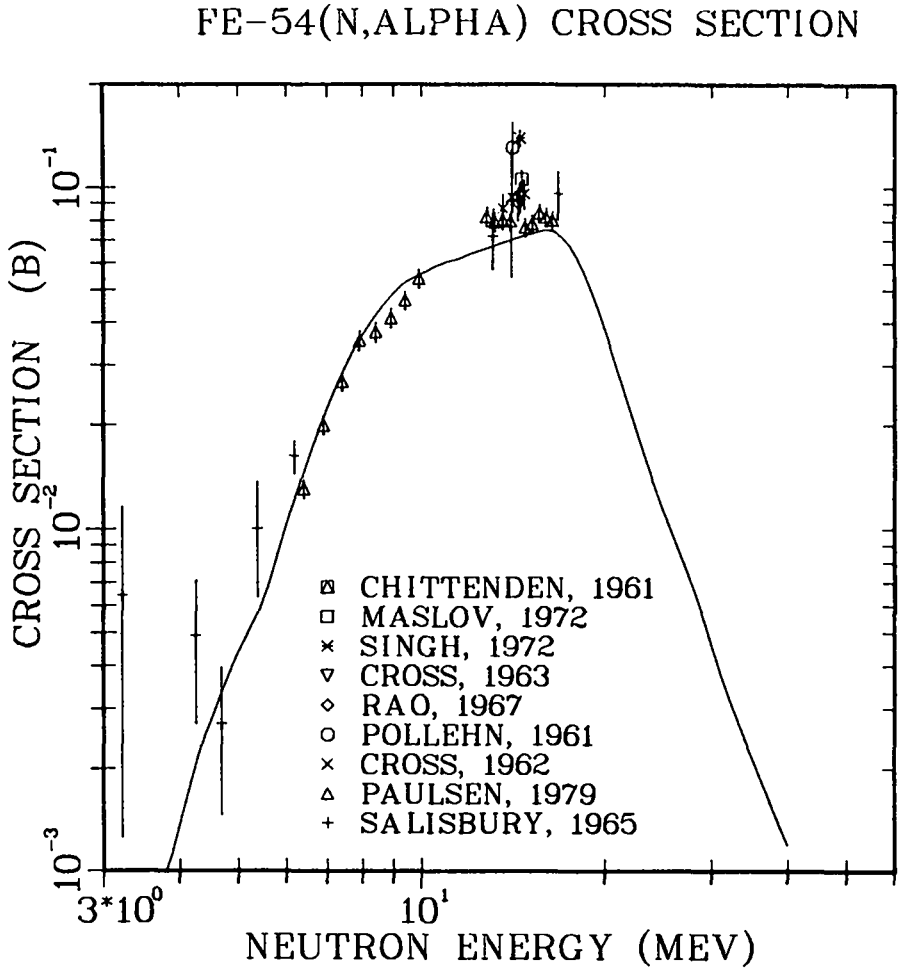


Fig. 30.
Calculated and measured $^{54}Fe(n,\alpha)$ cross sections from 3-40 MeV. Experimental results are from Refs. 100, 102, 105, 106, 112, 115, 118, 122, and 139.

section. These expressions were generally developed from higher-energy reaction data, and the present calculations provide a further opportunity to examine their applicability by comparison to neutron experimental data at lower incident energies.

Figure 30 compares the calculated $^{54}Fe(n,\alpha)$ cross section to data available between 1 and 19 MeV.[100,102,105,106,112,115,118,122,139] The sparsity of the data makes definite conclusions difficult concerning the models or parameters used in the calculations. The calculated results are lower than some of the data at 14-15 MeV but the total alpha-production cross section (75 mb) is in good agreement with the value of 79 $\pm$ 13 mb determined by integration of the

spectrum measured by Grimes et al.[138] Our results are compared to Grimes' measured alpha-emmission spectra from 15-MeV neutron bombardment of $^{54}Fe$ and $^{56}Fe$ in Figs. 31 and 32. In both cases the higher energy parts of the calculated spectra agree reasonably with the data, indicating the applicability of the pickup and knockout corrections applied. The disagreement at the lower energy portion of each spectrum [(n,nα) contributions)] probably indicates the alpha-particle optical parameters are not completely suited to produce low-energy transmission coefficients.

Since total charged-particle production cross sections are of interest to radiation damage calculations, theoretical curves for proton and alpha-particle production up to 40 MeV for $^{54}Fe$ and $^{56}Fe$ are shown in Fig. 33 along with available experimental data (see Refs. for Figs. 26-32). The arrows in Fig. 33 indicate thresholds for (n,pxn) and (n,αxn) reactions.

## F. Gamma-Ray Production

Gamma-ray production spectra have been measured on natural iron for neutron energies between 1 and 20 MeV using both continuous and discrete energy neutron sources. Comparisons to such measurements allow us to test the general consistency of theoretical calculations since the data provide information pertaining to all reactions having significant cross sections at a given neutron energy. These data are further supplemented by cross-section information for the production of discrete gamma-ray lines. These data often represent some of the main information available at higher energies through which nuclear model calculations can be verified.

Figures 34 through 40 compare calculated spectra to measurements of Chapman et al.[140] between 3.5 and 9.5 MeV. Good agreement exists except for portions of some calculated spectra that contain small contributions of discrete lines not seen in the data and parts of the continuum calculation between 5 and 8 MeV. The former problem results most likely from incorrect assignments in the gamma-ray branching information used in the calculation. The main discrete gamma-ray lines appearing in these spectra result from the 0.846- and 1.238-MeV gamma-rays produced from inelastic scattering on $^{56}Fe$. Measured excitation functions[141-153] for these 2 lines are compared to our theoretical results in Figs. 41 and 42. This comparison confirms not only the theoretical calculation of gamma-ray cascades populating low-lying levels in $^{56}Fe$ but also their population from compound nucleus and direct-reaction processes.

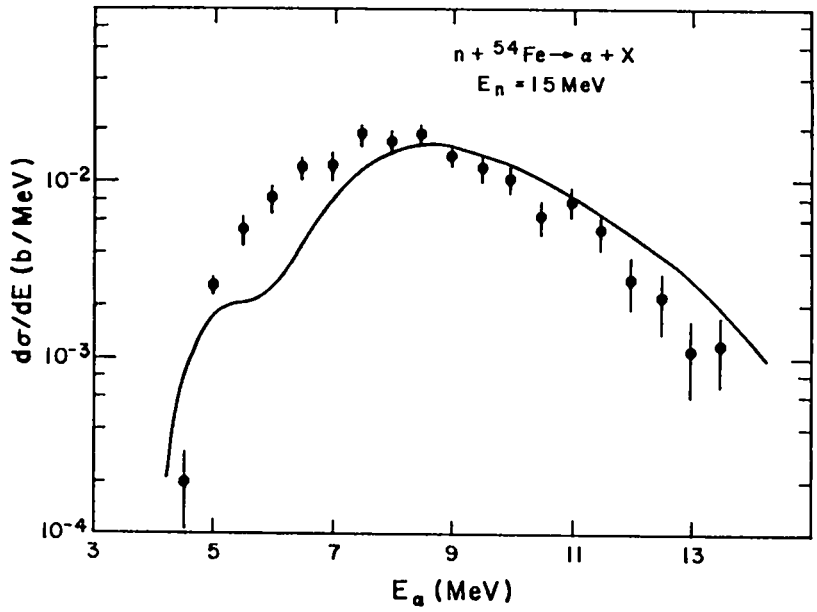


Fig. 31.
Calculated and measured[138] alpha emission spectra from 15-MeV neutron interactions with $^{54}Fe$.

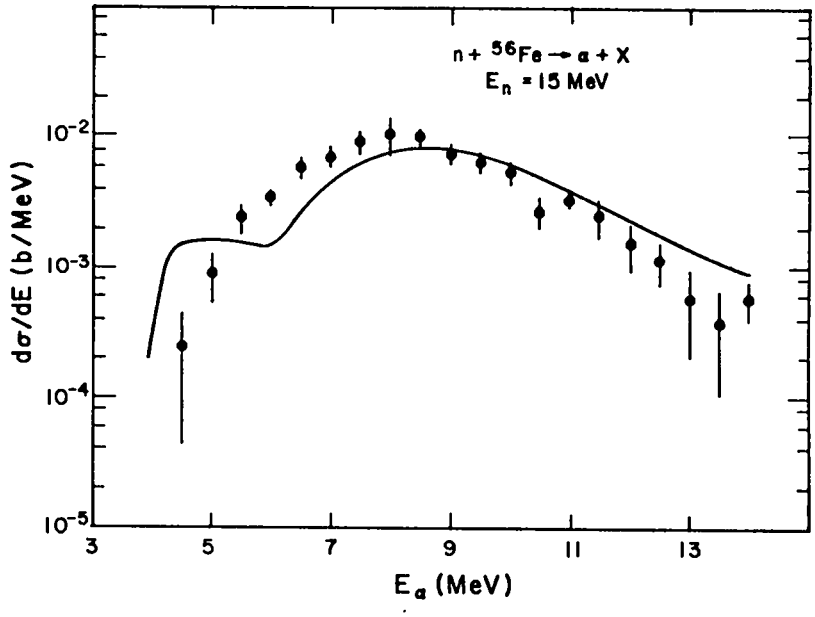


Fig. 32.
Calculated and measured[138] alpha emission spectra from 15-MeV neutron interactions with $^{56}Fe$.

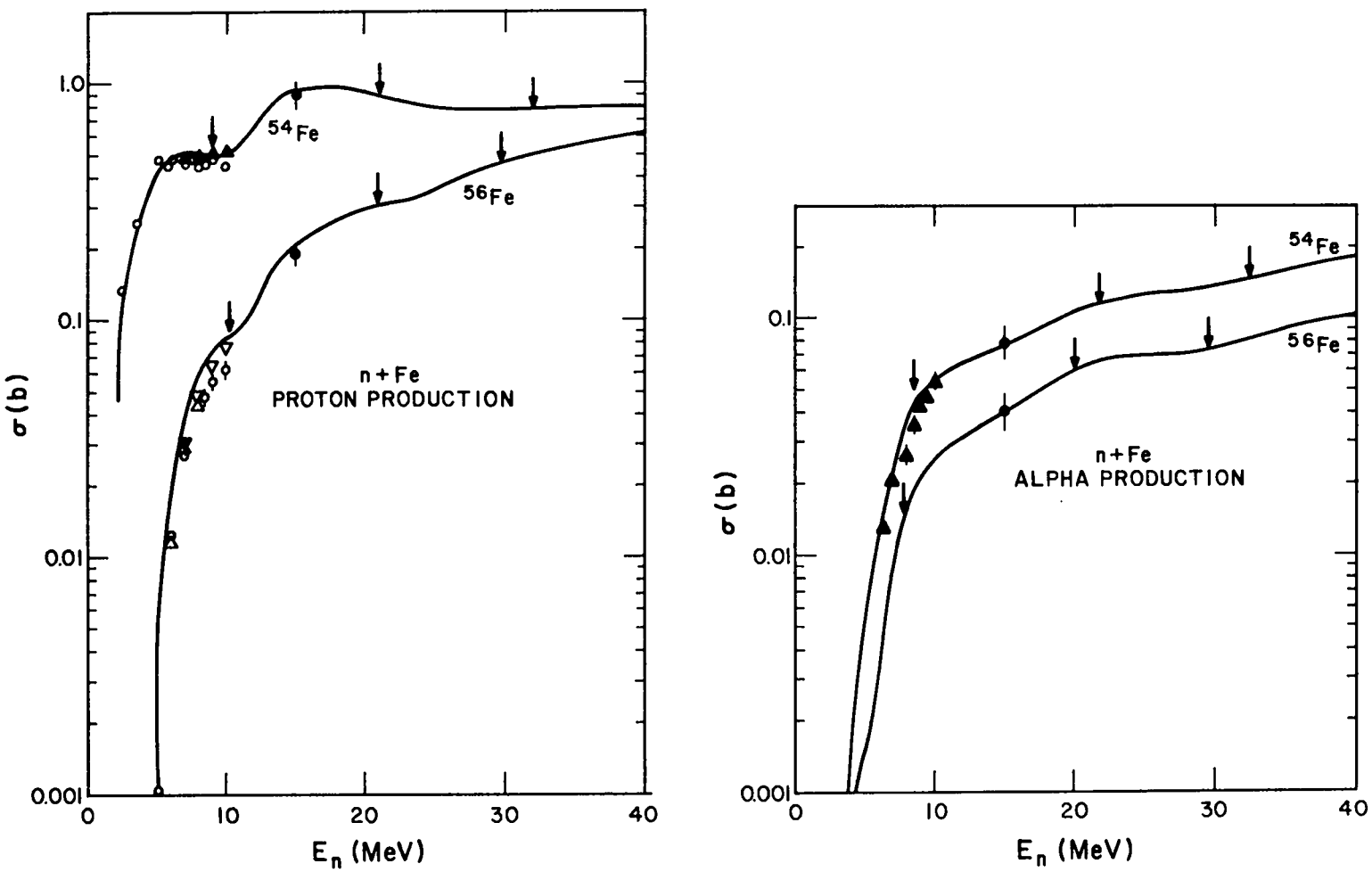


Fig. 33.
Proton and alpha production cross sections from $^{54}Fe$ and $^{56}Fe$.
See captions to Figs. 26-32 for experimental data references.
The arrows indicate thresholds for (n,pxn) and (n,αxn) reactions.

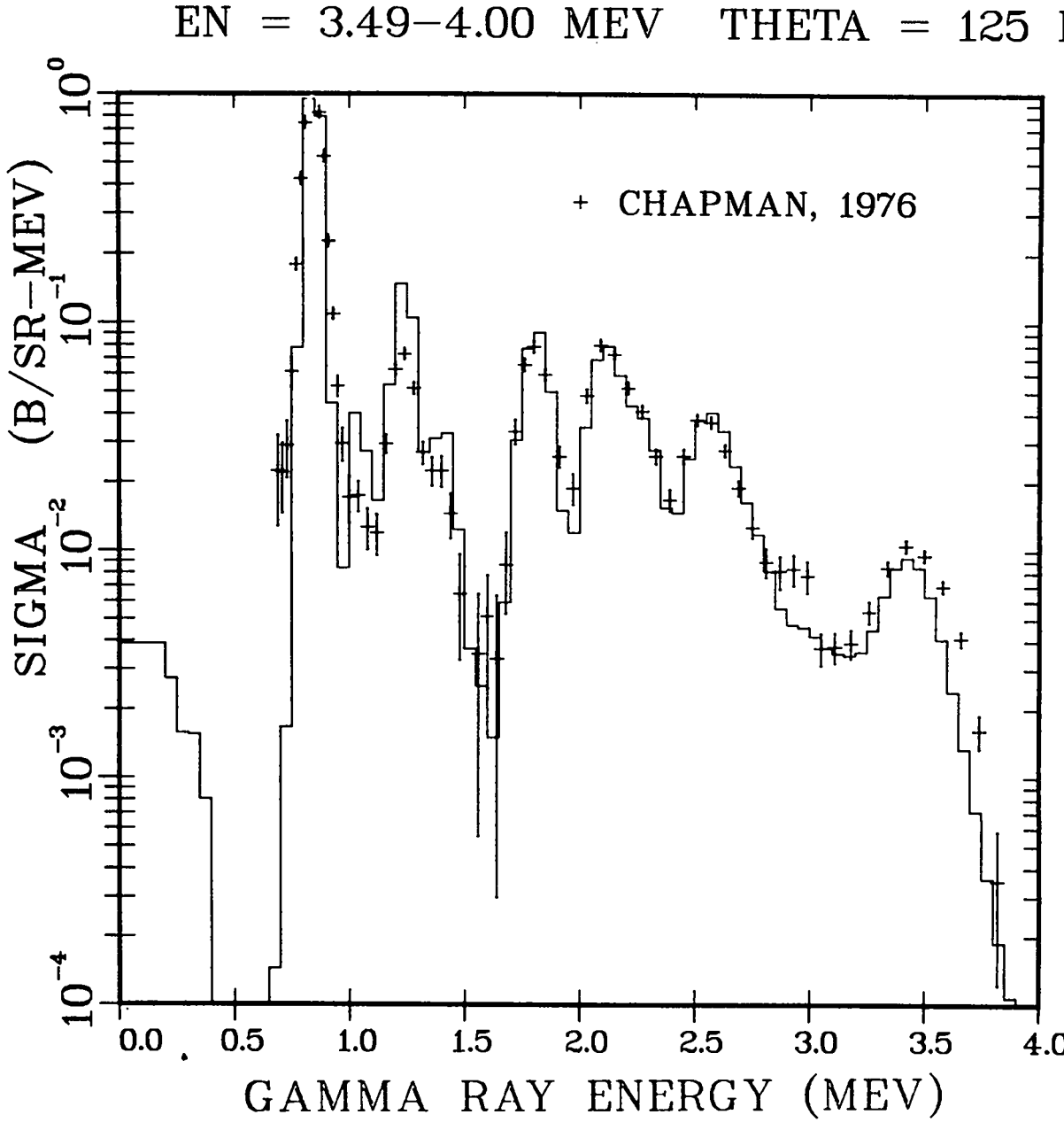


Fig. 34.
Calculated and measured $^{140}$ gamma-ray emission spectra from iron at 125 degrees for incident neutrons between 3.49 and 4.00 MeV.

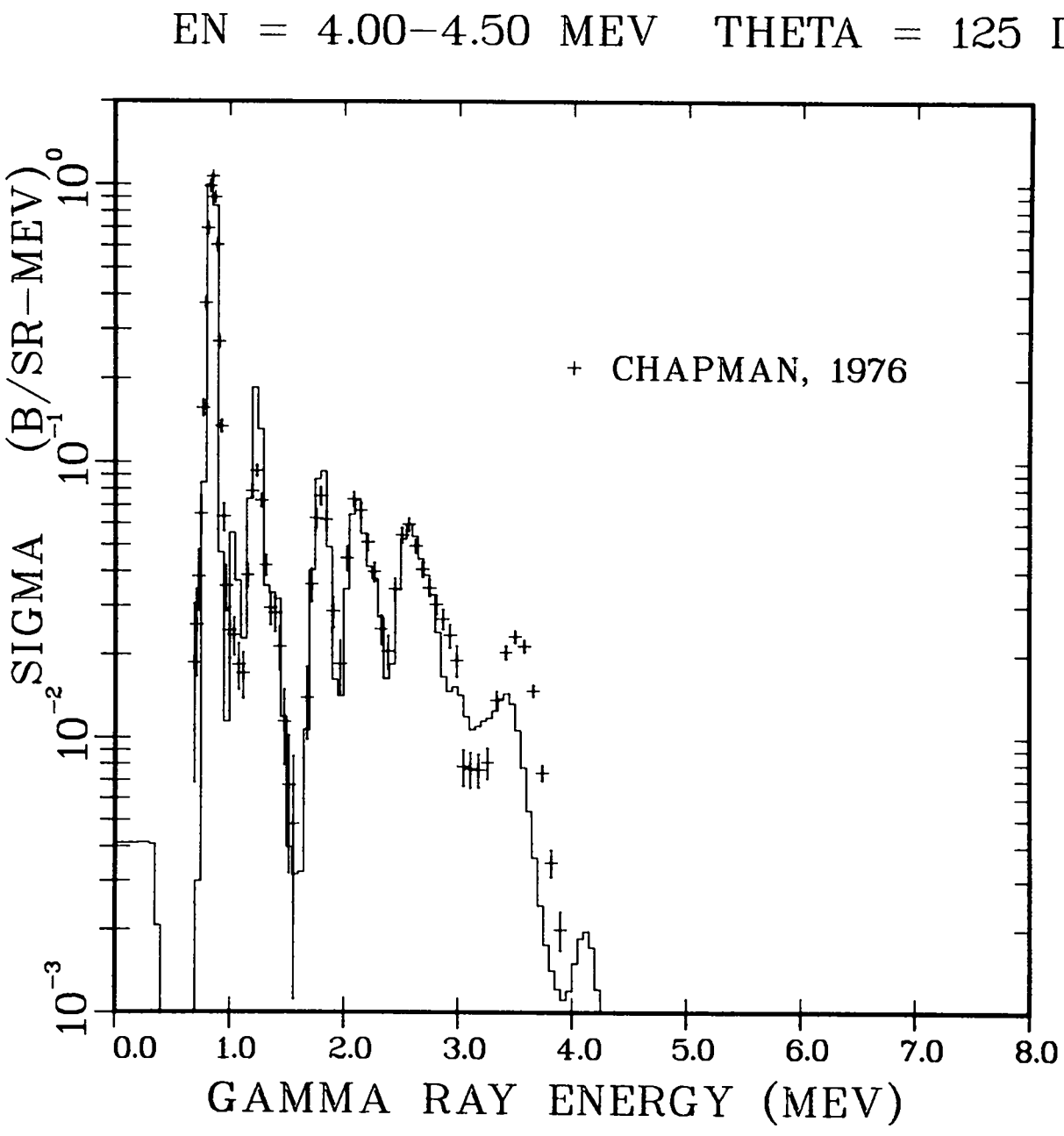


Fig. 35.
Calculated and measured[140] gamma-ray emission spectra from iron at 125 degrees for incident neutrons between 4.00 and 4.50 MeV.

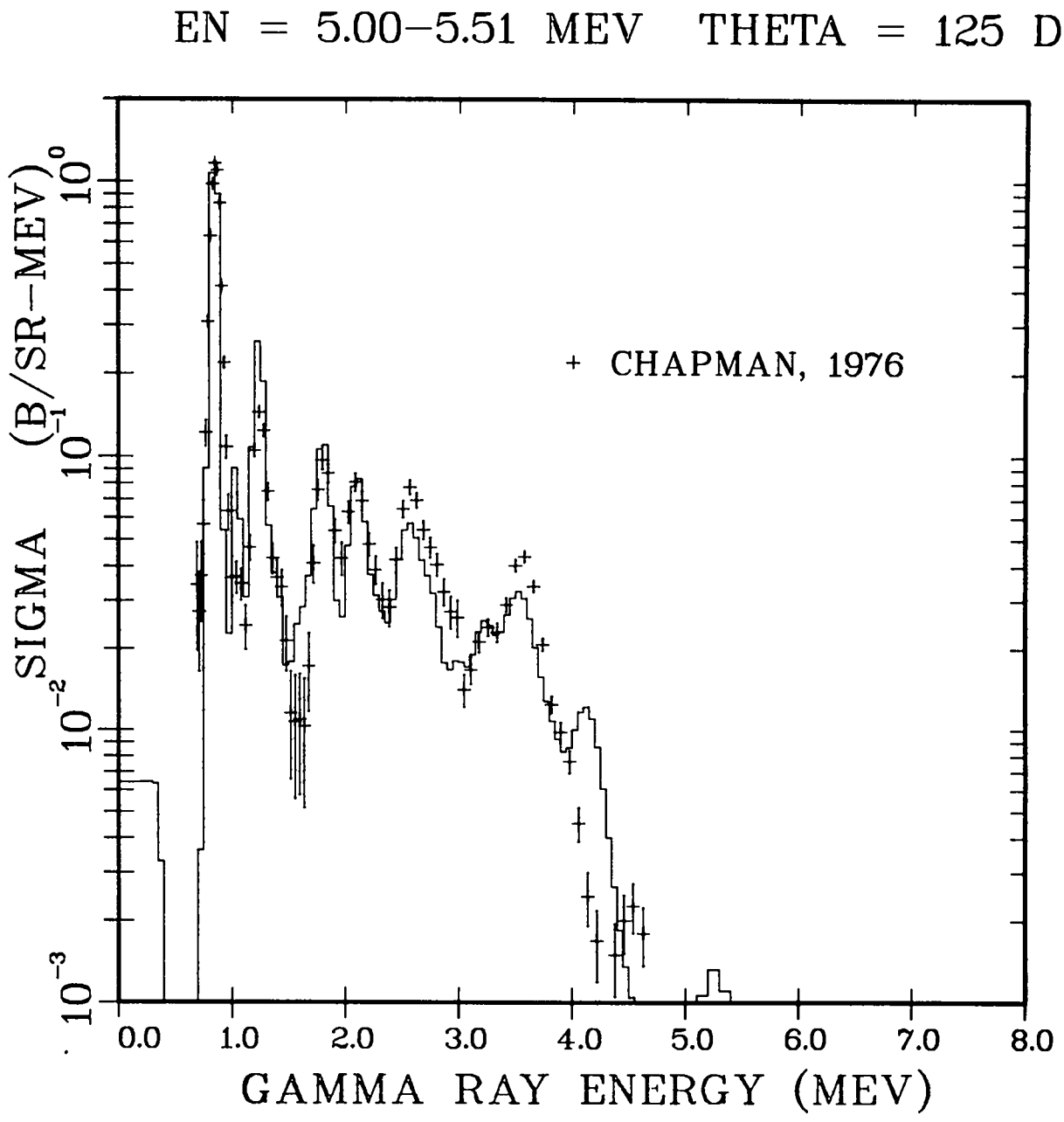


Fig. 36.
Calculated and measured[140] gamma-ray emission spectra from iron at 125 degrees for incident neutrons between 5.00 and 5.51 MeV.

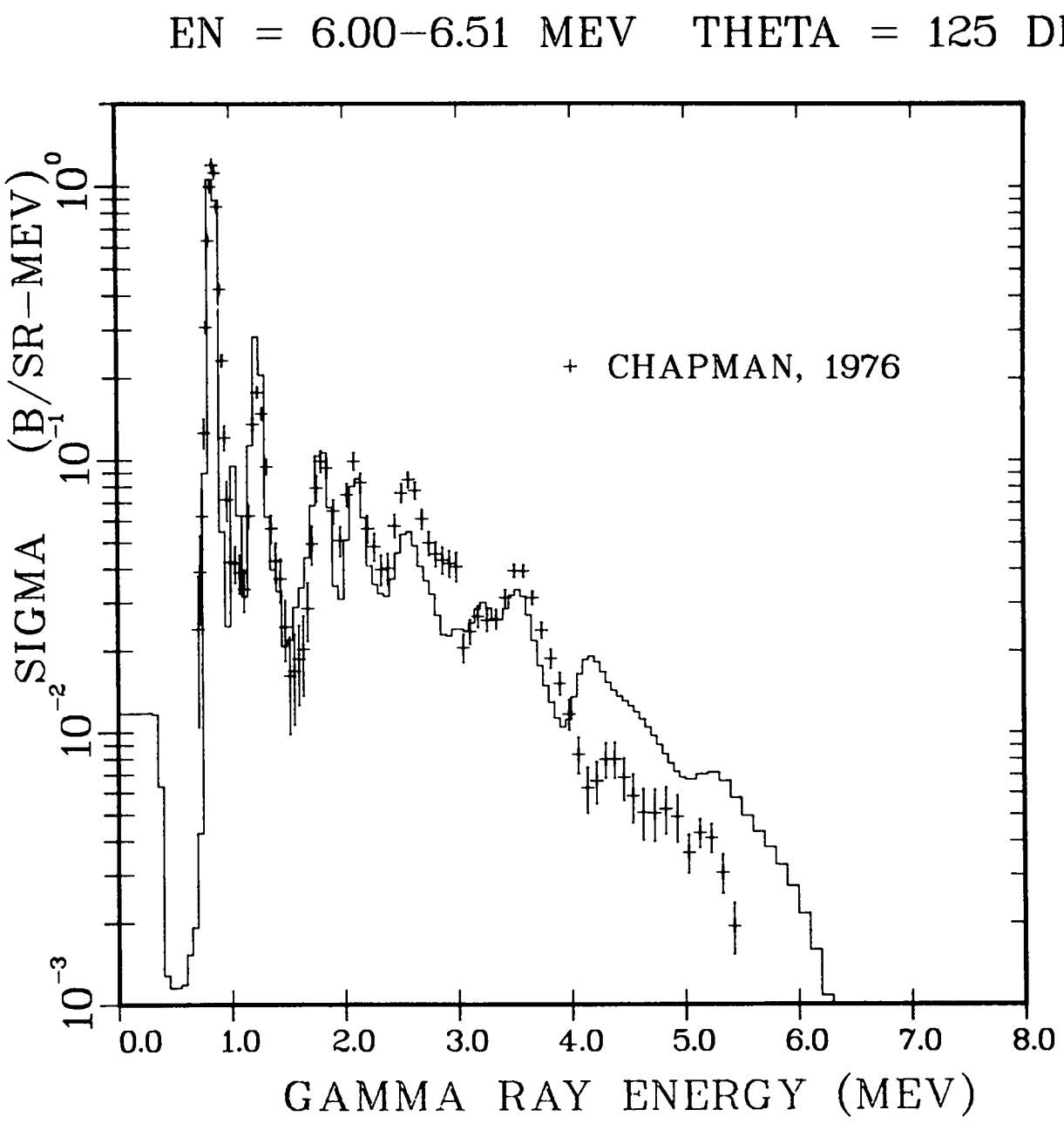


Fig. 37.
Calculated and measured $^{140}$ gamma-ray emission spectra from iron at 125 degrees for incident neutrons between 6.00 and 6.51 MeV.

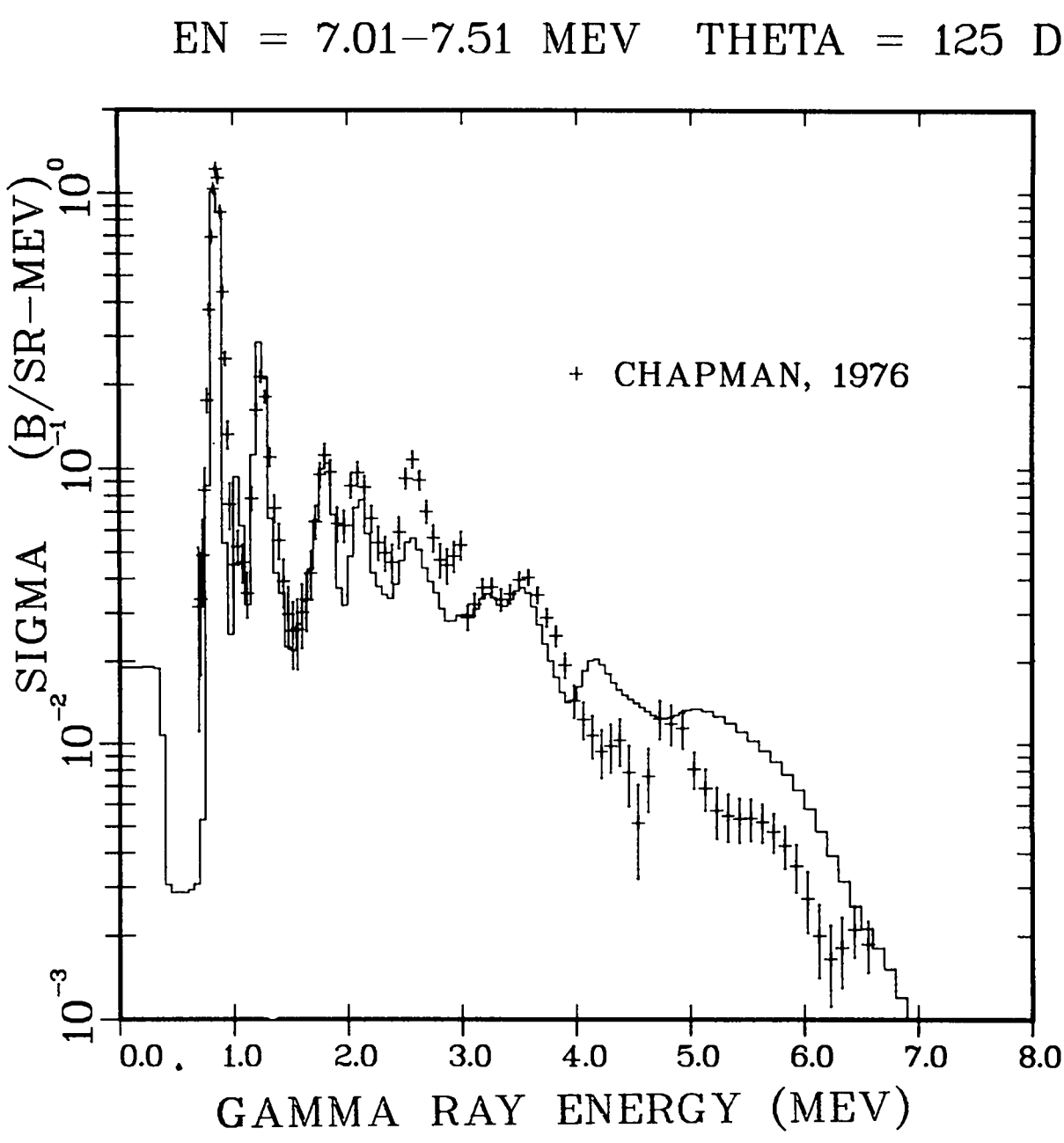


Fig. 38.
Calculated and measured[140] gamma-ray emission spectra from iron at 125 degrees for incident neutrons between 7.01 and 7.51 MeV.

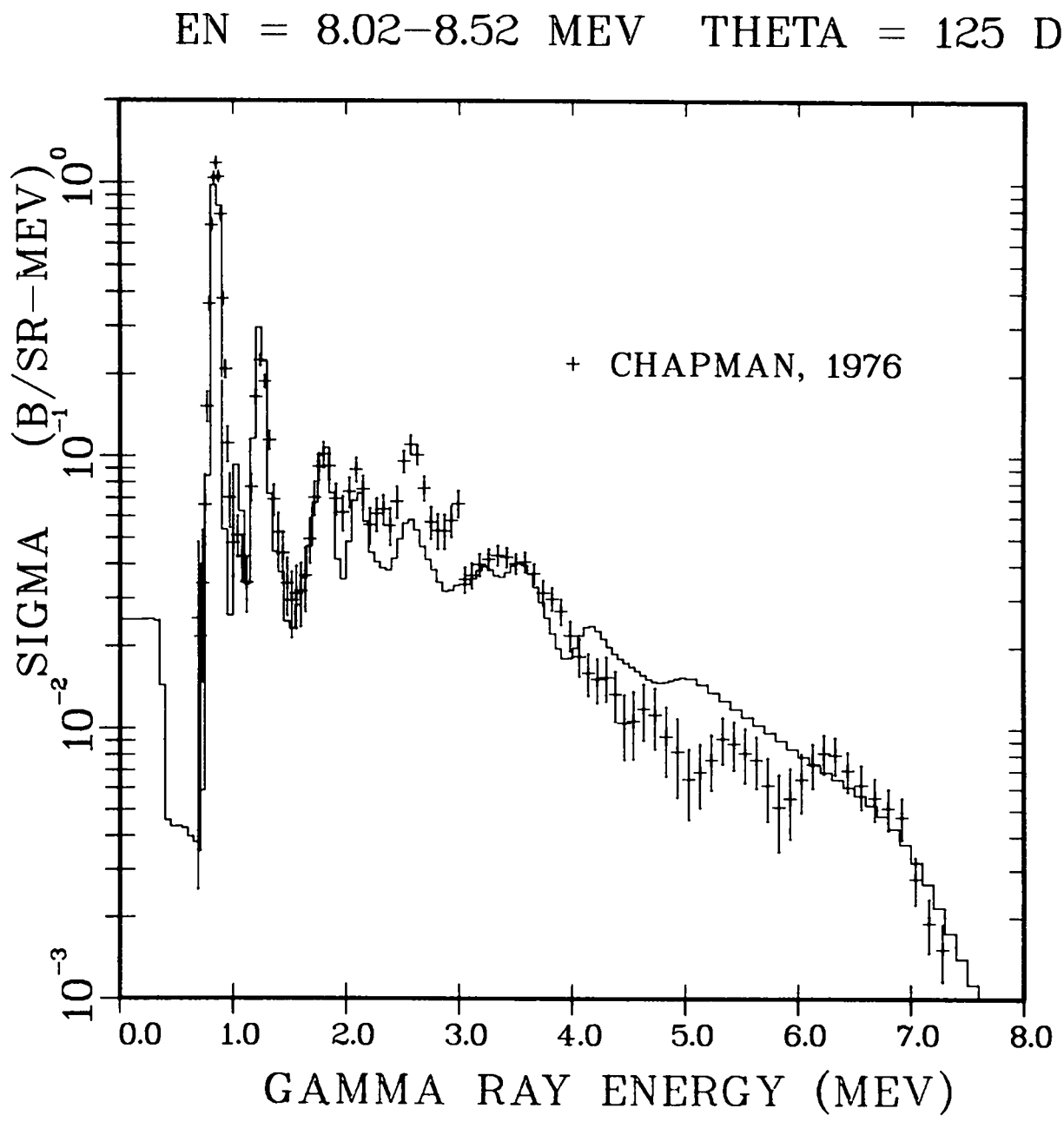


Fig. 39.
Calculated and measured[140] gamma-ray emission spectra from iron at 125 degrees for incident neutrons between 8.02 and 8.52 MeV.

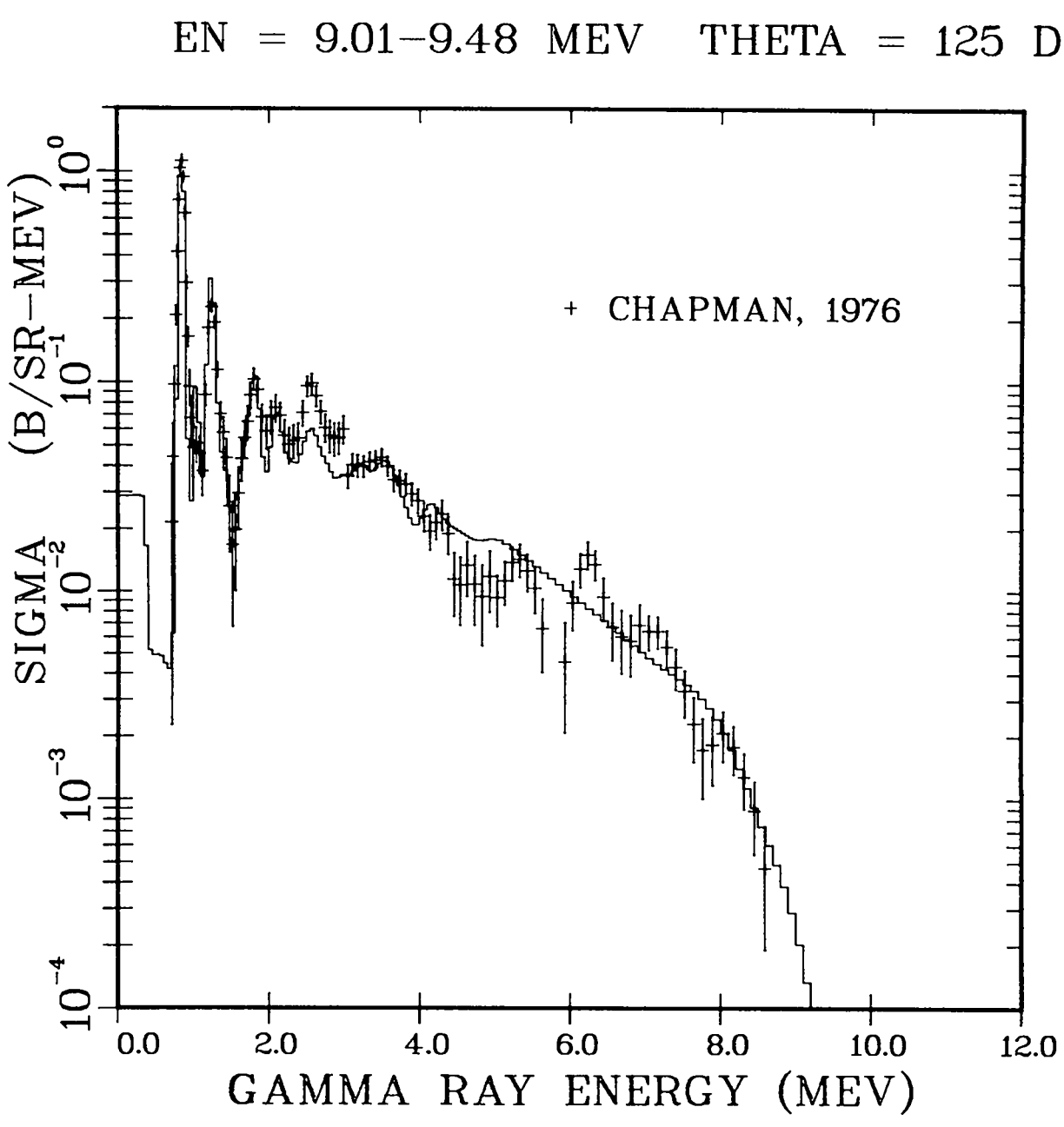


Fig. 40.
Calculated and measured[140] gamma-ray emission spectra from iron at 125 degrees for incident neutrons between 9.01 and 9.48 MeV.

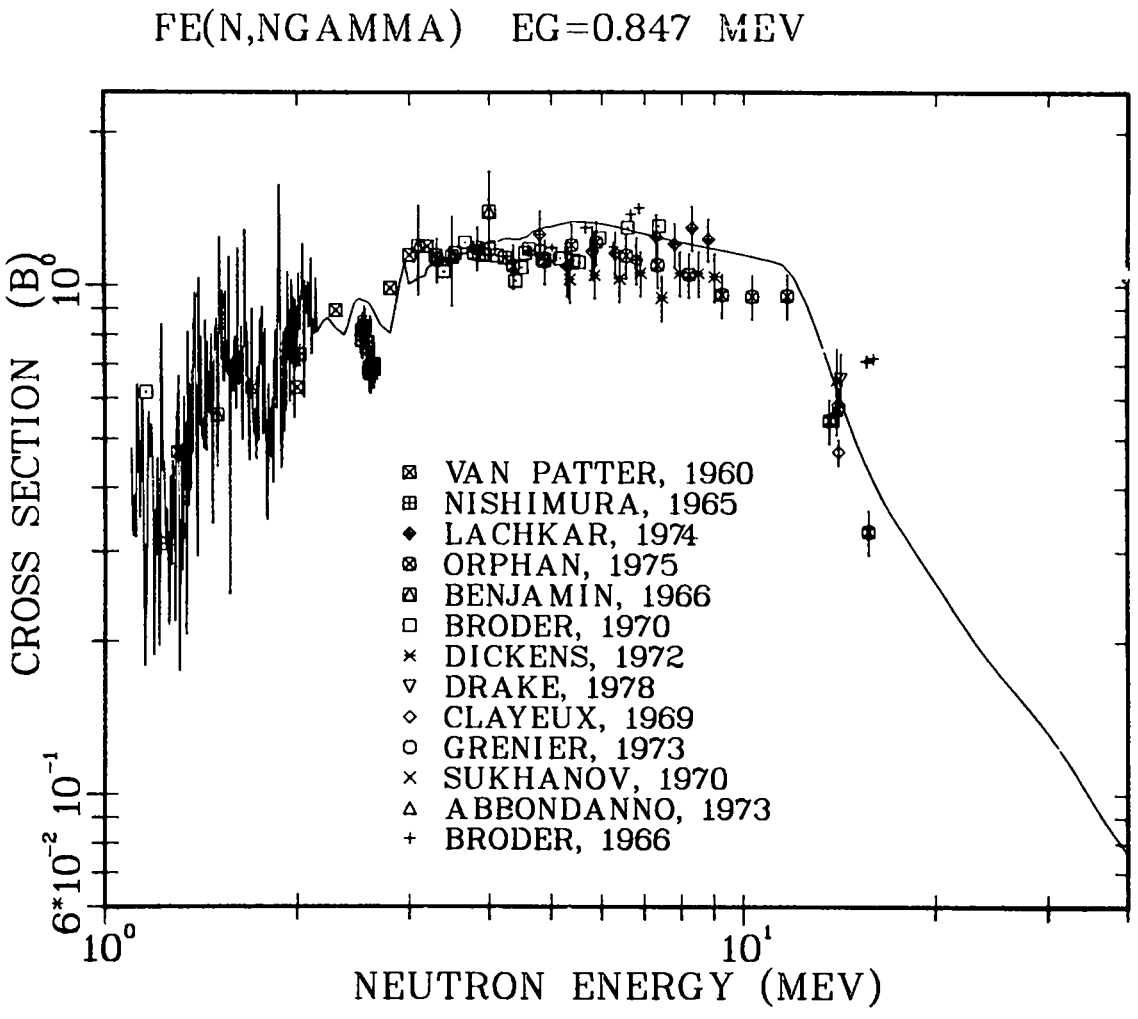


Fig. 41.
Calculated (above 3 MeV) and measured excitation functions for production of the 0.847-MeV gamma ray from iron. The experimental data are from Refs. 141-153.

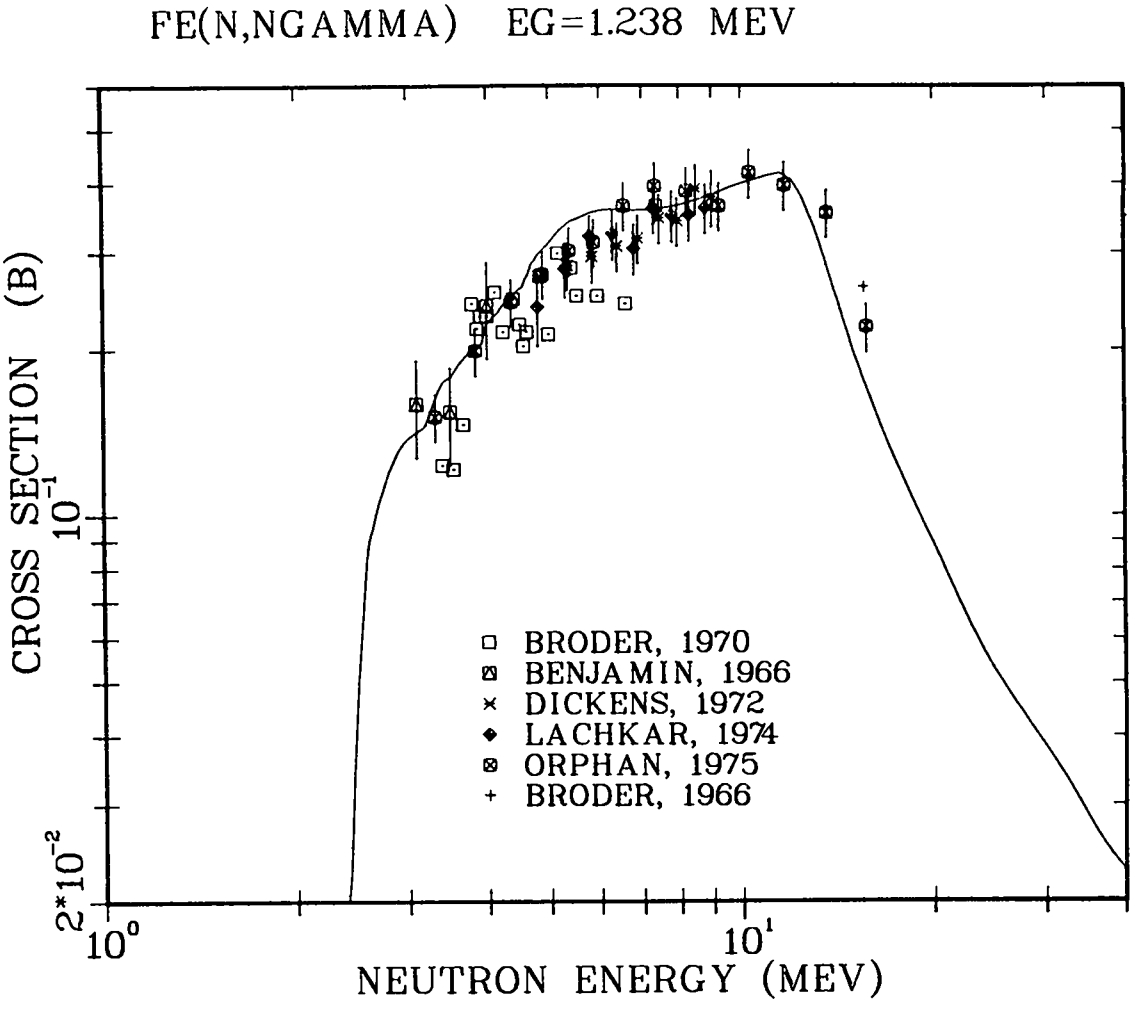


Fig. 42.
Calculated and measured excitation functions for production of the 1.238-MeV gamma ray from iron. The experimental data are from Refs. 143-147, 153.

Further comparisons to the measured spectra of Chapman[140] for neutron energies between 10 and 20 MeV appear in Figs. 43 through 49. Between 13 and 17 MeV there is a general deviation between our calculation and these data, which is somewhat surprising since the theoretical calculations of cross sections and secondary particle spectra around 14 MeV agreed well with several independent data sets. Furthermore, nuclear model calculations by Fu performed for ENDF/B-IV show similar departure in this energy range. Our results are in much better agreement with 14-MeV measurements made by Drake et al.[148] as shown in Fig. 50.

Between 17 and 20 MeV (Fig. 49), the calculations again agree generally well with the data of Chapman et al. The apparent underprediction of the discrete lines lying around 1-1.5 MeV in the theoretical gamma-ray spectrum results from use of spectrum bins to calculate (n,2nγ) contributions (dominant for these secondary energies), which were much larger than the width of the bins used to report the experimental results. The 0.846- and 1.238-MeV gamma-ray lines as well as others from inelastic scattering were not affected by such a problem since in the evaluation their production cross sections are given separately (see Sec. IV E).

Production cross sections have been measured[144,154] for the 0.931-MeV gamma-ray produced in the $^{56}$Fe(n,2nγ) reaction and are compared to our results in Fig. 51. The lower energy portion of the data of Corcalciuc et al.[154] (circles) appear to be in error since they exhibit a threshold shape in an incident energy region somewhat removed from the threshold for the (n,2nγ) reaction. Our results do agree well with the data of Orphan et al.[144] (squares) and with the higher energy portion of the Corcalciuc results.

## G. Comparison of Higher Energy Proton Cross Section Data

Since neutron reaction data are often sparse above neutron energies of 20 MeV, we compared calculated results for p + $^{56}$Fe reactions to experimental data available up to incident proton energies of 40 MeV. Two checks were made from (p,p') angular distribution measurements. Angular distributions measured for levels excited by proton inelastic scattering were analyzed using DWBA calculations and the proton optical parameters of Table II to test the applicability of these parameters at higher proton energies. Additionally, by making the assumption that the excitation of the collective levels in iron would be similar for inelastic neutron or proton scattering at higher energies, we checked the

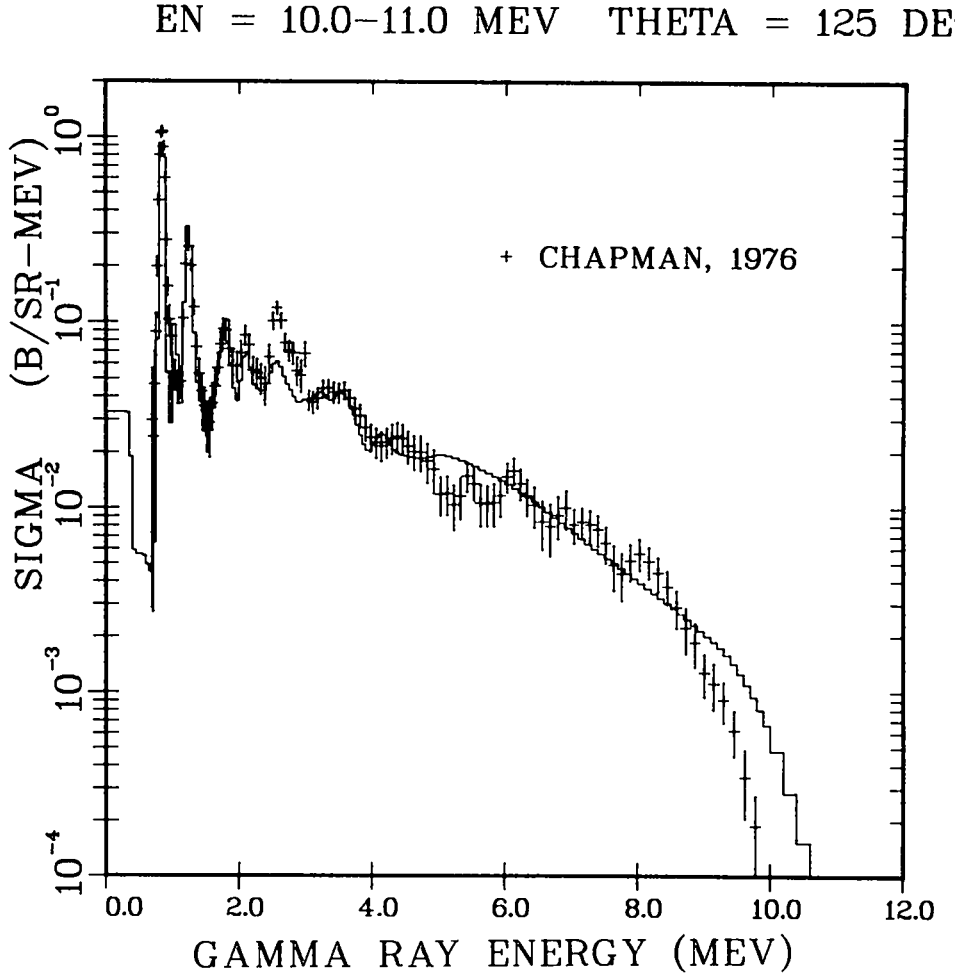


Fig. 43.
Calculated and measured[140] gamma-ray emission spectra from iron at 125 degrees for incident neutrons between 10 and 11 MeV.

angular distribution predictions from our DWBA calculation, which employed the neutron optical parameters of Table I.

Further tests were made through calculations of $^{56}Fe(p,xn)$ reactions using the GNASH code. Although the compound nuclei involved in the reaction chain for p + $^{56}Fe$ reactions are different from those for n + $^{56}Fe$ reactions, comparison to such proton data does provide additional checks on proton and neutron transmission coefficients, level-density parameters, and preequilibrium corrections. The agreement shown in Fig. 52 for calculated and measured[55,155] (p,n) and (p,2n) cross sections provides further confidence in the use of the parameters described in Sec. II at higher neutron energies.

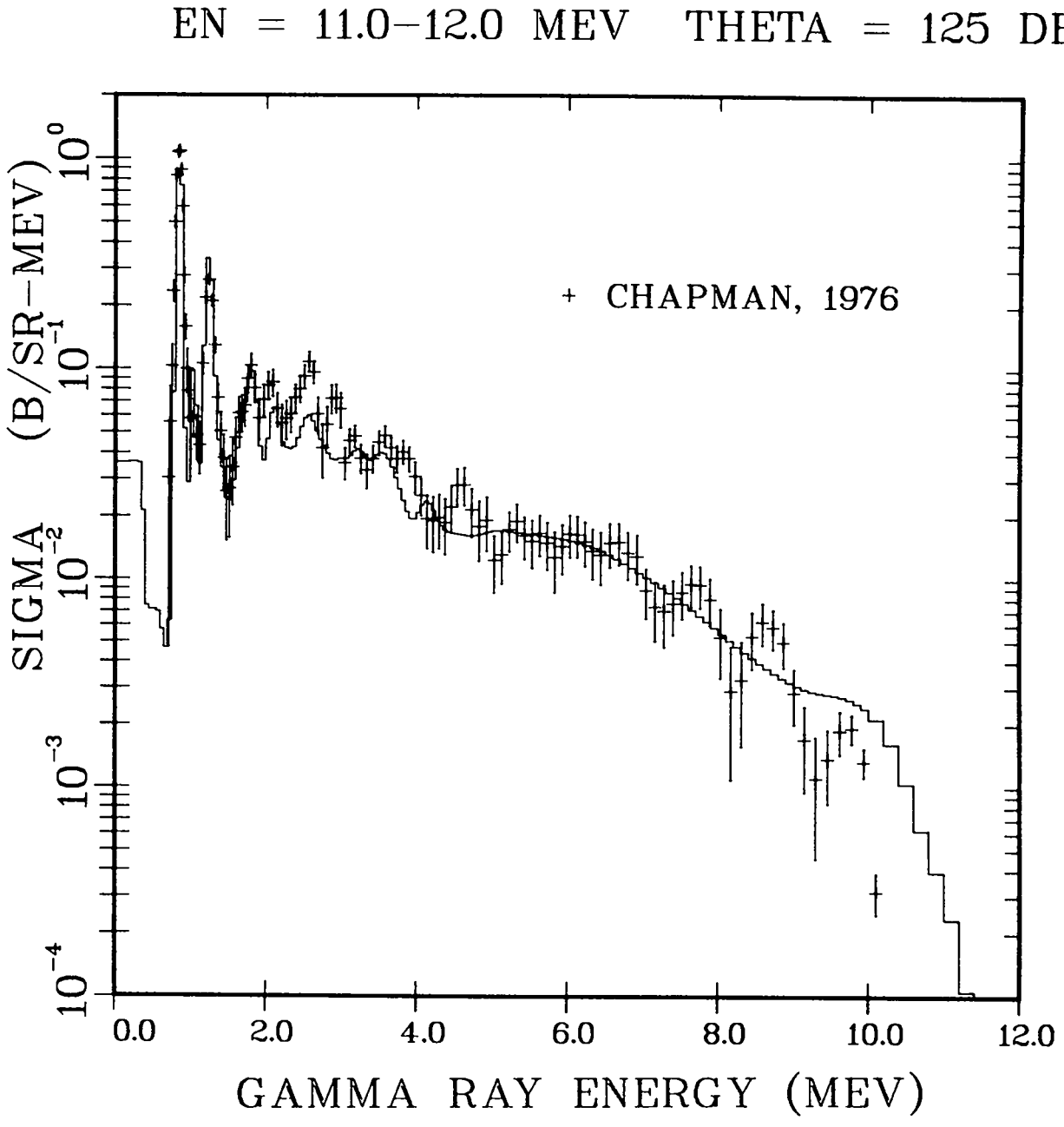


Fig. 44.
Calculated and measured[140] gamma-ray emission spectra from iron at 125 degrees for incident neutrons between 11 and 12 MeV.

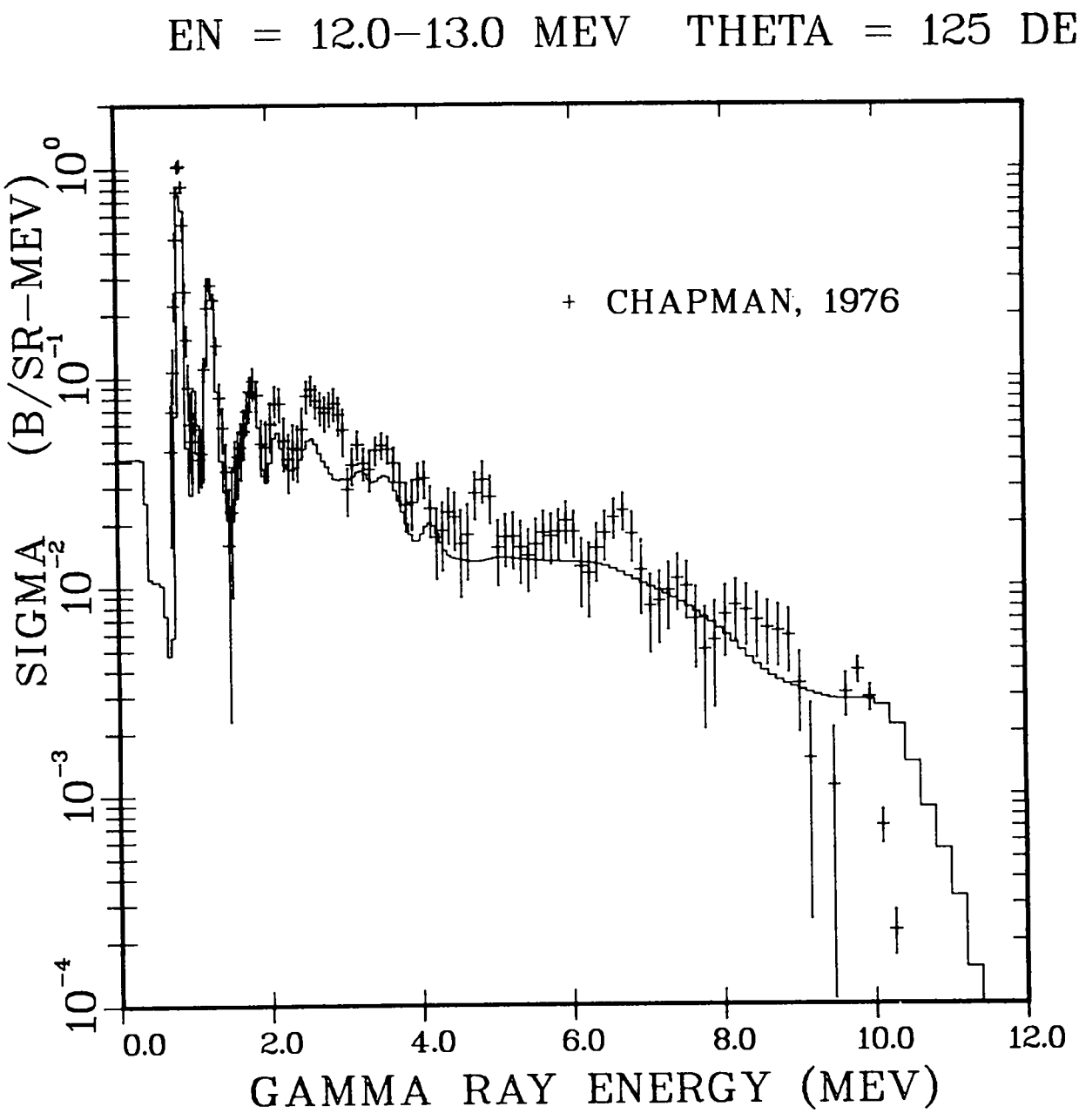


Fig. 45.
Calculated and measured[140] gamma-ray emission spectra from iron at 125 degrees for incident neutrons between 12 and 13 MeV.

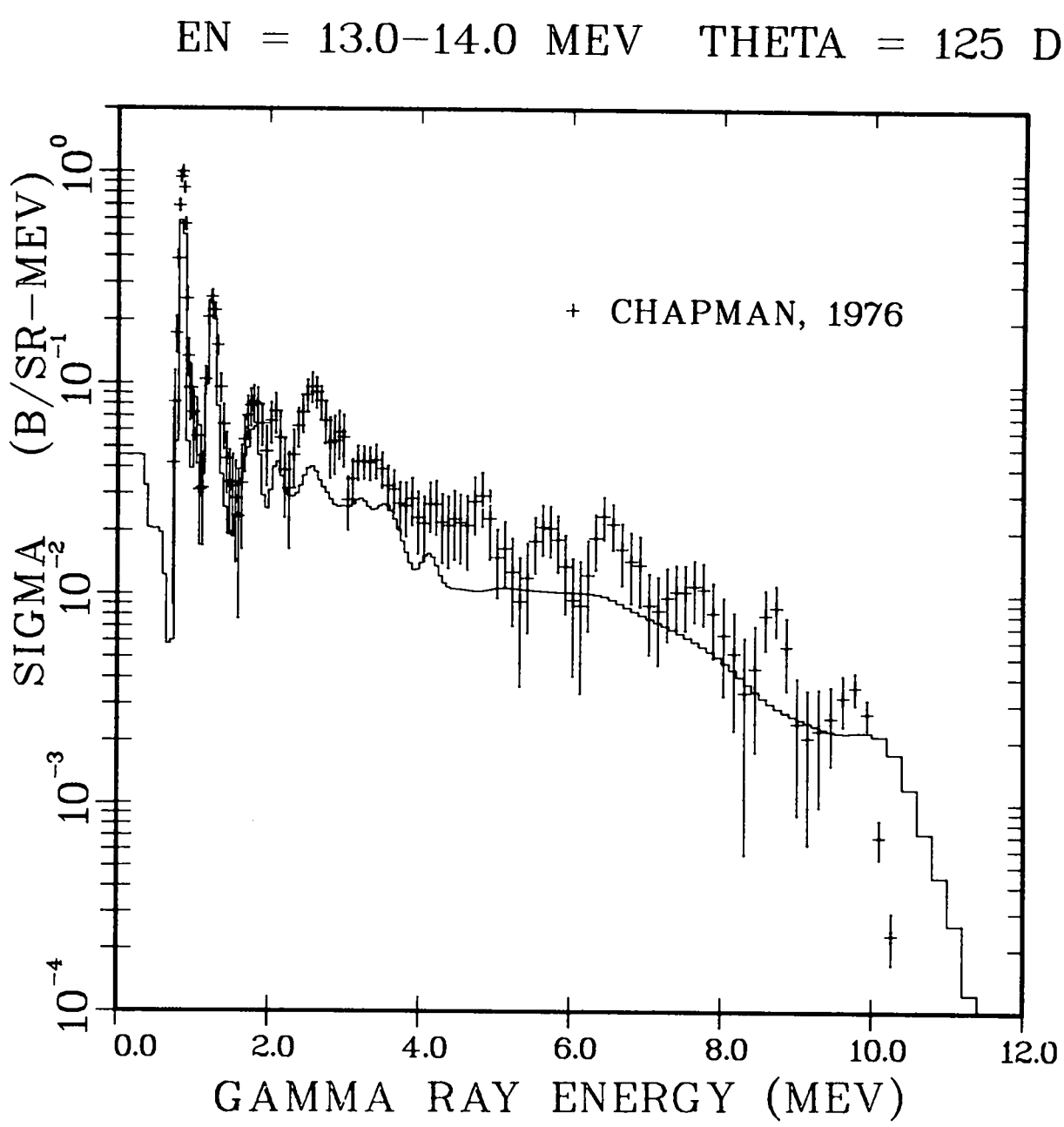


Fig. 46.
Calculated and measured $^{140}$ gamma-ray emission spectra from iron at 125 degrees for incident neutrons between 13 and 14 MeV.

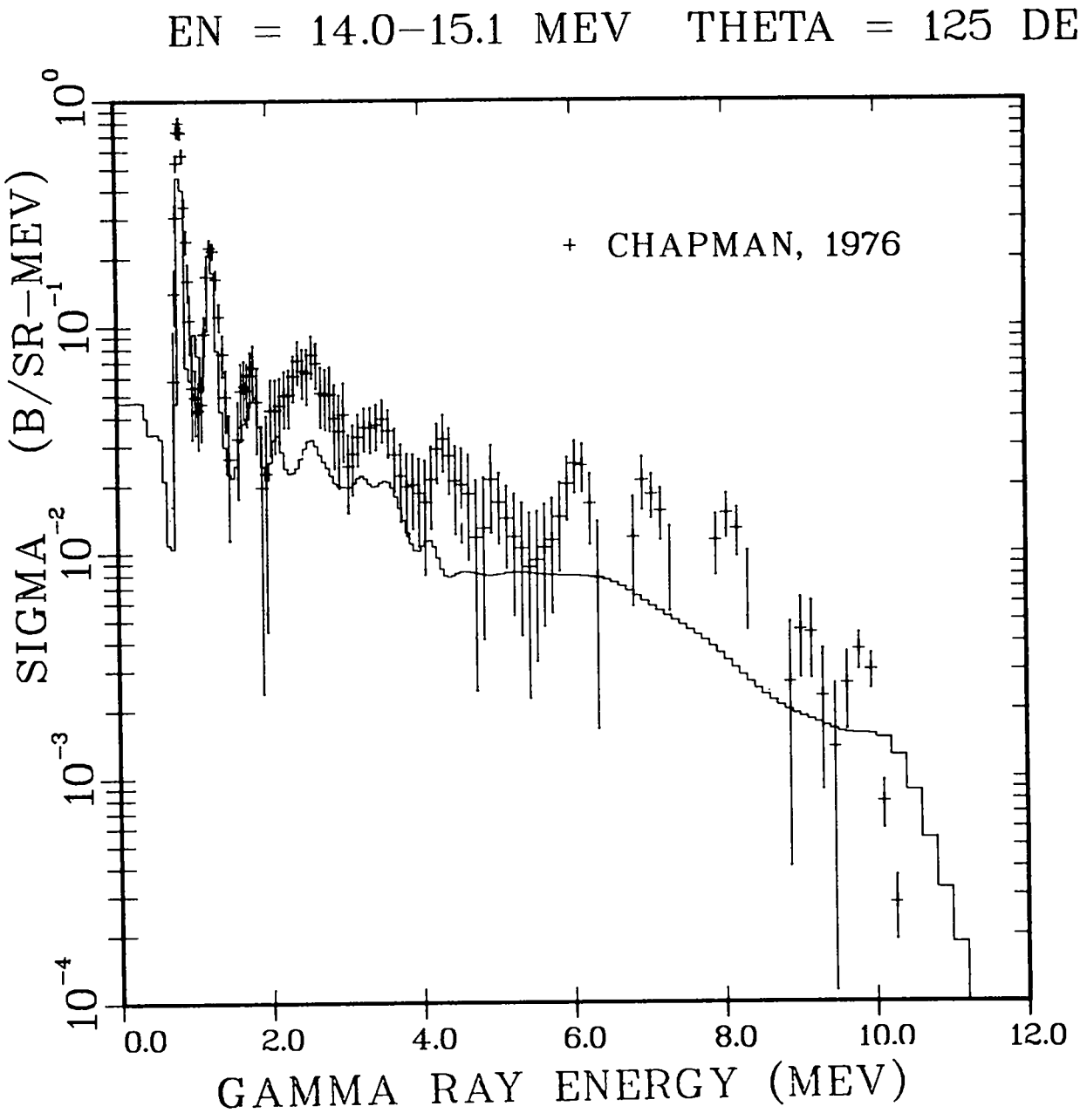


Fig. 47.
Calculated and measured[140] gamma-ray emission spectra from iron at 125 degrees for incident neutrons beteen 14 and 15.1 MeV.

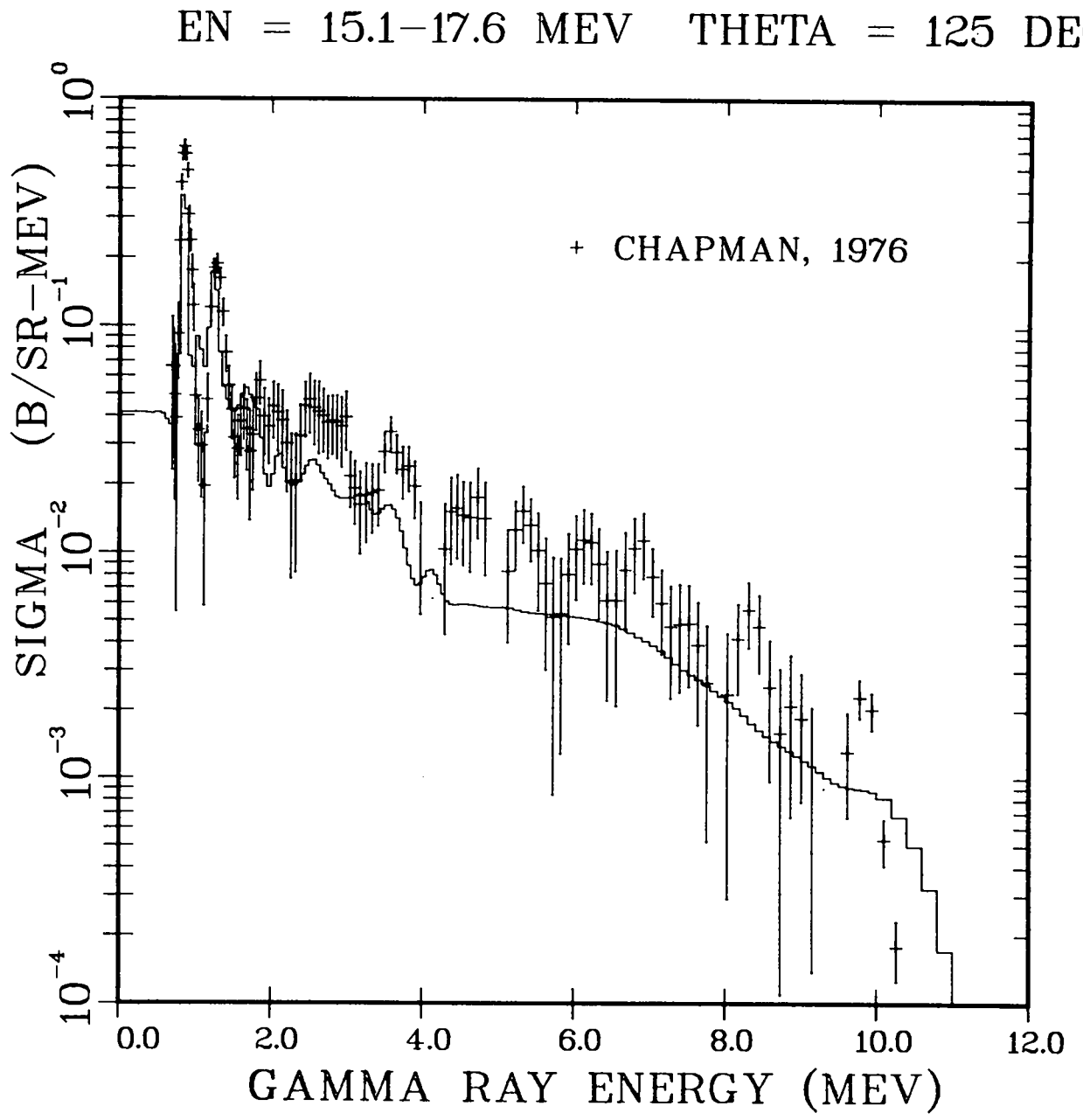


Fig. 48.
Calculated and measured[140] gamma-ray emission spectra from iron at 125 degrees for incident neutrons between 15.1 and 17.6 MeV.

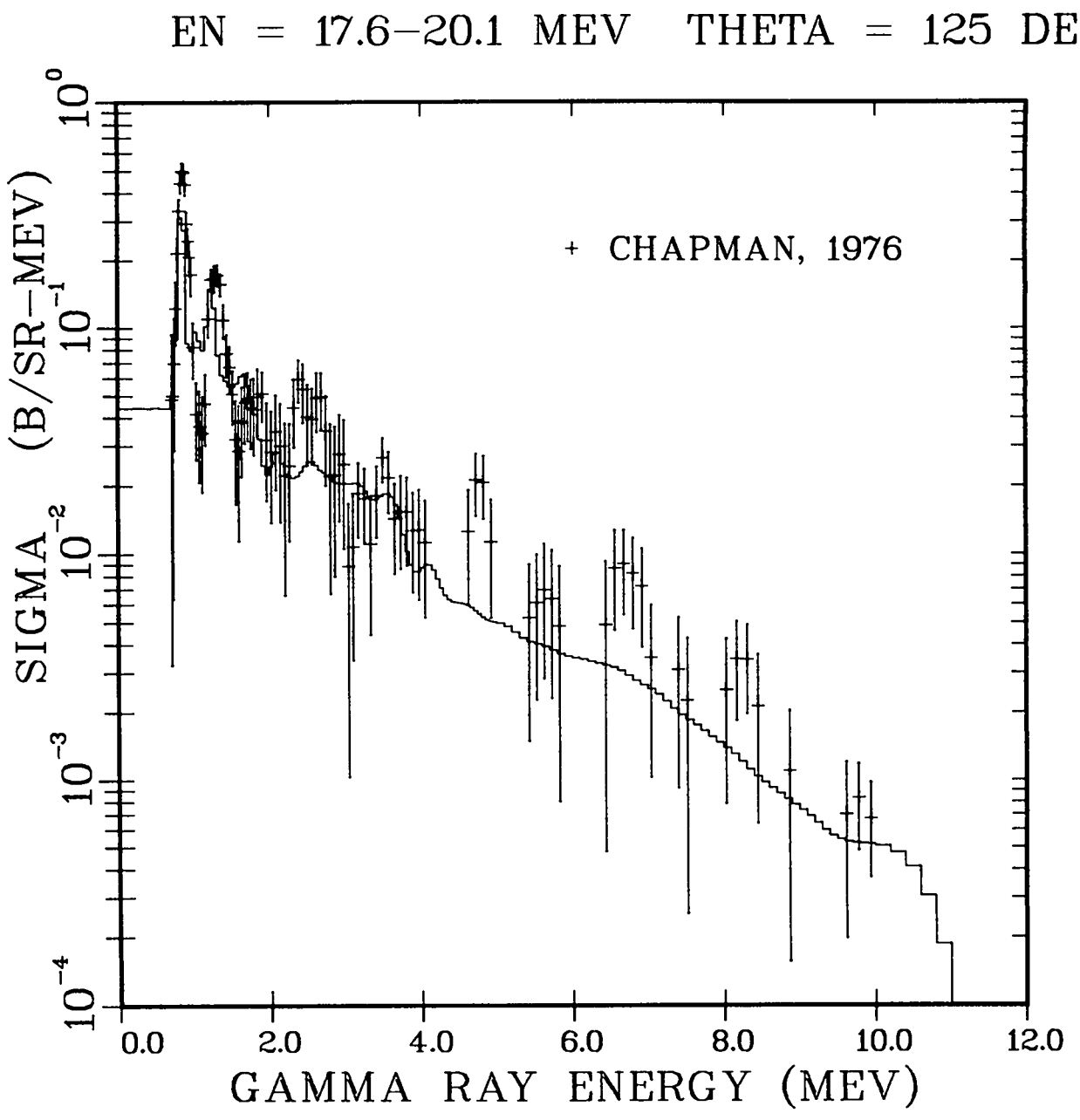


Fig. 49.
Calculated and measured[140] gamma-ray emission spectra from iron at 125 degrees for incident neutrons between 17.6 and 20.1 MeV.

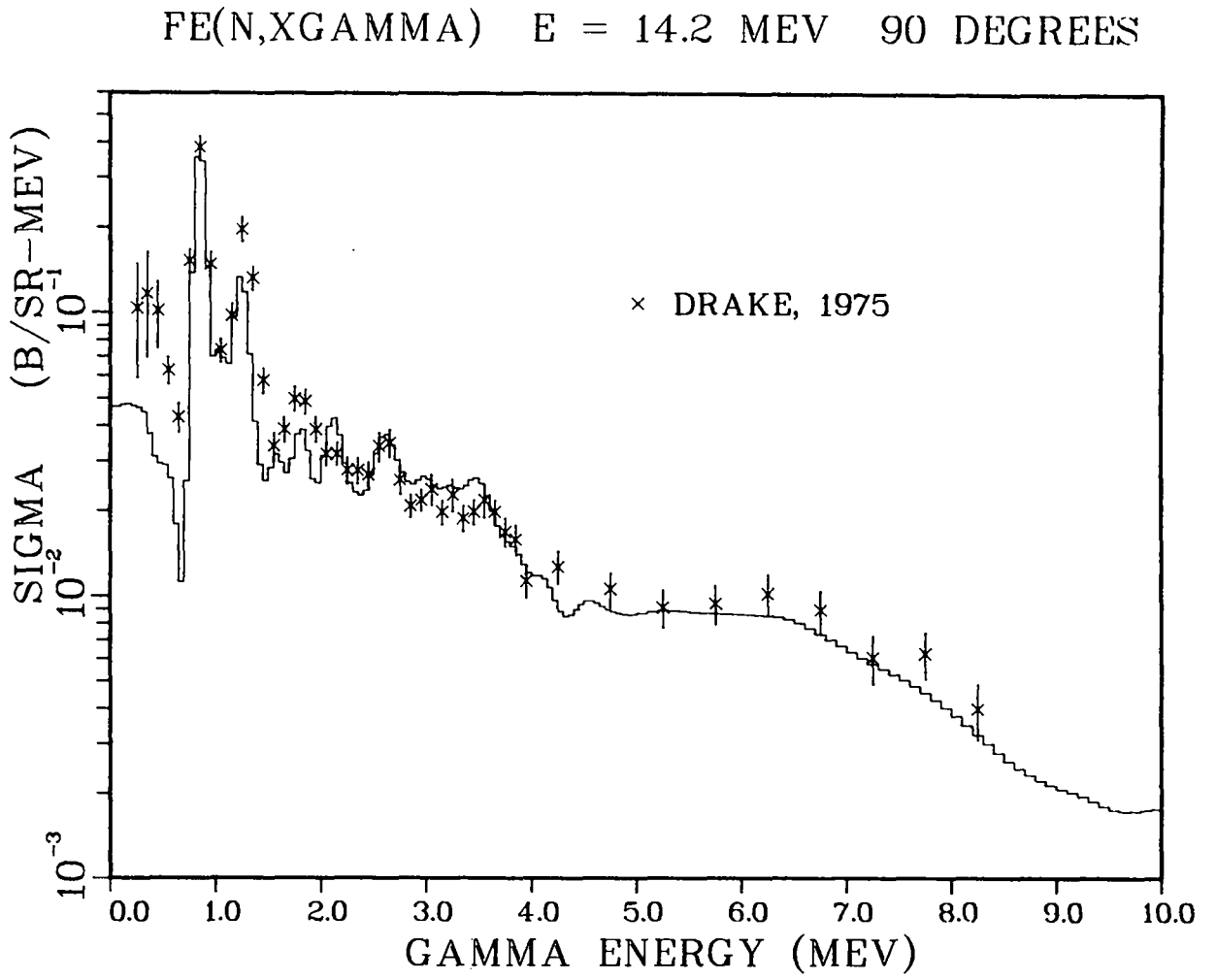


Fig. 50.
Comparison of calculated gamma-ray emission spectrum at 90 degrees for 14.1-MeV incident neutrons with the measurement of Drake et al.[148]

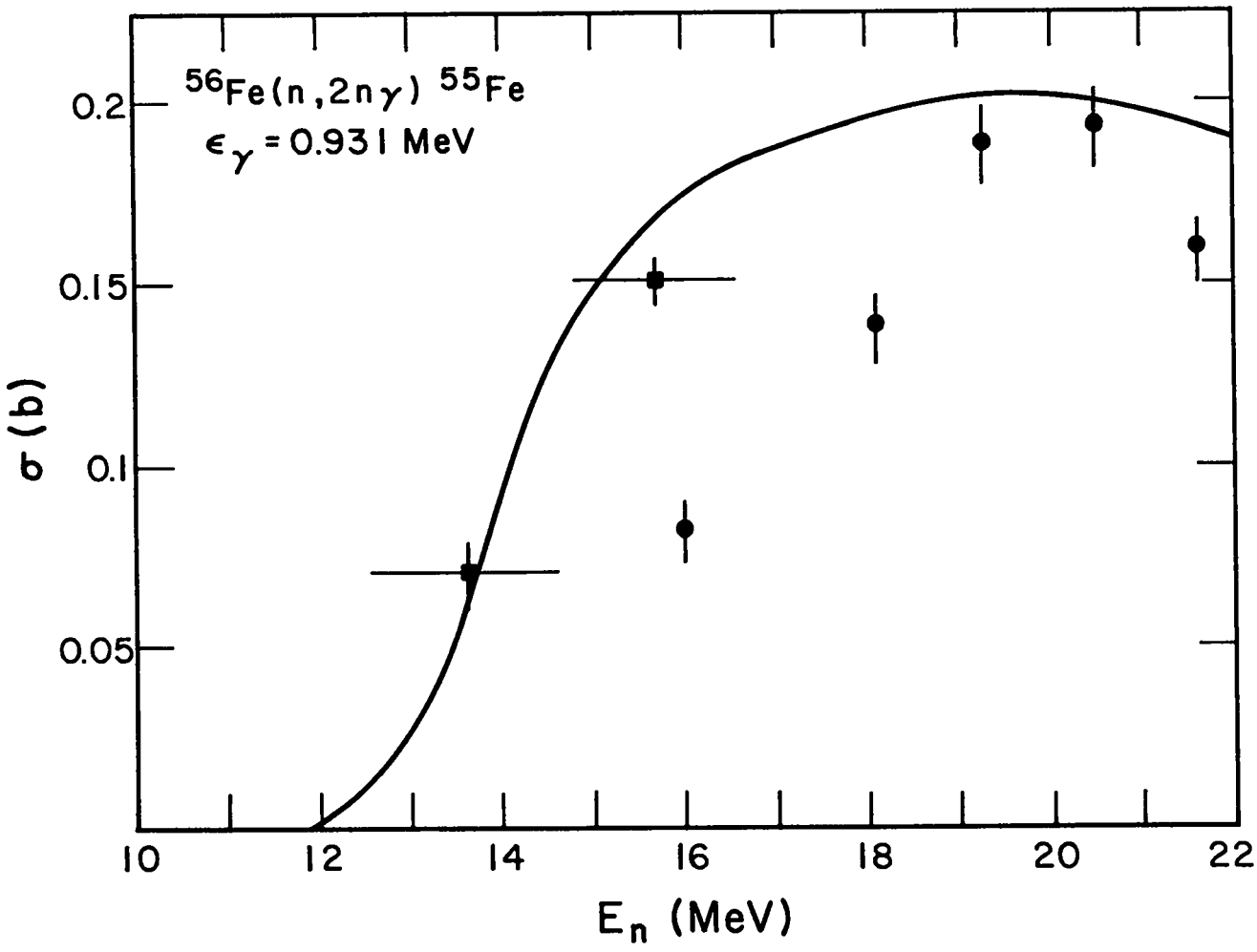


Fig. 51.
Comparison of the calculated production cross section for the 0.931-MeV gamma ray from the $^{56}Fe(n,2n\gamma)^{55}Fe$ reaction with the measurements of Orphan et al.[144] (solid squares) and Corcalciuc et al.[154] (solid circles).

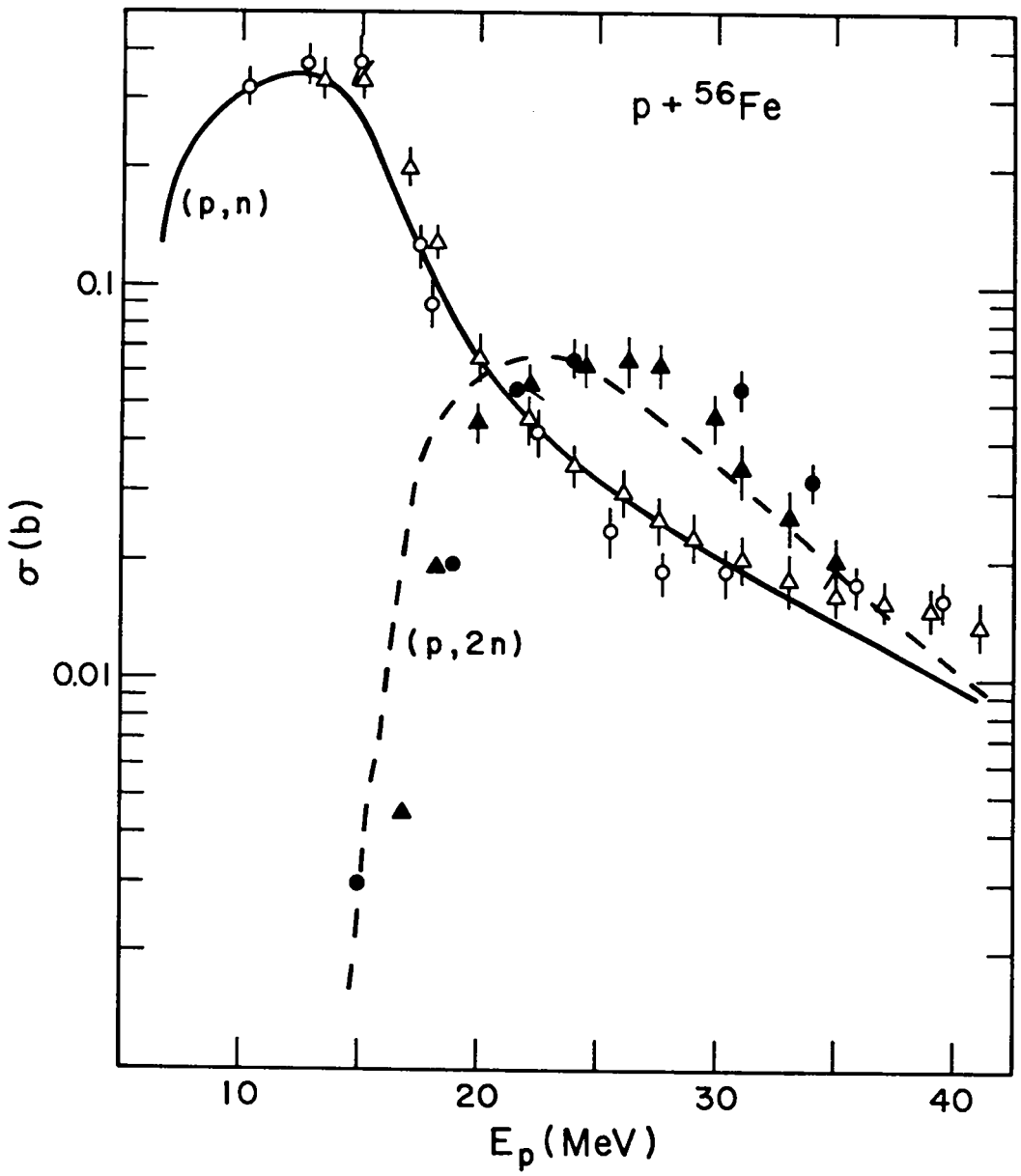


Fig. 52.
Comparison of the calculated (p,n) and (p,2n) cross sections for $^{56}Fe$ with the measurements of Michel et al.[155] (circles) and and Jenkins and Wain[55] (triangles).

## IV. EVALUATED DATA

The calculated cross sections described here were integrated with the existing ENDF/B-V file[2] to produce a new iron evaluation extending up to 40 MeV. Significant changes were made in the ENDF/B-V data at energies down to 3 MeV. In this new evaluation we chose to rely almost completely on the calculated results except for the total cross section. In particular, calculated values were used at all energies for reaction cross sections, angular distributions, and energy spectra, subject only to a small (<10%) renormalization of the nonelastic cross sections above 30 MeV. We made this choice since in general the calculations agree well with most available types of experimental data, and the resulting neutron and gamma-ray production cross sections and spectra are consistent with each other. In this manner we avoid energy imbalance problems that affect some ENDF evaluations. For example, the present ENDF/B-V evaluation for natural iron violates conservation of total energy by about 9% around 13 MeV. We felt also that extensions of cross sections from energy regions having experimental data up to 40 MeV would be more reliable through use of nuclear-model calculations employing consistent parameter sets.

Two evaluated data files were produced. The first contains dosimetry cross sections for neutrons incident on $^{54}Fe$ and $^{56}Fe$. The second is a complete ENDF/B evaluated data file for $^{NAT}Fe$, which includes cross sections, gamma-ray and neutron emission spectra, and their associated angular distributions. For the natural iron evaluation, we retained standard ENDF/B formats below 20 MeV to make this portion compatible with existing codes that use or process such data. Above 20 MeV, because of the necessity to include new reaction types not defined under present ENDF formats and in order to represent angular distributions associated with secondary neutron continuum energy distributions, we assigned new reaction type (MT) numbers and devised a method for representation of energy-angle correlated data. Details concerning methods used to represent the data both below and above 20 MeV as well as examples of evaluated cross sections and spectra are presented in the following sections.

### A. Reaction Type Labels (MT Numbers)

The ENDF/B reaction labels or MT numbers, either standard or newly defined, that were used for the dosimetry file are given in Table VI along with reaction thresholds. New reaction descriptors were required for the (n,2nα), (n,3nα),

(n,4n), (n,2np), and (n,3np) reactions, which are given respectively by MT=24, 25, 37, 41, and 42. Each dosimetry reaction is given over the entire energy range from threshold to 40 MeV.

Table VII lists the reactions and thresholds used for the natural iron evaluation, together with the energy ranges of applicability. Above 20 MeV, a new MT=99 was defined to be the sum of the reaction types MT=16, 17, 22, 24, 25, 28, 37, 41, 42, and 91. This MT represents a composite of all major reactions resulting in the emission of continuum neutrons. (Inelastic scattering from discrete levels is therefore not included under this label.)

B. Representation of Neutron Emission and Associated Angular Distributions

Below 20 MeV, neutron emission was described through a standard representation involving discrete inelastic level information along with contributions from continuum inelastic scattering, (n,2n), (n,np + n,pn) and (n,nα + n,αn) reactions. Angular distributions for neutrons produced by inelastic scattering from discrete levels were generally a combination of results calculated from the use of compound nucleus and direct reaction theory. For those levels not assumed to be excited through direct inelastic scattering, only a compound nucleus angular distribution was assumed. Continuous energy secondary neutron spectra for a given reaction type were expressed in tabulated (histogram) form so that preequilibrium contributions, where applicable, could be represented adequately. An angular distribution was assigned for each of these spectra based on its mean secondary energy though use of the Kalbach and Mann systematics[72] for the angular distributions of continuum neutrons (see Sec. II E). Information concerning the foward peaking of higher energy neutrons was suppressed due to the averaging of neutrons of low and high secondary energies that is inherent with this representation.

Above 20 MeV, angular distributions of secondary neutrons become much more forward peaked making it necessary to devise a method to represent such effects. As described in Sec. IV A, the use of MT numbers to represent individual reactions involving neutron emission was abandoned for the natural iron evaluation in favor of a new MT number, 99, which includes continuous neutron emission from all reactions present at a given energy. (The individual reaction cross sections are preserved in the dosimetry files.) The composite neutron emission spectrum denoted by MT=99 was subdivided into 7 secondary energy groups each 5 MeV wide. To each of these groups a separate angular distribution was assigned,

TABLE VI

REACTIONS, Q-VALUES, AND THRESHOLDS FOR THE $^{54}Fe$ and $^{56}Fe$ DOSIMETRY FILES

| | $^{54}Fe$ | | $^{56}Fe$ | | |
|---|---|---|---|---|---|
| MT | Q (MeV) | $E_{th}$ (MeV) | Q (MeV) | $E_{th}$ (MeV) | Reaction |
| 16 | -13.379 | 13.620 | -11.197 | 11.399 | (n,2n) |
| 17 | -24.062 | 24.497 | -20.496 | 20.866 | (n,3n) |
| 22 | - 8.418 | 8.570 | - 7.614 | 7.751 | (n,nα) |
| 24 | -21.419 | 21.806 | -19.653 | 20.008 | (n,2nα) |
| 25 | -32.001 | 32.579 | -28.914 | 29.436 | (n,3nα) |
| 28 | - 8.853 | 9.013 | -10.183 | 10.367 | (n,np) |
| 37 | --- | --- | -33.874 | 34.486 | (n,4n) |
| 41 | -20.908 | 21.285 | -20.410 | 20.779 | (n,2np) |
| 42 | -31.443 | 32.011 | -29.349 | 29.879 | (n,3np) |
| 103 | 0.085 | EXO | - 2.913 | 2.966 | (n,p) |
| 107 | 0.843 | EXO | 0.326 | EXO | (n,α) |

TABLE VII

REACTIONS, Q-VALUES, AND ENERGY RANGES INCLUDED IN NATURAL IRON EVALUATION

| MT | Q (MeV) | $E_{th}$ (MeV) | Energy Range (MeV) | Rection Description |
|---|---|---|---|---|
| 1 | 7.646 | EXO | $10^{-11}$-40 | Total |
| 2 | 0. | EXO | $10^{-11}$-40 | Elastic |
| 3 | 7.646 | EXO | $10^{-11}$-40 | Nonelastic |
| 4 | - 0.847 | 0.862 | 0.862-20 | Inelastic |
| 16 | -11.197 | 11.399 | 11.399-20 | (n,2n) |
| 22 | - 7.614 | 7.751 | 7.751-20 | (n,nα) |
| 28 | - 8.853 | 9.013 | 9.013-20 | (n,np) |
| 51-90 | - 0.847 | 0.862 | 0.862-40 | (n,n') discrete |
| 91 | - 4.878 | 4.966 | 4.966-20 | (n,n') continuum |
| 99 | -19.645 | 20.000 | 20-40 | Sum of MT=16,17,22 24,25,28,37,41, 42,91 |
| 102 | 7.646 | EXO | $10^{-11}$-40 | (n,γ) |
| 103 | 0.085 | EXO | $10^{-11}$-40 | (n,p) |
| 104 | - 7.959 | 8.102 | 8.102-40 | (n,d) |
| 105 | -11.928 | 12.144 | 12.144-40 | (n,t) |
| 106 | -10.533 | 10.723 | 10.723-40 | (n, $^{3}He$) |
| 107 | 0.326 | EXO | $10^{-11}$-40 | (n,α) |

again through use of the Kalbach systematics. In this manner, angular distribution effects were introduced for continuum neutrons and, along with discrete level angular distributions obtained through DWBA calculations, a reasonable representation was obtained for the physical processes occurring at higher incident energies. This method has some disadvantages as will be noted later, but for this evaluation it represents a first step towards ENDF formats that will describe energy-angle correlations.

## C. Neutron Cross Sections

The evaluated cross sections for the reaction types listed in Table VI were determined purely from the theoretical results as described earlier. In this section we present cross-section curves only for reaction types not already compared to experimental data in Sec. III. Further detail regarding some of these cross sections appears in Appendix B, which tabulates the dosimetry cross sections calculated for individual reactions with $^{54}Fe$ and $^{56}Fe$.

1. Total, Elastic, and Nonelastic Cross Sections. The evaluated total cross section for natural iron is compared to experimental measurements[6-19] and to ENDF/B-V[2] in Fig. 53. The total consists of ENDF/B-V values below 10 MeV and then follows the recent measurements of Larson[13] to 40 MeV. These data were chosen since they cover the widest range of incident energies and agree well with the previous measurements of Perey,[6] which cover a similar although somewhat smaller energy range.

The evaluated elastic cross section is shown with experimental data (Refs. 22-24,26,32,47,87) and ENDF/B-V in Fig. 54. The evaluated elastic was joined to the ENDF/B-V values at 8 MeV. Between 8 and 40 MeV, it was determined from the difference between the evaluated total and the sum of the various components of the reaction cross section.

The nonelastic cross section used in the evaluation is compared to experimental data[37-50] and to ENDF/B-V in Fig. 55. The nonelastic cross section was generally derived from values calculated with the optical parameters of Table I except in the region around 30-40 MeV where these values were renormalized downward by a maximum of 10% to agree with the recent results of Brady et al.,[37] which were not available for use in the determination of the optical parameters.

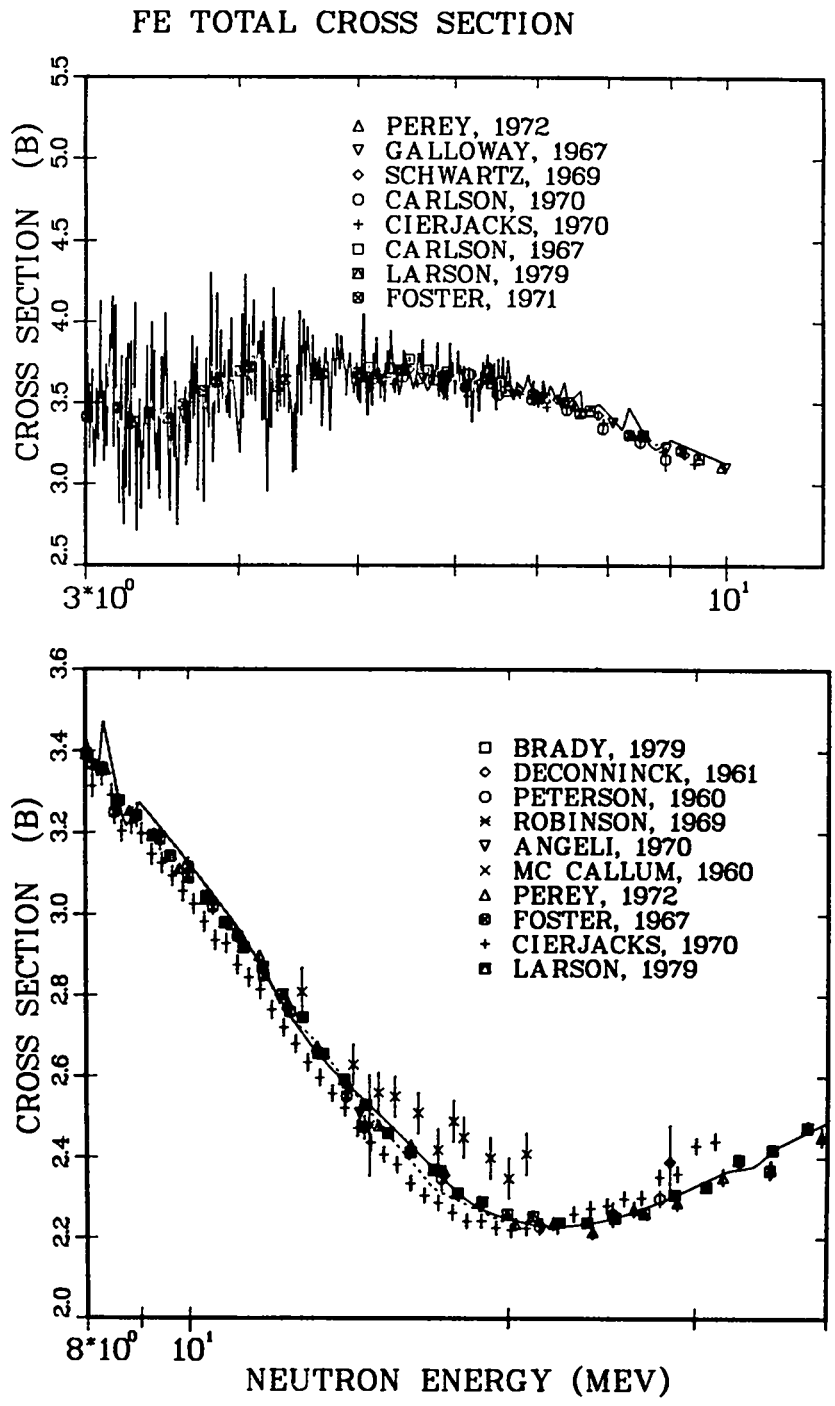


Fig. 53.
Evaluated and measured total cross section for iron. The dashed curve is ENDF/B-V, the solid curve is the present evaluation, and the experimental data are from Refs. 6-19.

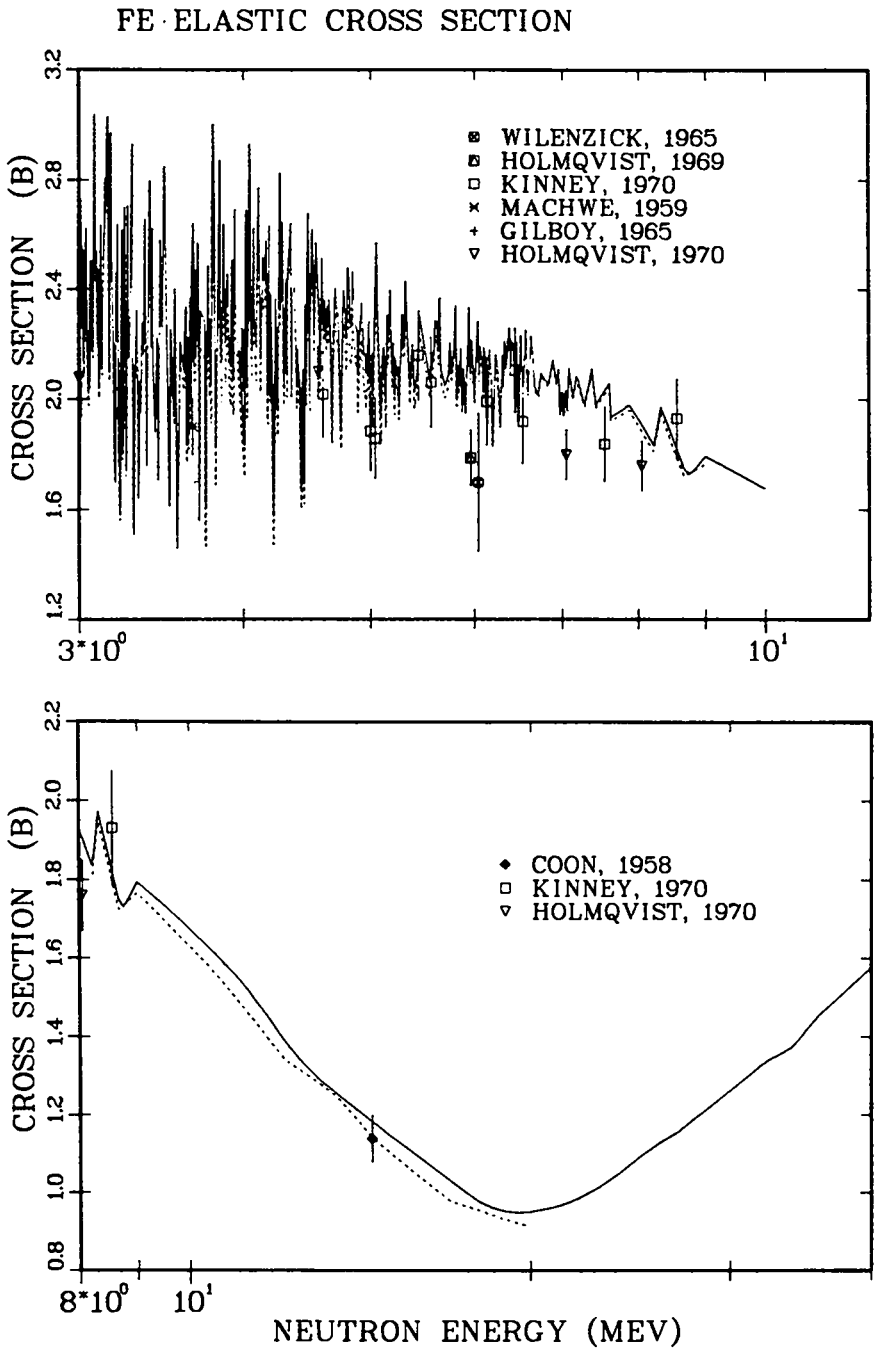


Fig. 54.
Evaluated and measured elastic cross section for iron. Experimental data are from Refs. 22-24, 26, 32, 47, 87. See caption of Fig. 53 for curves.

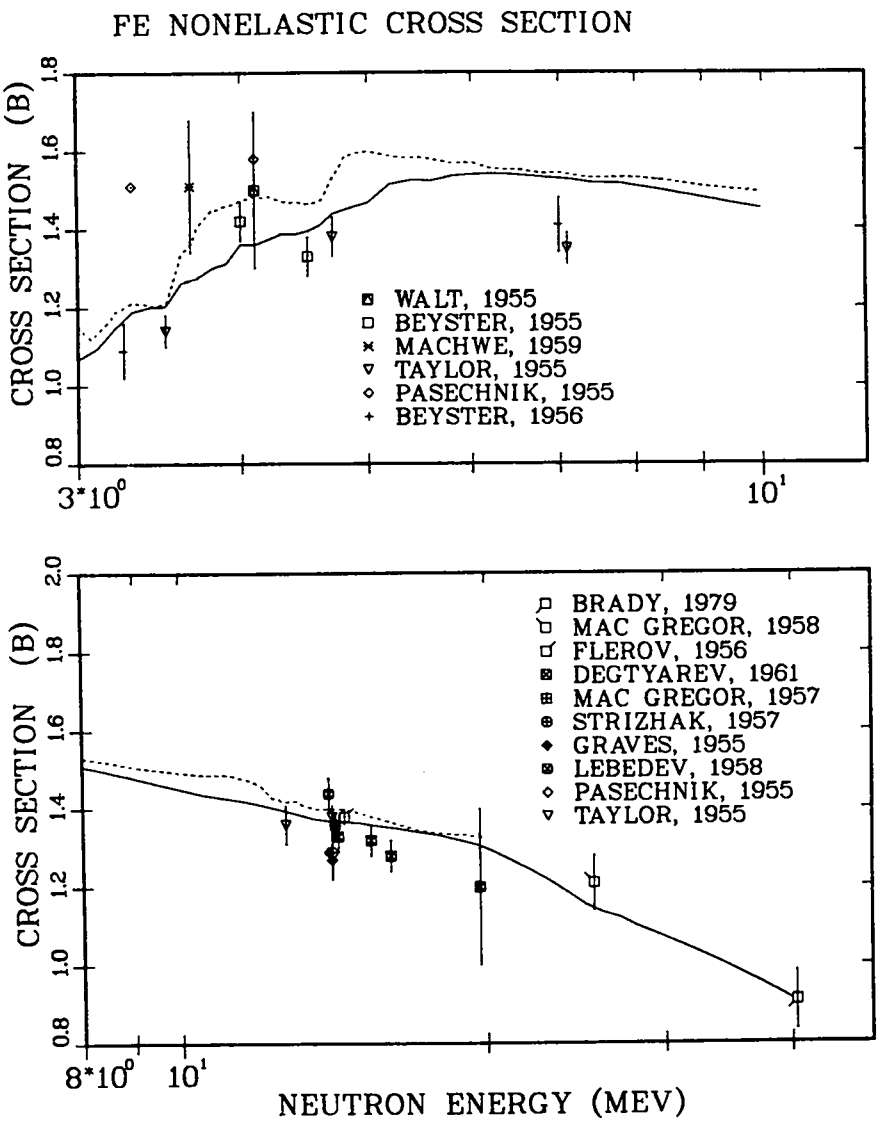


Fig. 55.
Evaluated and measured nonelastic cross section for iron. Experimental data are from Refs. 37-50. See caption of Fig. 53 for curves.

2. Inelastic Cross Sections. Discrete inelastic cross sections for the lowest 33 levels in $^{56}Fe$ and the lowest 7 levels* in $^{54}Fe$ are included from threshold to 40 MeV in the evaluation. Continuum inelastic scattering ($E_{th}$ = 5 MeV) is tabulated in MT=91 below 20 MeV and is combined in MT=99 above 20 MeV with all other neutron-emitting reactions except discrete (n,n').

Comparisons of the calculated and measured excitation cross sections for low-lying levels of $^{54}Fe$ and $^{56}Fe$ were presented in Figs. 13-19 of Sec. III. B. Figures 56-58 compare the $^{NAT}Fe$ excitation functions for the first 10 levels included in the evaluation with ENDF/B-V values in cases where the latter exist for the same states. These levels include the low-lying collective states of these nuclei that have a significant cross section up to 40 MeV because of calculated direct reaction components. These cross sections as well as the remainder of the discrete level inelastic cross sections (MT=61-90) were joined to the ENDF/B-V results near 3 MeV.

The total inelastic cross section (MT=4) is compared to available experimental data[86,137,146,156-161] and to ENDF/B-V from 2 to 20 MeV in Fig. 59. The very old measurement of Landon[160] (1958) near 14 MeV disagrees with both ENDF/B-V and the present evaluation.

3. Fe(n,γ) Cross Section. The (n,γ) cross section is represented explicitly under MT=102 at all energies to 40 MeV. Statistical theory GNASH calculations were coupled with a preequilibrium-like semi-direct calculation above 3 MeV to obtain the evaluated curve. The results are compared to ENDF/B-V and to the available experimental data[162-164] in Fig. 60.

4. Fe(n,2n) Cross Section. The (n,2n) cross section is represented under MT=16 below 20 MeV and is included in MT=99 at higher energies. The results for $^{54}Fe$ and $^{NAT}Fe$ were compared to experimental data in Figs. 24 and 25 of Sec. III C. The results for $^{NAT}Fe$ are compared to ENDF/B-V and to additional experimental data[165,166] in Fig. 61.

5. The Fe(n,p) and Fe(n,α) Cross Sections. The evaluated (n,p) and (n,α) cross sections for natural iron are given explicitly under MT=103 and 107 from $10^{-5}$ eV to 40 MeV. Comparisons of the present results with ENDF/B-V are included in Fig. 62. Comparisons of the constituent isotopic results to experiment were presented earlier in Figs. 26-33 of Secs. III D and E.

*The $J^{\pi} = 6^{+}$ fourth excited state of $^{54}Fe$ at $E_x$ = 2.9501 MeV was omitted due to its small cross section.

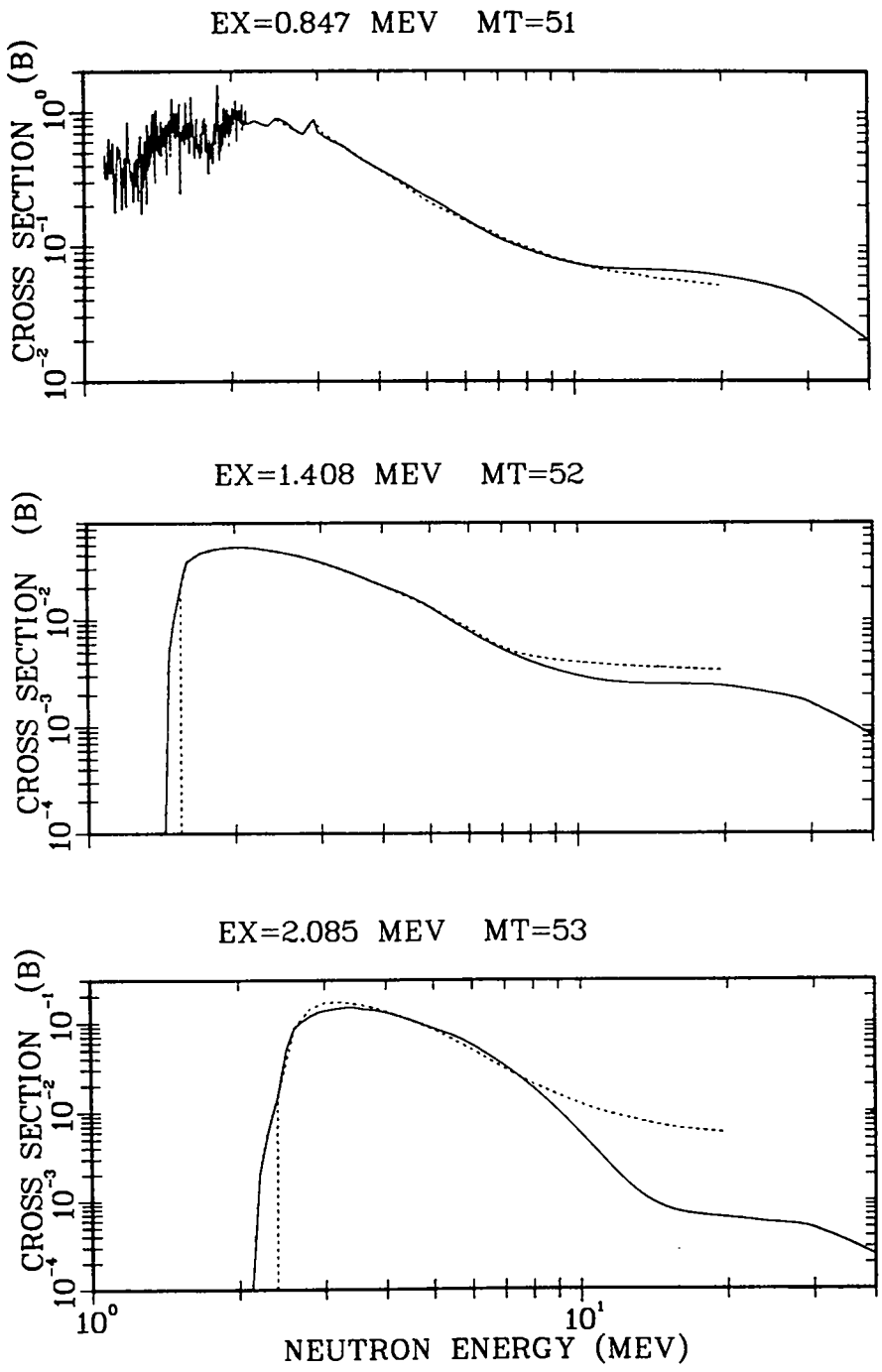


Fig. 56.
Evaluated Fe(n,n') cross sections for the first three discrete states. The solid curve is the present evaluation and the dashed curve is ENDF/B-V.

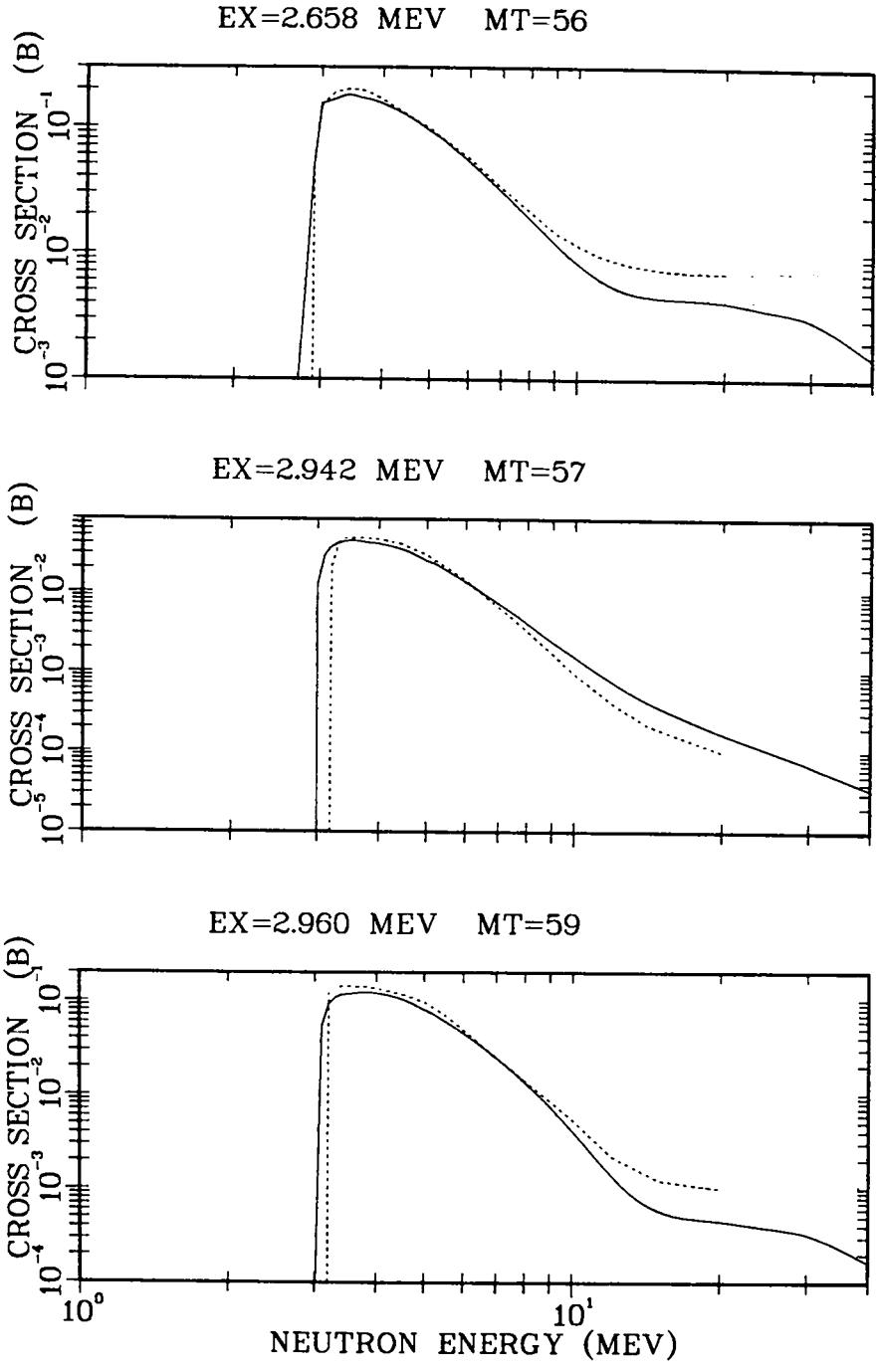


Fig. 57
Evaluated Fe(n,n') cross sections for the 6th, 7th, and 9th discrete states. See caption of Fig. 56 for curves.

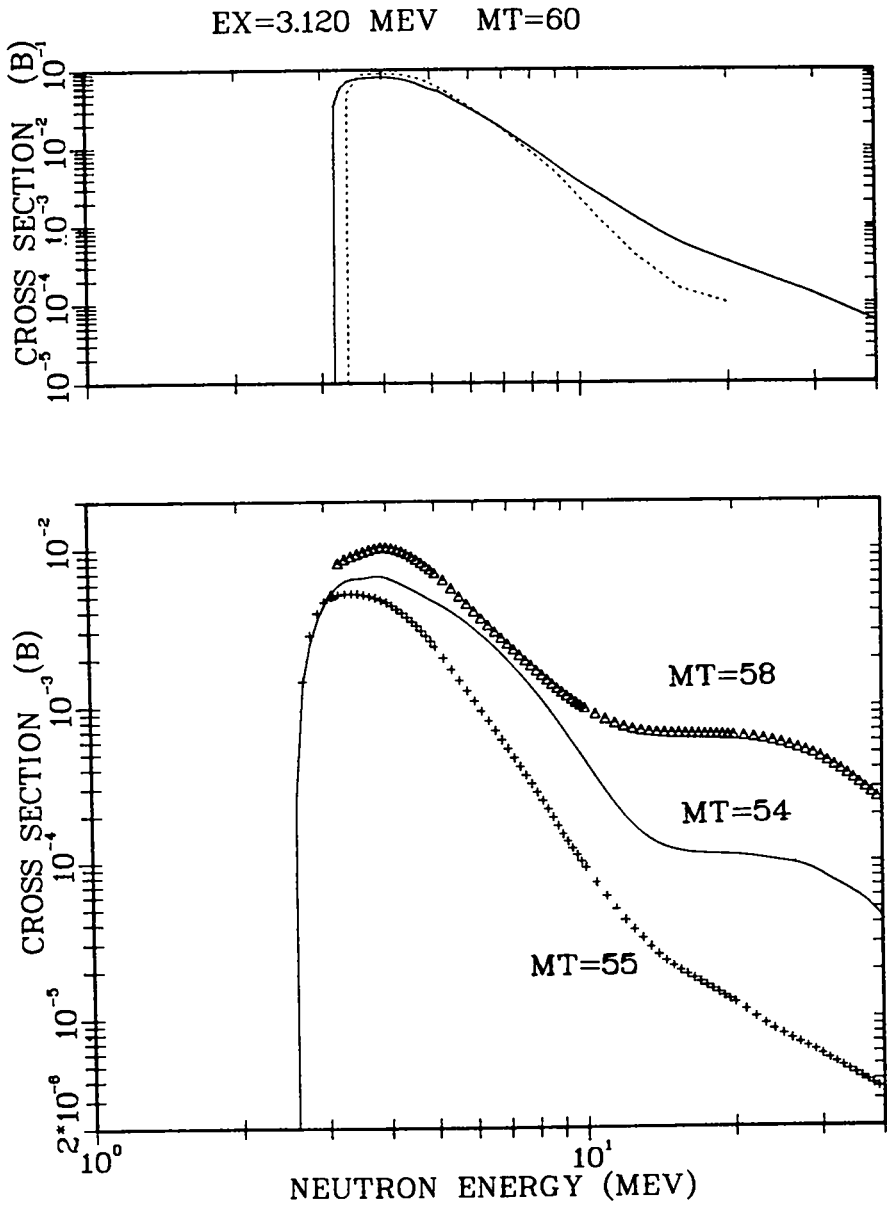


Fig. 58.
Evaluated Fe(n,n') cross sections for the 4th, 5th, 8th, and 10th discrete states. The dashed curve is ENDF/B-V; the solid curves, triangles, and crosses are the present evaluation.

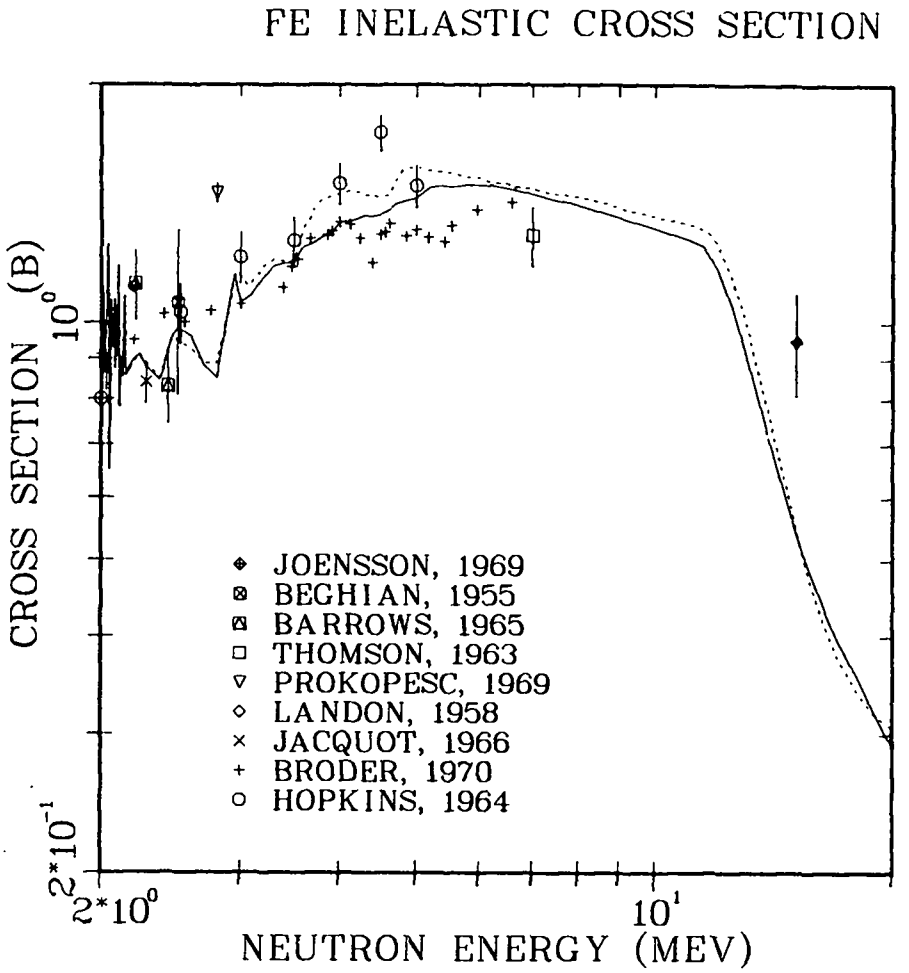


Fig. 59.
The inelastic cross section of iron from 2 to 20 MeV. The solid curve is the present evaluation; the dashed curve is ENDF/B-V; and the experimental data are from Refs. 86, 137, 146, 156-161.

6. The Fe(n,np) and Fe(n,nα) Cross Sections. The evaluated (n,np) and (n,nα) cross sections for natural iron are given to 20 MeV under MT=28 and 22, respectively. These results are compared to ENDF/B-V in Fig. 63. At higher energies, contributions from these reactions are included in the MT=99 composite for $^{NAT}$Fe but are tabulated individually in the $^{54}$Fe and $^{56}$Fe dosimetry file.

7. Fe(n,d), Fe(n,t), and Fe(n,$^3$He) Cross Sections. The evaluated cross sections for the (n,d), (n,t), and (n,$^3$He) reactions are shown in Fig. 64. We did not attempt to calculate these with theoretical models since their cross sections are small and the parameters and reaction mechanisms associated with them are somewhat uncertain. For the (n,d) reaction, we assumed a shape similar

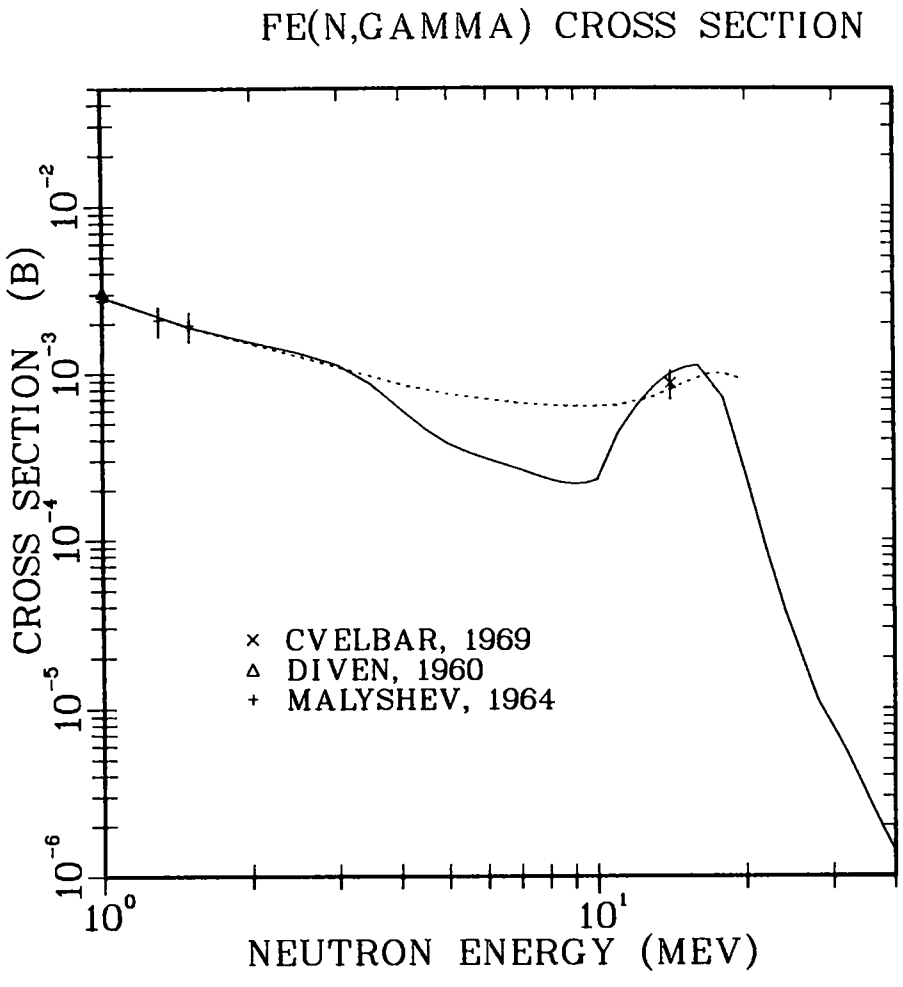


Fig. 60.
Evaluated and measured[162-164] cross section for the Fe(n,γ) reaction. See caption to Fig. 59 for curves.

to that for the (n,p) cross section (adjusted for threshold differences) and normalized the curve to the integrated deuteron emission spectrum measured by Grimes et al.[138] at 14 MeV, since at this energy the (n,d) reaction dominates. A similar approach was followed for the (n,t) reaction with the normalization determined from the 14-MeV systematics of (n,t) reactions as described by Qaim.[167] For the (n,$^3$He) reaction, the cross section was assumed to have a shape similar to that for the (n,α) reaction (again adjusted for threshold differences), and the Qaim (n,$^3$He) systematics were used for absolute normalization at 14 MeV. The present results for the (n,d), (n,t) and (n,$^3$He) cross sections are seen in Fig. 64 to be significantly lower than ENDF/B-V.

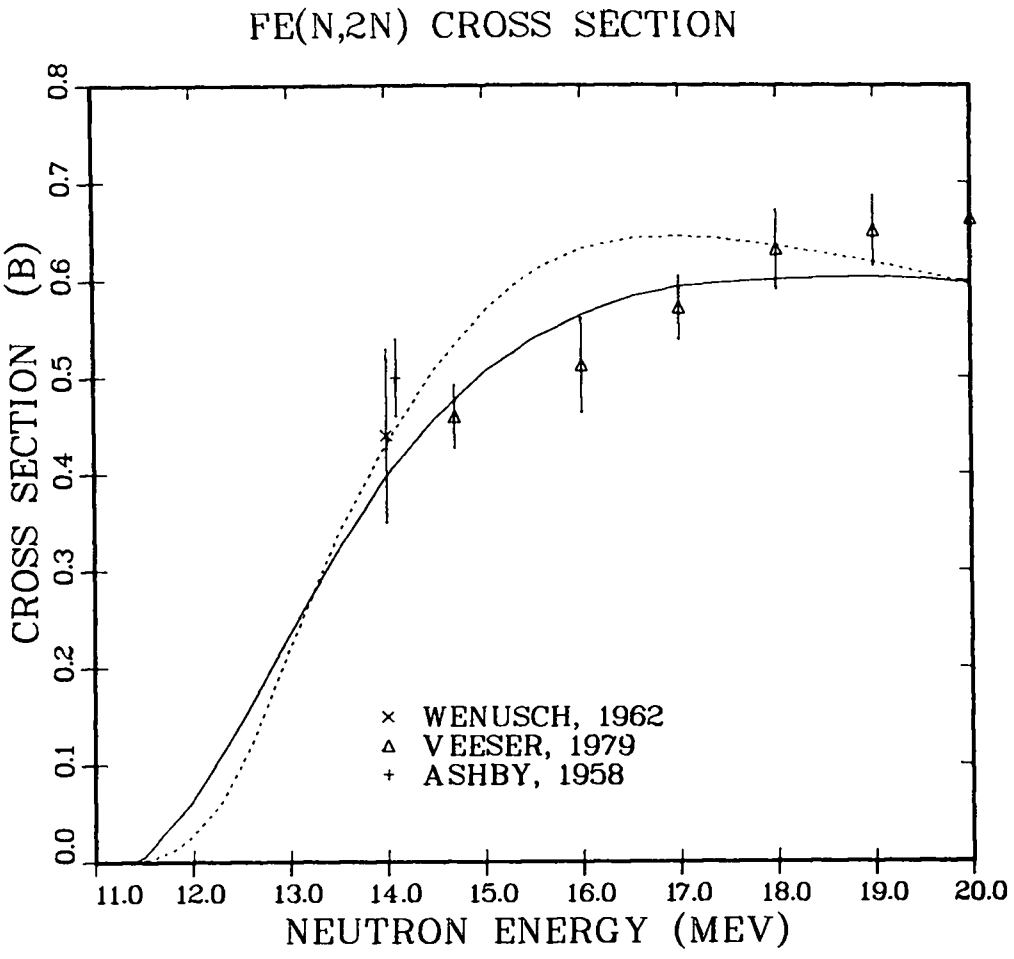


Fig. 61.
Evaluated and measured[97,165,166] cross section for the Fe(n,2n) reaction. See caption to Fig. 59 for curves.

## D. Neutron Emission Spectra

Comparisons to experimental spectra measured for 14-MeV neutrons shown in Sec. III B indicate that the calculated spectra provide a realistic representation of this data. Here we show examples of neutron emission spectra calculated at higher incident energies to illustrate angular distribution effects that are present as well as the need to incorporate them into the evaluated data file. Figure 65 shows the laboratory angle dependence of the secondary neutron spectra induced by 36-MeV neutrons. The higher energy portions of the spectra contain discrete level cross sections (elastic and inelastic) that exhibit a large

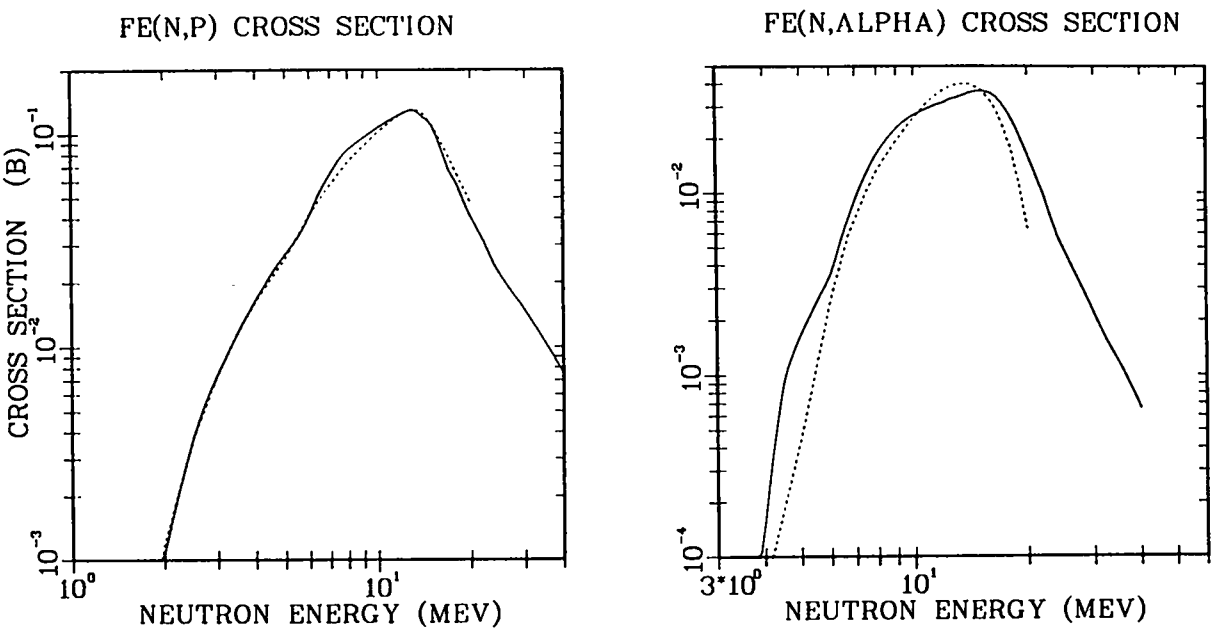


Fig. 62.
Evaluated (n,p) and (n,α) cross sections for iron. Curves are the same as described for Fig. 59.

degree of forward peaking. Likewise, the continuum energy region between 10 and 25 MeV exhibits a similar dependence with almost a factor of ten difference in cross section between forward and backward angles. The discontinuities shown are artificial and arise from the assignment of one angular distribution to each 5-MeV wide group of secondary energies. This problem indicates that a format should be devised that would allow angular distributions to be assigned for smaller secondary energy ranges in a compact manner. Such an effort is in progress.

## E. Gamma-Ray Cross Sections and Spectra

Discrete gamma-ray lines from inelastic scattering are included in the evaluation from threshold to 40 MeV. The discrete data are given as multiplicities in ENDF/B File 12 and are assumed to have isotropic angular distributions. Gamma lines from all other reactions were binned with the continuum gamma rays

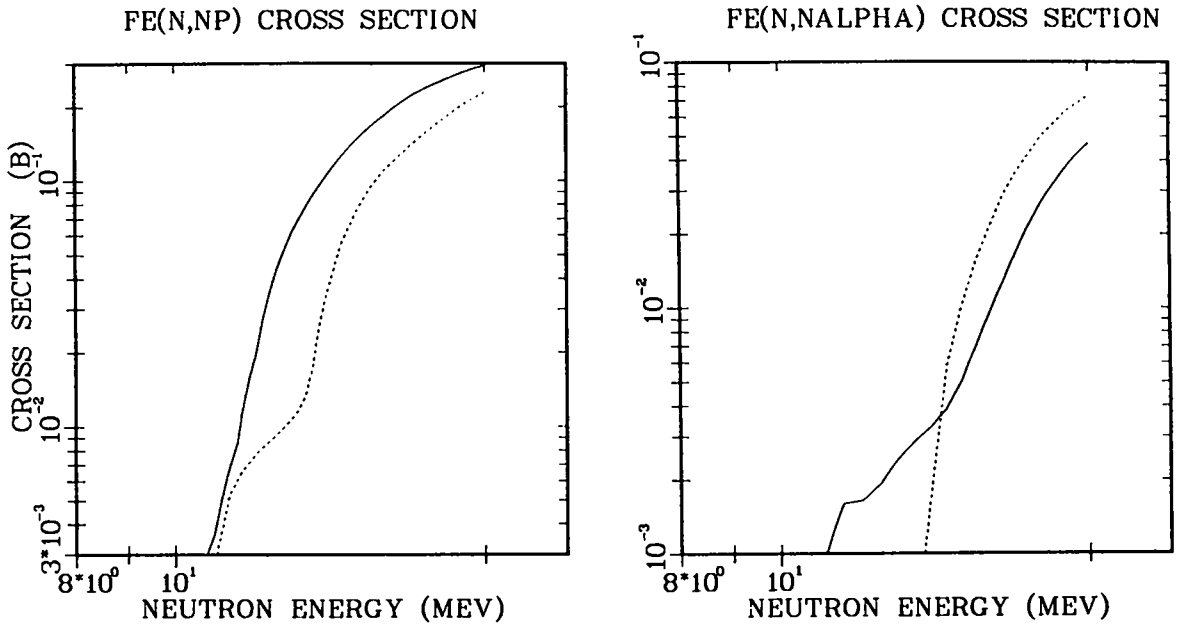


Fig. 63.
Evaluated (n,np) and (n,nα) cross sections for iron. The curves are described in the caption to Fig. 59.

and are represented as tabulations in Files 13 and 15. Again, isotropy is assumed in all cases. As with the neutron files, gamma rays resulting from all reactions that produce neutrons (except discrete inelastic) were lumped under MT=99 for incident neutron energies above 20 MeV.

A large portion of the gamma-ray production spectra has been compared in Sec. III F to experimental data available up to neutron energies of 20 MeV. We show here in Fig. 66 examples of gamma-ray production spectra calculated for higher incident neutron energies (28 and 40 MeV). These spectra illustrate the increasing importance of continuum gamma-ray contributions with a decreased contribution from discrete lines. However, the 0.846- and 1.238-MeV gamma rays from $^{56}Fe(n,n')$ and the 0.953-MeV gamma ray from $^{56}Fe(n,2n)$ are still identifiable at these higher energies. The total calculated gamma-production cross section maintains an almost constant value of about 2 barns in the neutron energy range between 20 and 40 MeV.

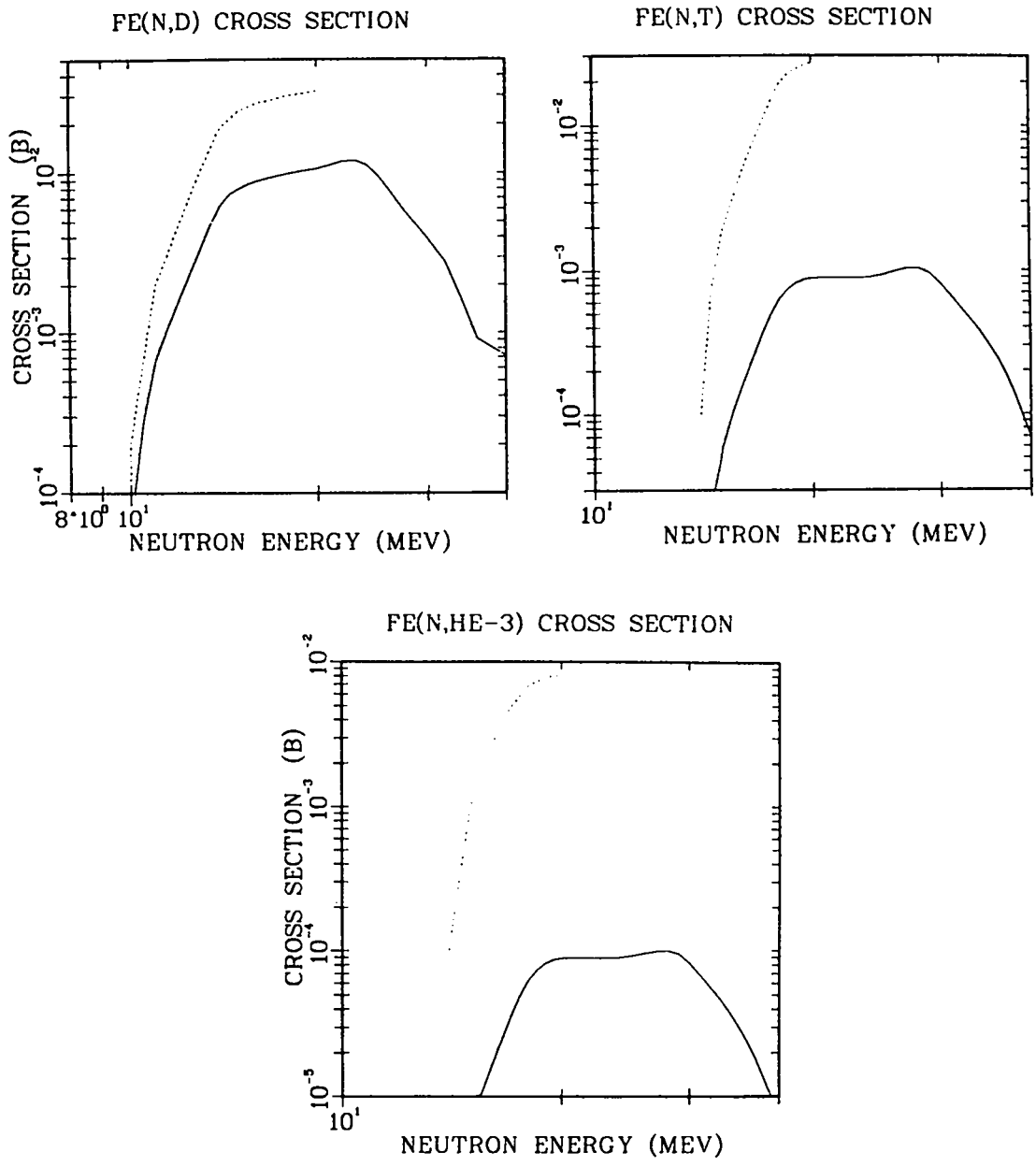


Fig. 64.
Evaluated (n,d), (n,t), and (n,$^3$He) cross sections for iron.
The curves are described in the caption to Fig. 59.

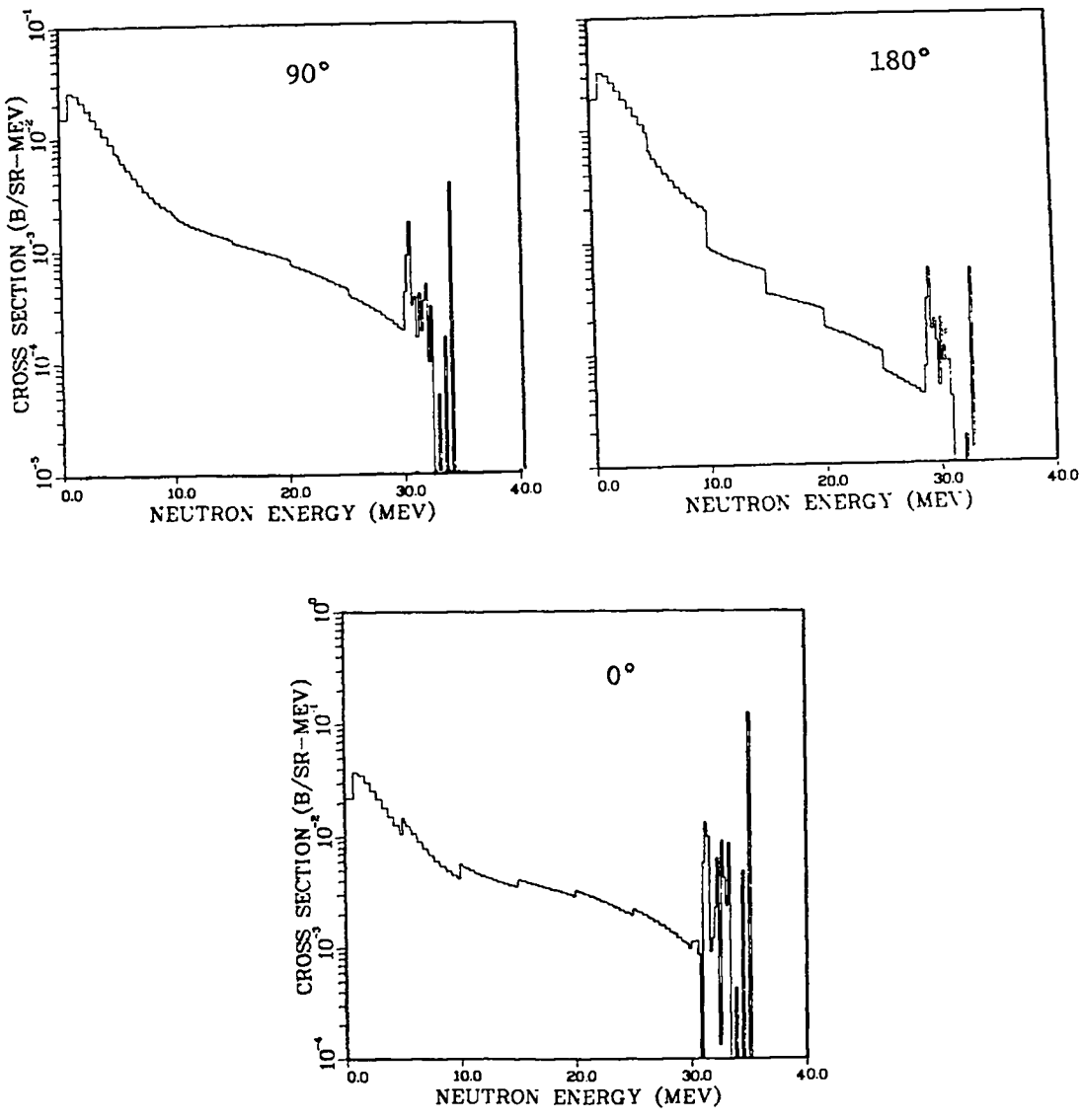


Fig. 65.
Calculated neutron emission spectra at 0, 90, and 180 degrees for 36-MeV neutrons incident on iron.

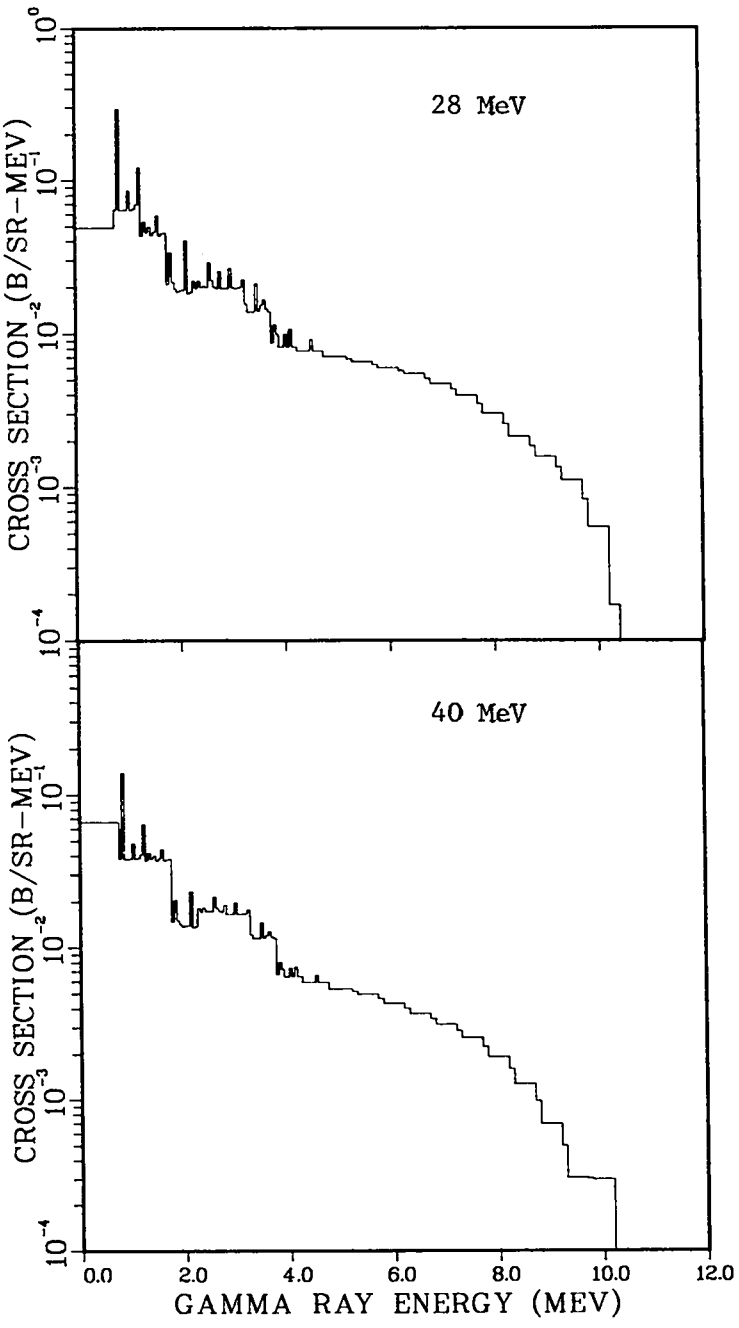


Fig. 66.
Calculated gamma-ray emission spectra at 90 degrees for 28- and 40-MeV neutrons incident on iron.

## V. SUMMARY

A consistent set of nuclear models and parameters for calculating neutron-induced reactions on $^{54}Fe$ and $^{56}Fe$ between 3 and 40 MeV has been presented. The calculations were made using a multistep Hauser-Feshbach statistical model with corrections for preequilibrium and direct-reaction effects. A spherical optical model was used to determine neutron, proton, and alpha transmission coefficients, and gamma-ray strengths were parameterized to calculate photon emission. Extensive comparisons with experimental data, including neutron-, proton-, and alpha-induced reactions, show that the calculations are in general agreement with most of the available experimental data.

The calculated data were used to develop two ENDF/B-formatted evaluated data files: a dosimetry file, which includes individual $^{54}Fe$ and $^{56}Fe$ neutron-induced reaction cross sections to 40 MeV; and a complete, general purpose $^{NAT}Fe$ file, which was joined at lower energies to ENDF/B-V and which includes neutron- and photon-production cross sections, angular distributions, and energy spectra from $10^{-5}$ eV to 40 MeV. To describe the data above 20 MeV, new formats, procedures, and reaction type "labels" were developed for the ENDF representation, and some lumping of reactions was found desirable for the natural Fe evaluation. Both evaluated data files have been provided to the ENDF/A library in the National Nuclear Data Center at Brookhaven National Laboratory.

The use of nuclear theory to augment the rather sparse experimental data base above 20 MeV has been suggested[169] as the most feasible way to extend evaluated data files to the 40-50 MeV regime in the detail needed for certain applications. The present work verifies that such extensions are indeed feasible and can lead to internally consistent evaluations that are in good overall agreement with experimental results.

APPENDIX A

DISCRETE LEVELS USED IN THE CALCULATIONS

| Nucleus | Level Energy (MeV) | Spin Parity |
|---|---|---|
| 24048 | 0.0000 | 0.0 + |
| | 0.7524 | 2.0 + |
| | 1.8590 | 4.0 + |
| | 3.4200 | 0.0 + |
| | 3.4520 | 6.0 + |
| 24049 | 0.0000 | 2.5 − |
| | 0.2720 | 3.5 − |
| | 1.0850 | 4.5 − |
| | 1.5630 | 5.5 − |
| | 1.7040 | 1.5 − |
| | 1.7420 | 1.5 − |
| | 1.9820 | 1.5 + |
| | 2.1690 | 1.5 − |
| | 2.4330 | 2.5 − |
| | 2.4980 | 6.5 − |
| 24050 | 0.0000 | 0.0 + |
| | 0.7833 | 2.0 + |
| | 1.8814 | 4.0 + |
| | 2.9250 | 2.0 + |
| | 3.1611 | 2.0 + |
| | 3.1637 | 6.0 + |
| | 3.3246 | 4.0 + |
| | 3.5945 | 3.0 + |
| | 3.6110 | 4.0 + |
| | 3.6300 | 1.0 + |
| | 3.6900 | 0.0 + |
| | 3.6980 | 2.0 + |
| | 3.7920 | 5.0 + |
| | 3.8254 | 6.0 + |
| 24051 | 0.0000 | 3.5 − |
| | 0.7490 | 1.5 − |
| | 0.7770 | 0.5 − |
| | 1.1645 | 4.5 − |
| | 1.3500 | 2.5 − |
| | 1.4803 | 5.5 − |
| | 1.5574 | 3.5 − |
| | 1.8994 | 1.5 − |
| | 2.0010 | 2.5 − |
| | 2.2557 | 7.5 − |
| | 2.3130 | 3.5 − |
| | 2.3796 | 3.5 − |
| | 2.3856 | 6.5 − |
| 24052 | 0.0000 | 0.0 + |
| | 1.4342 | 2.0 + |
| | 2.3698 | 4.0 + |
| | 2.6470 | 0.0 + |
| | 2.7680 | 4.0 + |
| | 2.9650 | 2.0 + |
| | 3.1138 | 6.0 + |
| | 3.1620 | 2.0 + |
| | 3.4153 | 3.0 + |
| | 3.6166 | 5.0 + |
| | 3.7710 | 2.0 + |
| | 3.9510 | 1.0 + |
| | 4.0154 | 5.0 + |
| | 4.0400 | 4.0 + |
| | 4.5630 | 3.0 − |
| 24053 | 0.0000 | 3.5 − |
| | 0.5641 | 0.5 − |
| | 1.0060 | 2.5 − |
| | 1.2895 | 3.5 − |
| | 1.5365 | 3.5 − |
| | 1.9736 | 2.5 − |
| | 2.1724 | 5.5 − |
| | 2.2332 | 4.5 − |
| | 2.3205 | 1.5 − |
| | 2.4530 | 3.5 − |
| | 2.6570 | 2.5 − |
| | 2.6700 | 0.5 − |
| 24055 | 0.0000 | 1.5 − |
| | 0.2440 | 0.5 − |
| | 0.5210 | 2.5 − |
| | 0.5720 | 1.5 − |
| | 0.8850 | 2.5 − |
| 25051 | 0.0000 | 2.5 − |
| | 0.2370 | 3.5 − |
| | 1.1395 | 4.5 − |
| | 1.4881 | 5.5 − |
| | 1.8170 | 1.5 + |
| | 1.8246 | 1.5 − |
| | 1.9589 | 0.5 − |
| | 2.1403 | 1.5 − |
| | 2.2559 | 3.5 − |
| | 2.2759 | 0.5 + |

| Nucleus | Level Energy (MeV) | Spin Parity |
|---|---|---|
| 25052 | 0.0000 | 6.0 + |
| | 0.3778 | 2.0 + |
| | 0.5459 | 1.0 + |
| | 0.7315 | 4.0 + |
| | 0.8252 | 3.0 + |
| | 0.8697 | 7.0 + |
| 25053 | 0.0000 | 3.5 − |
| | 0.3780 | 2.5 − |
| | 1.2897 | 1.5 − |
| | 1.4414 | 5.5 − |
| | 1.6210 | 4.5 − |
| | 2.2740 | 2.5 − |
| | 2.4070 | 1.5 − |
| | 2.5630 | 6.5 − |
| | 2.5730 | 3.5 − |
| | 2.6710 | 0.5 − |
| | 2.6870 | 3.5 − |
| | 2.6935 | 7.5 − |
| | 2.6973 | 5.5 − |
| | 2.7070 | 0.5 + |
| 25054 | 0.0000 | 3.0 + |
| | 0.0545 | 2.0 + |
| | 0.1562 | 4.0 + |
| | 0.3680 | 5.0 + |
| | 0.4078 | 3.0 + |
| | 0.8389 | 4.0 + |
| | 1.0097 | 3.0 + |
| | 1.0732 | 6.0 + |
| | 1.1366 | 5.0 + |
| | 1.3745 | 3.0 + |
| | 1.3905 | 1.0 + |
| | 1.4542 | 1.0 + |
| | 1.5085 | 3.0 + |
| | 1.5437 | 3.0 + |
| | 1.6340 | 2.0 + |
| | 1.6508 | 1.0 + |
| | 1.7840 | 7.0 + |

| Nucleus | Level Energy (MeV) | Spin Parity |
|---|---|---|
| 25055 | 0.0000 | 2.5 − |
| | 0.1260 | 3.5 − |
| | 0.9843 | 4.5 − |
| | 1.2922 | 5.5 − |
| | 1.5298 | 1.5 − |
| | 1.8850 | 3.5 − |
| | 2.1985 | 3.5 − |
| | 2.2153 | 2.5 − |
| | 2.2525 | 1.5 − |
| | 2.2690 | 0.5 − |
| | 2.3118 | 6.5 − |
| | 2.3660 | 2.5 − |
| 25056 | 0.0000 | 3.0 + |
| | 0.0266 | 2.0 + |
| | 0.1105 | 1.0 + |
| | 0.2120 | 4.0 + |
| | 0.2150 | 2.0 + |
| | 0.3355 | 5.0 + |
| | 0.3410 | 3.0 + |
| | 0.4540 | 4.0 + |
| | 0.4860 | 3.0 + |
| | 0.7160 | 3.0 + |
| | 0.7540 | 3.0 + |
| | 0.8400 | 3.0 + |
| | 0.8530 | 1.0 + |
| | 1.1660 | 1.0 + |
| 25057 | 0.0000 | 2.5 − |
| 25058 | 0.0000 | 3.0 + |
| 26051 | 0.0000 | 2.5 − |
| | 0.2700 | 3.5 − |
| 26052 | 0.0000 | 0.0 + |
| | 0.8400 | 2.0 + |
| | 2.3600 | 4.0 + |
| | 2.7400 | 2.0 + |
| | 3.5500 | 2.0 + |
| | 3.5900 | 4.0 + |

| Nucleus | Level Energy (MeV) | Spin Parity |
|---|---|---|
| 26053 | 0.0000 | 3.5 − |
| | 0.7420 | 1.5 − |
| | 1.3280 | 4.5 − |
| | 1.4240 | 2.5 − |
| | 1.6970 | 3.5 − |
| | 2.0430 | 1.5 − |
| | 2.3390 | 5.5 − |
| 26054 | 0.0000 | 0.0 + |
| | 1.4084 | 2.0 + |
| | 2.5384 | 4.0 + |
| | 2.5613 | 0.0 + |
| | 2.9500 | 6.0 + |
| | 2.9590 | 2.0 + |
| | 3.1661 | 2.0 + |
| | 3.2952 | 4.0 + |
| | 3.3450 | 3.0 + |
| | 3.8340 | 4.0 + |
| | 4.0290 | 3.0 + |
| | 4.0480 | 4.0 + |
| | 4.0740 | 3.0 + |
| | 4.2650 | 4.0 + |
| | 4.2920 | 0.0 + |
| | 4.5790 | 2.0 + |
| 26055 | 0.0000 | 1.5 − |
| | 0.4115 | 0.5 − |
| | 0.9313 | 2.5 − |
| | 1.3167 | 3.5 − |
| | 1.4086 | 3.5 − |
| | 1.9190 | 0.5 − |
| | 2.0520 | 1.5 − |
| | 2.1442 | 2.5 − |
| | 2.2119 | 4.5 − |
| | 2.3009 | 4.5 − |
| | 2.4700 | 1.5 − |
| | 2.5390 | 5.5 − |
| | 2.5779 | 2.5 − |
| | 2.8130 | 6.5 − |
| | 2.8720 | 2.5 − |
| | 2.9390 | 3.5 − |
| | 2.9830 | 5.5 − |
| | 2.9840 | 1.5 − |
| | 3.0270 | 1.5 − |
| | 3.0720 | 4.5 − |
| | 3.1090 | 2.5 − |

| Nucleus | Level Energy (MeV) | Spin Parity |
|---|---|---|
| 26056 | 0.0000 | 0.0 + |
| | 0.8468 | 2.0 + |
| | 2.0851 | 4.0 + |
| | 2.6576 | 2.0 + |
| | 2.9417 | 0.0 + |
| | 2.9600 | 2.0 + |
| | 3.1200 | 1.0 + |
| | 3.1230 | 4.0 + |
| | 3.3702 | 2.0 + |
| | 3.3880 | 6.0 + |
| | 3.4450 | 3.0 + |
| | 3.4500 | 1.0 + |
| | 3.6019 | 2.0 + |
| | 3.6070 | 0.0 + |
| | 3.7558 | 6.0 + |
| | 3.8320 | 2.0 + |
| | 3.8565 | 3.0 + |
| | 4.0490 | 3.0 + |
| | 4.1003 | 3.0 + |
| | 4.1200 | 4.0 + |
| | 4.2980 | 4.0 + |
| | 4.3020 | 0.0 + |
| | 4.3950 | 3.0 + |
| | 4.4010 | 2.0 + |
| | 4.4580 | 3.0 + |
| | 4.5100 | 3.0 − |
| | 4.5395 | 1.0 + |
| | 4.5540 | 3.0 + |
| | 4.6120 | 2.0 + |
| | 4.6600 | 3.0 + |
| | 4.6847 | 3.0 + |
| | 4.7299 | 0.0 + |
| | 4.7396 | 2.0 + |
| | 4.8780 | 2.0 + |
| 26057 | 0.0000 | 0.5 − |
| | 0.0144 | 1.5 − |
| | 0.1365 | 2.5 − |
| | 0.3667 | 1.5 − |
| | 0.7064 | 2.5 − |
| | 1.0071 | 3.5 − |
| | 1.1980 | 4.5 − |
| | 1.2650 | 0.5 − |
| | 1.3657 | 3.5 − |
| | 1.6277 | 1.5 − |
| | 1.7257 | 1.5 − |
| | 1.9750 | 0.5 − |
| | 1.9894 | 4.5 − |
| | 2.1170 | 2.5 − |
| | 2.2070 | 2.5 − |
| | 2.2190 | 1.5 − |
| | 2.3350 | 0.5 − |
| | 2.3550 | 5.5 − |
| | 2.4550 | 4.5 + |
| | 2.5060 | 2.5 + |

APPENDIX B

LISTING OF THE $^{54}Fe$ AND $^{56}Fe$ DOSIMETRY FILES IN ENDF/B FORMAT
(See Table VI in the text for definition of the MT numbers)

```
2,6050E+04 5.5365E+01          0          0          1          0265410 16     0
0.        -1.3379E+07          0          0          2          35265410 16    1
         2          2         35          5                     265410 16     2
1,3620E+07 0.          1.3750E+07 2.1700E-04 1.4000E+07 1.3900E-03265410 16    3
1,4500E+07 6.7200E-03 1.5000E+07 1.5500E-02 1.5500E+07 2.5840E-02265410 16    4
1,6000E+07 3.7300E-02 1.6500E+07 4.7520E-02 1.7000E+07 5.6800E-02265410 16    5
1,7500E+07 6.4610E-02 1.8000E+07 7.1300E-02 1.8500E+07 7.6480E-02265410 16    6
1,9000E+07 8.0900E-02 1.9500E+07 8.4650E-02 2.0000E+07 8.7500E-02265410 16    7
2,1000E+07 9.1030E-02 2.2000E+07 9.4000E-02 2.3000E+07 9.6780E-02265410 16    8
2,4000E+07 9.8400E-02 2.5000E+07 9.7120E-02 2.6000E+07 9.3000E-02265410 16    9
2.7000E+07 8.7410E-02 2.8000E+07 8.1400E-02 2.9000E+07 7.5679E-02265410 16    10
3,0000E+07 6.9548E-02 3.1000E+07 6.3662E-02 3.2000E+07 5.8662E-02265410 16    11
3,3000E+07 5.4284E-02 3.4000E+07 5.0144E-02 3.5000E+07 4.6364E-02265410 16    12
3,6000E+07 4.2963E-02 3.7000E+07 4.0147E-02 3.8000E+07 3.7491E-02265410 16    13
3.9000E+07 3.5403E-02 4.0000E+07 3.3439E-02                     265410 16     14
                                                                265410  0     15
2,6054E+04 5.5365E+01          0          0          1          0265410 17     0
0.        -2.4062E+07          0          0          2          17265410 17    1
         5          2         17          5                     265410 17     2
2,4497E+07 0.          2.5000E+07 1.4359E-04 2.6000E+07 4.2906E-04265410 17    3
2,7000E+07 7.1453E-04 2.8000E+07 1.0000E-03 2.9000E+07 1.5568E-03265410 17    4
3,0000E+07 2.2490E-03 3.1000E+07 3.0242E-03 3.2000E+07 3.8092E-03265410 17    5
3,3000E+07 4.5560E-03 3.4000E+07 5.2448E-03 3.5000E+07 5.8390E-03265410 17    6
3,6000E+07 6.3049E-03 3.7000E+07 6.6957E-03 3.8000E+07 6.9679E-03265410 17    7
3.9000E+07 7.1728E-03 4.0000E+07 7.2140E-03                     265410 17     8
                                                                265410  0     9
2,6054E+04 5.5365E+01          0          0          1          0265410 22     0
0.        -8.4180E+06          0          0          2          53265410 22    1
        15          2         53          5                     265410 22     2
8,5700E+06 0.          8.6000E+06 1.5309E-07 8.7500E+06 9.1852E-07265410 22    3
8,8000E+06 1.1737E-06 9.0000E+06 2.1942E-06 9.2000E+06 3.2148E-06265410 22    4
9,2500E+06 3.4700E-06 9.4000E+06 4.2354E-06 9.5000E+06 4.7457E-06265410 22    5
9,6000E+06 5.2560E-06 9.7500E+06 6.0214E-06 9.8000E+06 6.2765E-06265410 22    6
1,0000E+07 7.2971E-06 1.0500E+07 9.8486E-06 1.1000E+07 1.2400E-05265410 22    7
1,1500E+07 5.9300E-05 1.2000E+07 6.4800E-05 1.2500E+07 7.4400E-05265410 22    8
1,3000E+07 1.0000E-04 1.3500E+07 2.9400E-04 1.4000E+07 7.0500E-04265410 22    9
1,4500E+07 1.3950E-03 1.5000E+07 2.3300E-03 1.5500E+07 3.8550E-03265410 22    10
1,6000E+07 6.2800E-03 1.6500E+07 1.0160E-02 1.7000E+07 1.6200E-02265410 22    11
1,7500E+07 2.3860E-02 1.8000E+07 3.2200E-02 1.8500E+07 4.1400E-02265410 22    12
1,9000E+07 5.0700E-02 1.9500E+07 5.9790E-02 2.0000E+07 6.8000E-02265410 22    13
2,1000E+07 8.1670E-02 2.2000E+07 9.3200E-02 2.3000E+07 1.0140E-01265410 22    14
2,4000E+07 1.0700E-01 2.5000E+07 1.1350E-01 2.6000E+07 1.1780E-01265410 22    15
2,7000E+07 1.1300E-01 2.8000E+07 9.6000E-02 2.9000E+07 7.4740E-02265410 22    16
3,0000E+07 5.6693E-02 3.1000E+07 4.8954E-02 3.2000E+07 3.3331E-02265410 22    17
3,3000E+07 2.6445E-02 3.4000E+07 2.1091E-02 3.5000E+07 1.6876E-02265410 22    18
3,6000E+07 1.3511E-02 3.7000E+07 1.0813E-02 3.8000E+07 8.5721E-03265410 22    19
3.9000E+07 6.8308E-03 4.0000E+07 5.4317E-03                     265410 22     20
                                                                265410  0     21
2,6054E+04 5.5365E+01          0          0          1          0265410 24     0
0.        -2.1419E+07          0          0          2          20265410 24    1
         4          2         20          5                     265410 24     2
2,1806E+07 0.          2.2000E+07 8.8423E-06 2.3000E+07 5.4421E-05265410 24    3
2,4000E+07 1.0000E-04 2.5000E+07 6.7390E-04 2.6000E+07 3.3480E-03265410 24    4
2,7000E+07 1.1500E-02 2.8000E+07 2.6000E-02 2.9000E+07 4.4564E-02265410 24    5
3,0000E+07 6.6957E-02 3.1000E+07 8.8080E-02 3.2000E+07 1.0190E-01265410 24    6
```

```
3.3000E+07 1.1041E-01 3.4000E+07 1.1855E-01 3.5000E+07 1.2593E-01265410 24     7
3.6000E+07 1.3150E-01 3.7000E+07 1.3658E-01 3.8000E+07 1.4079E-01265410 24     8
3.9000E+07 1.4535E-01 4.0000E+07 1.4852E-01                      265410 24     9
                                                                 265410  0    10

2.6054E+04 5.5365E+01          0          0          1          0265410 25     0
0.        -3.8001E+07          0          0          2          9265410 25     1
        9          2          9          5                     265410 25     2
3.2579E+07 0.         3.3000E+07 2.6723E-09 3.4000E+07 8.8954E-09265410 25     3
3.5000E+07 1.4929E-08 3.6000E+07 2.0760E-08 3.7000E+07 2.6487E-08265410 25     4
3.8000E+07 3.1861E-08 3.9000E+07 3.7275E-08 4.0000E+07 4.2439E-08265410 25     5
                                                                 265410  0     6

2.6054E+04 5.5365E+01          0          0          1          0265410 28     0
0.        -8.8530E+06          0          0          2          49265410 28    1
       10          2         49          5                     265410 28     2
9.0130E+06 0.         9.2000E+06 1.9618E-03 9.2500E+06 2.4863E-03265410 28     3
9.4000E+06 4.0600E-03 9.5000E+06 5.1091E-03 9.6000E+06 6.1582E-03265410 28     4
9.7500E+06 7.7318E-03 9.8000E+06 8.2564E-03 1.0000E+07 1.0355E-02265410 28     5
1.0500E+07 1.5600E-02 1.1000E+07 6.8700E-02 1.1500E+07 1.3900E-01265410 28     6
1.2000E+07 2.1900E-01 1.2500E+07 3.0600E-01 1.3000E+07 3.9700E-01265410 28     7
1.3500E+07 4.8800E-01 1.4000E+07 5.7400E-01 1.4500E+07 6.4600E-01265410 28     8
1.5000E+07 7.0300E-01 1.5500E+07 7.4100E-01 1.6000E+07 7.7100E-01265410 28     9
1.6500E+07 7.9640E-01 1.7000E+07 8.1700E-01 1.7500E+07 8.3180E-01265410 28    10
1.8000E+07 8.4200E-01 1.8500E+07 8.4830E-01 1.9000E+07 8.5200E-01265410 28    11
1.9500E+07 8.5310E-01 2.0000E+07 8.5100E-01 2.1000E+07 8.3870E-01265410 28    12
2.2000E+07 8.2200E-01 2.3000E+07 8.0210E-01 2.4000E+07 7.8000E-01265410 28    13
2.5000E+07 7.5740E-01 2.6000E+07 7.3120E-01 2.7000E+07 6.9940E-01265410 28    14
2.8000E+07 6.6100E-01 2.9000E+07 6.1561E-01 3.0000E+07 5.5964E-01265410 28    15
3.1000E+07 5.0323E-01 3.2000E+07 4.5425E-01 3.3000E+07 4.1113E-01265410 28    16
3.4000E+07 3.7108E-01 3.5000E+07 3.3570E-01 3.6000E+07 3.0534E-01265410 28    17
3.7000E+07 2.8019E-01 3.8000E+07 2.5646E-01 3.9000E+07 2.3728E-01265410 28    18
4.0000E+07 2.1981E-01                                            265410 28    19
                                                                 265410  0    20

2.6054E+04 5.5365E+01          0          0          1          0265410 41     0
0.        -2.0908E+07          0          0          2          20265410 41    1
        4          2         20          5                     265410 41     2
2.1285E+07 0.         2.2000E+07 3.9503E-04 2.3000E+07 9.4751E-04265410 41     3
2.4000E+07 1.5000E-03 2.5000E+07 6.0420E-03 2.6000E+07 1.9610E-02265410 41     4
2.7000E+07 4.9080E-02 2.8000E+07 9.1600E-02 2.9000E+07 1.4019E-01265410 41     5
3.0000E+07 1.9410E-01 3.1000E+07 2.4505E-01 3.2000E+07 2.8474E-01265410 41     6
3.3000E+07 3.1739E-01 3.4000E+07 3.4934E-01 3.5000E+07 3.7688E-01265410 41     7
3.6000E+07 3.9541E-01 3.7000E+07 4.0868E-01 3.8000E+07 4.1661E-01265410 41     8
3.9000E+07 4.2253E-01 4.0000E+07 4.2096E-01                      265410 41     9
                                                                 265410  0    10

2.6054E+04 5.5385E+01          0          0          1          0265410 42     0
0.        -3.1443E+07          0          0          2          9265410 42     1
        5          2          9          5                     265410 42     2
3.2011E+07 0.         3.3000E+07 1.4015E-05 3.4000E+07 2.7796E-05265410 42     3
3.5000E+07 4.1146E-05 3.6000E+07 5.4042E-05 3.7000E+07 3.3763E-04265410 42     4
3.8000E+07 1.4899E-03 3.9000E+07 4.8250E-03 4.0000E+07 1.1627E-02265410 42     5
                                                                 265410  0     6

2.6054E+04 5.5365E+01          0          0          1          0265410103     0
0.         8.5300E+04          0          0          2          123265410103   1
        2          2        123          5                     265410103     2
1.0000E-05 0.         4.6011E+05 3.0000E-05 9.2000E+05 1.0000E-04265410103     3
1.0000E+06 1.6020E-04 1.1000E+06 3.0000E-04 1.2000E+06 5.2600E-04265410103     4
1.3000E+06 9.3314E-04 1.4000E+06 1.7233E-03 1.5000E+06 2.7668E-03265410103     5
1.6000E+06 3.9400E-03 1.7000E+06 5.1916E-03 1.8000E+06 8.8691E-03265410103     6
1.9000E+06 1.3047E-02 2.0000E+06 1.8200E-02 2.1000E+06 2.4428E-02265410103     7
2.2000E+06 3.2027E-02 2.3000E+06 4.1162E-02 2.4000E+06 5.2000E-02265410103     8
2.5000E+06 6.3877E-02 2.6000E+06 7.6012E-02 2.7000E+06 8.8390E-02265410103     9
2.8000E+06 1.0100E-01 2.9000E+06 1.1368E-01 3.0000E+06 1.2644E-01265410103    10
3.1000E+06 1.3947E-01 3.2000E+06 1.5300E-01 3.3000E+06 1.6730E-01265410103    11
3.4000E+06 1.8236E-01 3.5000E+06 1.9800E-01 3.6000E+06 2.1400E-01265410103    12
```

```
3,7000E+06 2,3012E-01 3,8000E+06 2,4660E-01 3,9000E+06 2,6328E-012654 3103     5
4,0000E+06 2,8000E-01 4,1000E+06 2,9691E-01 4,2000E+06 3,1373E-012654 3103     6
4,3000E+06 3,3034E-01 4,4000E+06 3,4664E-01 4,5000E+06 3,6251E-012654 3103     7
4,6000E+06 3,7785E-01 4,7000E+06 3,9256E-01 4,8000E+06 4,0654E-012654 3103     8
4,9000E+06 4,1972E-01 5,0000E+06 4,3200E-01 5,2000E+06 4,5307E-012654 3103     9
5,2500E+06 4,9758E-01 5,4000E+06 4,6939E-01 5,5000E+06 4,7594E-012654 3103    10
5,6000E+06 4,8154E-01 5,7500E+06 4,8832E-01 5,8000E+06 4,9022E-012654 3103    11
6,0000E+06 4,9690E-01 6,2000E+06 5,0050E-01 6,2500E+06 5,0158E-012654 3103    12
6,4000E+06 5,0458E-01 6,5000E+06 5,0634E-01 6,6000E+06 5,0787E-012654 3103    13
6,7500E+06 5,0965E-01 6,8000E+06 5,1009E-01 7,0000E+06 5,1100E-012654 3103    14
7,2000E+06 5,1116E-01 7,2500E+06 5,1118E-01 7,4000E+06 5,1120E-012654 3103    15
7,5000E+06 5,1115E-01 7,6000E+06 5,1105E-01 7,7500E+06 5,1079E-012654 3103    16
7,8000E+06 5,1067E-01 8,0000E+06 5,1000E-01 8,2000E+06 5,0916E-012654 3103    17
8,2500E+06 5,0894E-01 8,4000E+06 5,0822E-01 8,5000E+06 5,0769E-012654 3103    18
8,6000E+06 5,0710E-01 8,7500E+06 5,0609E-01 8,8000E+06 5,0572E-012654 3103    19
9,0000E+06 5,0400E-01 9,2000E+06 5,0173E-01 9,2500E+06 5,0108E-012654 3103    20
9,4000E+06 4,9898E-01 9,5000E+06 4,9753E-01 9,6000E+06 4,9609E-012654 3103    21
9,8000E+06 4,9334E-01 1,0000E+07 4,9100E-01 1,0500E+07 4,8721E-012654 3103    22
1,1000E+07 4,8400E-01 1,1500E+07 4,7738E-01 1,2000E+07 4,6800E-012654 3103    23
1,2500E+07 4,5199E-01 1,3000E+07 4,2500E-01 1,3500E+07 3,8761E-012654 3103    24
1,4000E+07 3,4800E-01 1,4500E+07 3,0407E-01 1,5000E+07 2,6500E-012654 3103    25
1,5500E+07 2,2836E-01 1,6000E+07 1,9500E-01 1,6500E+07 1,6475E-012654 3103    26
1,7000E+07 1,4000E-01 1,7500E+07 1,2080E-01 1,8000E+07 1,0500E-01265410103    33
1,8500E+07 9,1930E-02 1,9000E+07 8,1200E-02 1,9500E+07 7,2660E-02265410103    34
2,0000E+07 6,5800E-02 2,1000E+07 5,5000E-02 2,2000E+07 4,6900E-02265410103    35
2,3000E+07 4,0640E-02 2,4000E+07 3,6100E-02 2,5000E+07 3,2710E-02265410103    36
2,6000E+07 2,9700E-02 2,7000E+07 2,7240E-02 2,8000E+07 2,5000E-02265410103    37
2,9000E+07 2,2992E-02 3,0000E+07 2,0924E-02 3,1000E+07 1,9009E-02265410103    38
3,2000E+07 1,7427E-02 3,3000E+07 1,6289E-02 3,4000E+07 1,5460E-02265410103    39
3,5000E+07 1,4707E-02 3,6000E+07 1,3871E-02 3,7000E+07 1,3027E-02265410103    40
3,8000E+07 1,2142E-02 3,9000E+07 1,1373E-02 4,0000E+07 1,0609E-02265410103    41
                                                                265410  0     42
2,6050E+04 5,5365E+01          0          0          1          0265410107     0
0.         8,4290E+05          0          0          2         11265410107     1
        23          2        117          5                     265410107     2
1,0000E-05 0.          1,0000E+06 1,0192E-05 1,1000E+06 1,1400E-05265410107     3
1,2000E-06 1,2633E-05 1,3000E+06 1,3887E-05 1,4000E+06 1,5160E-05265410107     4
1,5000E+06 1,6449E-05 1,6000E+06 1,7752E-05 1,7000E+06 1,9066E-05265410107     5
1,8000E+06 2,0389E-05 1,9000E+06 2,1718E-05 2,0000E+06 2,3051E-05265410107     6
2,1000E+06 2,4384E-05 2,2000E+06 2,5716E-05 2,3000E+06 2,7043E-05265410107     7
2,4000E+06 2,8364E-05 2,5000E+06 2,9675E-05 2,6000E+06 3,0974E-05265410107     8
2,7000E+06 3,2259E-05 2,8000E+06 3,3527E-05 2,9000E+06 3,4774E-05265410107     9
3,0000E+06 3,6000E-05 3,1000E+06 3,7633E-05 3,2000E+06 4,0000E-05265410107    10
3,3000E+06 8,8300E-05 3,4000E+06 1,9000E-04 3,5000E+06 3,3910E-04265410107    11
3,6000E+06 5,4000E-04 3,7000E+06 7,5330E-04 3,8000E+06 9,6000E-04265410107    12
3,9000E+06 1,1530E-03 4,0000E+06 1,3700E-03 4,1000E+06 1,6130E-03265410107    13
4,2000E+06 1,8900E-03 4,3000E+06 2,2000E-03 4,4000E+06 2,5100E-03265410107    14
4,5000E+06 2,7600E-03 4,6000E+06 3,0600E-03 4,7000E+06 3,3850E-03265410107    15
4,8000E+06 3,7140E-03 4,9000E+06 4,0450E-03 5,0000E+06 4,3900E-03265410107    16
5,2000E+06 5,0560E-03 5,2500E+06 5,2220E-03 5,4000E+06 5,7870E-03265410107    17
5,6000E+06 6,8820E-03 5,7500E+06 8,0240E-03 5,8000E+06 8,4540E-03265410107    18
6,0000E+06 1,0300E-02 6,2000E+06 1,2310E-02 6,2500E+06 1,2850E-02265410107    19
6,4000E+06 1,4580E-02 6,6000E+06 1,7060E-02 6,7500E+06 1,8990E-02265410107    20
6,8000E+06 1,9660E-02 7,0000E+06 2,2400E-02 7,2000E+06 2,5270E-02265410107    21
7,2500E+06 2,6000E-02 7,4000E+06 2,8210E-02 7,6000E+06 3,1190E-02265410107    22
7,7500E+06 3,3400E-02 7,8000E+06 3,4130E-02 8,0000E+06 3,6900E-02265410107    23
8,2000E+06 3,9490E-02 8,2500E+06 4,0120E-02 8,4000E+06 4,1980E-02265410107    24
8,6000E+06 4,4410E-02 8,7500E+06 4,6200E-02 8,8000E+06 4,6780E-02265410107    25
9,0000E+06 4,9000E-02 9,2000E+06 5,0970E-02 9,2500E+06 5,1410E-02265410107    26
9,4000E+06 5,2570E-02 9,6000E+06 5,3730E-02 9,7500E+06 5,4460E-02265410107    27
9,8000E+06 5,4690E-02 1,0000E+07 5,5700E-02 1,0500E+07 5,8600E-02265410107    28
1,1000E+07 6,0500E-02 1,1500E+07 6,1700E-02 1,2000E+07 6,3800E-02265410107    29
```

```
1,2500E+07 6,5400E-02 1,3000E+07 6,7000E-02 1,3500E+07 6,8600E-02265410107    30
1,4000E+07 7,0100E-02 1,4500E+07 7,1600E-02 1,5000E+07 7,2900E-02265410107    31
1,5500E+07 7,4110E-02 1,6000E+07 7,5200E-02 1,6500E+07 7,4480E-02265410107    32
1,7000E+07 7,1600E-02 1,7500E+07 6,7470E-02 1,8000E+07 6,1900E-02265410107    33
1,8500E+07 5,5680E-02 1,9000E+07 4,9400E-02 1,9500E+07 4,3460E-02265410107    34
2,0000E+07 3,8003E-02 2,1000E+07 2,8730E-02 2,2000E+07 2,2000E-02265410107    35
2,3000E+07 1,7180E-02 2,4000E+07 1,3700E-02 2,5000E+07 1,1230E-02265410107    36
2,6000E+07 9,4030E-03 2,7000E+07 7,9400E-03 2,8000E+07 6,7000E-03265410107    37
2,9000E+07 5,6035E-03 3,0000E+07 4,6162E-03 3,1000E+07 3,8192E-03265410107    38
3,2000E+07 3,2378E-03 3,3000E+07 2,8046E-03 3,4000E+07 2,4454E-03265410107    39
3,5000E+07 2,1461E-03 3,6000E+07 1,8915E-03 3,7000E+07 1,6779E-03265410107    40
3,8000E+07 1,4847E-03 3,9000E+07 1,3269E-03 4,0000E+07 1,1882E-03265410107    41
                                                          265410  0           42
                                                          2654 0  0
                                                            0 0  0
2,6056E+04 5,5365E+01          0          0          1          0265610 16     0
0.        -1,1197E+07          0          0          2          39265610 16    1
        2          2          39          5                     265610 16     2
1,1399E+07 0.          1,1500E+07 5,7900E-03 1,2000E+07 6,6800E-02265610 16    3
1,2500E+07 1,5260E-01 1,3000E+07 2,4970E-01 1,3500E+07 3,4270E-01265610 16     4
1,4000E+07 4,2390E-01 1,4500E+07 4,8650E-01 1,5000E+07 5,3680E-01265610 16     5
1,5500E+07 5,7250E-01 1,6000E+07 5,9830E-01 1,6500E+07 6,1730E-01265610 16     6
1,7000E+07 6,2820E-01 1,7500E+07 6,3220E-01 1,8000E+07 6,3470E-01265610 16     7
1,8500E+07 6,3620E-01 1,9000E+07 6,3690E-01 1,9500E+07 6,3490E-01265610 16     8
2,0000E+07 6,3030E-01 2,1000E+07 6,1490E-01 2,2000E+07 5,9410E-01265610 16     9
2,3000E+07 5,6850E-01 2,4000E+07 5,3040E-01 2,5000E+07 4,8180E-01265610 16     10
2,6000E+07 4,3230E-01 2,7000E+07 3,8570E-01 2,8000E+07 3,4650E-01265610 16     11
2,9000E+07 3,1445E-01 3,0000E+07 2,8282E-01 3,1000E+07 2,5422E-01265610 16     12
3,2000E+07 2,3074E-01 3,3000E+07 2,1094E-01 3,4000E+07 1,9297E-01265610 16     13
3,5000E+07 1,7682E-01 3,6000E+07 1,6249E-01 3,7000E+07 1,5027E-01265610 16     14
3,8000E+07 1,3852E-01 3,9000E+07 1,2898E-01 4,0000E+07 1,2009E-01265610 16     15
                                                          265610  0           16
2,6056E+04 5,5365E+01          0          0          1          0265610 17     0
0.        -2,0496E+07          0          0          2          21265610 17    1
        3          2          21          5                     265610 17     2
2,0866E+07 0.          2,1000E+07 1,1817E-04 2,2000E+07 1,0000E-03265610 17    3
2,3000E+07 5,7140E-03 2,4000E+07 1,8000E-02 2,5000E+07 3,4880E-02265610 17     4
2,6000E+07 5,3700E-02 2,7000E+07 7,2850E-02 2,8000E+07 9,0300E-02265610 17     5
2,9000E+07 1,0282E-01 3,0000E+07 1,1289E-01 3,1000E+07 1,1996E-01265610 17     6
3,2000E+07 1,2380E-01 3,3000E+07 1,2549E-01 3,4000E+07 1,2552E-01265610 17     7
3,5000E+07 1,2401E-01 3,6000E+07 1,2069E-01 3,7000E+07 1,1666E-01265610 17     8
3,8000E+07 1,1139E-01 3,9000E+07 1,0624E-01 4,0000E+07 1,0015E-01265610 17     9
                                                          265610  0           10
2,6056E+04 5,5365E+01          0          0          1          0265610 22     0
0.        -7,6140E+06          0          0          2          59265610 22    1
       20          2          59          5                     265610 22     2
7,7510E+06 0.          7,8000E+06 2,8324E-07 8,0000E+06 1,4393E-06265610 22    3
8,2000E+06 2,5954E-06 8,2500E+06 2,8844E-06 8,4000E+06 3,7514E-06265610 22     4
8,5000E+06 4,3295E-06 8,6000E+06 4,9075E-06 8,7500E+06 5,7746E-06265610 22     5
8,8000E+06 6,0636E-06 9,0000E+06 7,2197E-06 9,2000E+06 8,3757E-06265610 22     6
9,2500E+06 8,6647E-06 9,4000E+06 9,5318E-06 9,5000E+06 1,0110E-05265610 22     7
9,6000E+06 1,0688E-05 9,7500E+06 1,1555E-05 9,8000E+06 1,1844E-05265610 22     8
1,0000E+07 1,3000E-05 1,0500E+07 3,1000E-04 1,1000E+07 9,6600E-04265610 22     9
1,1500E+07 1,7000E-03 1,2000E+07 1,7500E-03 1,2500E+07 2,0500E-03265610 22     10
1,3000E+07 2,5900E-03 1,3500E+07 3,0400E-03 1,4000E+07 3,4700E-03265610 22     11
1,4500E+07 4,0600E-03 1,5000E+07 5,2300E-03 1,5500E+07 7,2460E-03265610 22     12
1,6000E+07 9,9400E-03 1,6500E+07 1,3270E-02 1,7000E+07 1,7390E-02265610 22     13
1,7500E+07 2,2050E-08 1,8000E+07 2,6900E-02 1,8500E+07 3,1730E-02265610 22     14
1,9000E+07 3,6500E-02 1,9500E+07 4,1350E-02 2,0000E+07 4,5600E-02265610 22     15
2,1000E+07 5,2060E-02 2,2000E+07 5,7800E-02 2,3000E+07 6,3350E-02265610 22     16
```

```
2.4000E+07 6.7960E-02 2.5000E+07 6.9760E-02 2.6000E+07 6.9600E-02265610 22   17
2.7000E+07 6.8540E-02 2.8000E+07 6.5000E-02 2.9000E+07 5.8613E-02265610 22   18
3.0000E+07 5.0151E-02 3.1000E+07 4.1621E-02 3.2000E+07 3.4283E-02265610 22   19
3.3000E+07 2.7848E-02 3.4000E+07 2.2289E-02 3.5000E+07 1.7975E-02265610 22   20
3.6000E+07 1.4862E-02 3.7000E+07 1.2653E-02 3.8000E+07 1.0869E-02265610 22   21
3.9000E+07 9.5465E-03 4.0000E+07 8.4870E-03                     265610 22   22
                                                                265610  0   23
2.6056E+04 5.5365E+01          0          0          1          0265610 24    0
0.        -1.9653E+07          0          0          2         21265610 24    1
        5          2         21          5                     265610 24    2
2.0008E+07 0.         2.1000E+07 6.2124E-07 2.2000E+07 1.2475E-06265610 24    3
2.3000E+07 1.8737E-06 2.4000E+07 2.5000E-06 2.5000E+07 1.1830E-05265610 24    4
2.6000E+07 6.7900E-05 2.7000E+07 6.8330E-04 2.8000E+07 4.9400E-03265610 24    5
2.9000E+07 1.2910E-02 3.0000E+07 2.3376E-02 3.1000E+07 3.3963E-02265610 24    6
3.2000E+07 4.0568E-02 3.3000E+07 4.7717E-02 3.4000E+07 5.5328E-02265610 24    7
3.5000E+07 6.2325E-02 3.6000E+07 6.7282E-02 3.7000E+07 7.1038E-02265610 24    8
3.8000E+07 7.3988E-02 3.9000E+07 7.6407E-02 4.0000E+07 7.6977E-02265610 24    9
                                                                265610  0   10
2.6056E+04 5.5365E+01          0          0          1          0265610 25    0
0.        -2.8914E+07          0          0          2         12265610 25    1
        8          2         12          5                     265610 25    2
2.9436E+07 0.         3.0000E+07 4.2322E-08 3.1000E+07 1.1507E-07265610 25    3
3.2000E+07 1.8599E-07 3.3000E+07 2.5576E-07 3.4000E+07 3.2300E-07265610 25    4
3.5000E+07 3.8789E-07 3.6000E+07 4.5035E-07 3.7000E+07 8.5016E-07265610 25    5
3.8000E+07 1.8597E-06 3.9000E+07 4.7155E-06 4.0000E+07 1.3579E-05265610 25    6
                                                                265610  0    7
2.6056E+04 5.5365E+01          0          0          1          0265610 28    0
0.        -1.0183E+07          0          0          2         41265610 28    1
        4          2         41          5                     265610 28    2
1.0367E+07 0.         1.0500E+07 3.1460E-05 1.1000E+07 1.4973E-04265610 28    3
1.1500E+07 2.6800E-04 1.2000E+07 7.8970E-03 1.2500E+07 2.3860E-02265610 28    4
1.3000E+07 4.0480E-02 1.3500E+07 5.6000E-02 1.4000E+07 7.2950E-02265610 28    5
1.4500E+07 9.1600E-02 1.5000E+07 1.1100E-01 1.5500E+07 1.2950E-01265610 28    6
1.6000E+07 1.4800E-01 1.6500E+07 1.6730E-01 1.7000E+07 1.8500E-01265610 28    7
1.7500E+07 1.9960E-01 1.8000E+07 2.1300E-01 1.8500E+07 2.2640E-01265610 28    8
1.9000E+07 2.3900E-01 1.9500E+07 2.4990E-01 2.0000E+07 2.5960E-01265610 28    9
2.1000E+07 2.7750E-01 2.2000E+07 2.9400E-01 2.3000E+07 3.0750E-01265610 28   10
2.4000E+07 3.1800E-01 2.5000E+07 3.2370E-01 2.6000E+07 3.2100E-01265610 28   11
2.7000E+07 3.0900E-01 2.8000E+07 2.8600E-01 2.9000E+07 2.5939E-01265610 28   12
3.0000E+07 2.3268E-01 3.1000E+07 2.0815E-01 3.2000E+07 1.8760E-01265610 28   13
3.3000E+07 1.7005E-01 3.4000E+07 1.5404E-01 3.5000E+07 1.3975E-01265610 28   14
3.6000E+07 1.2700E-01 3.7000E+07 1.1604E-01 3.8000E+07 1.0564E-01265610 28   15
3.9000E+07 9.7102E-02 4.0000E+07 8.9114E-02                     265610 28   16
                                                                265610  0   17
2.6056E+04 5.5365E+01          0          0          1          0265610 37    0
0.        -3.3874E+07          0          0          2          7265610 37    1
        7          2          7          5                     265610 37    2
3.4480E+07 0.         3.5000E+07 8.6216E-05 3.6000E+07 2.4802E-04265610 37    3
3.7000E+07 4.0594E-04 3.8000E+07 5.5625E-04 3.9000E+07 7.0551E-04265610 37    4
4.0000E+07 8.4870E-04                                           265610 37    5
                                                                265610  0    6
2.6056E+04 5.5365E+01          0          0          1          0265610 41    0
0.        -2.0410E+07          0          0          2         21265610 41    1
        3          2         21          5                     265610 41    2
2.0779E+07 0.         2.1000E+07 9.8500E-05 2.2000E+07 5.0000E-04265610 41    3
2.3000E+07 1.6430E-03 2.4000E+07 5.1100E-03 2.5000E+07 1.5130E-02265610 41    4
2.6000E+07 4.2100E-02 2.7000E+07 8.3410E-02 2.8000E+07 1.1800E-01265610 41    5
2.9000E+07 1.5757E-01 3.0000E+07 2.0037E-01 3.1000E+07 2.4186E-01265610 41    6
3.2000E+07 2.7712E-01 3.3000E+07 3.0684E-01 3.4000E+07 3.3327E-01265610 41    7
3.5000E+07 3.5487E-01 3.6000E+07 3.6749E-01 3.7000E+07 3.7560E-01265610 41    8
```

```
3.8000E+07 3.7710E-01 3.9000E+07 3.7609E-01 4.0000E+07 3.6834E-01265610 41    9
                                                                 265610  0   10
2.6056E+04 5.5365E+01          0          0          1           0265610 42    0
0.        -2.9349E+07          0          0          2          12265610 42    1
        4           2         12          5                     265610 42    2
2.9879E+07 0.          3.0000E+07 5.6199E-10 3.1000E+07 5.1050E-09265610 42    3
3.2000E+07 9.5230E-09 3.3000E+07 1.0344E-06 3.4000E+07 4.6213E-05265610 42    4
3.5000E+07 9.1438E-04 3.6000E+07 8.5927E-03 3.7000E+07 1.7339E-02265610 42    5
3.8000E+07 3.2711E-02 3.9000E+07 4.4803E-02 4.0000E+07 6.5095E-02265610 42    6
                                                                 265610  0    7
2.6056E+04 5.5365E+01          0          0          1           0265610103    0
0.        -2.9130E+06          0          0          2          90265610103    1
       15           2         90          5                     265610103    2
2.9660E+06 0.          3.0000E+06 3.0308E-06 3.1000E+06 1.1945E-05265610103    3
3.2000E+06 2.0859E-05 3.3000E+06 2.9773E-05 3.4000E+06 3.8687E-05265610103    4
3.5000E+06 4.7601E-05 3.6000E+06 5.6515E-05 3.7000E+06 6.5429E-05265610103    5
3.8000E+06 7.4344E-05 3.9000E+06 8.3258E-05 4.0000E+06 9.2172E-05265610103    6
4.1000E+06 1.0109E-04 4.2000E+06 1.1000E-04 4.3000E+06 2.1210E-04265610103    7
4.4000E+06 3.7660E-04 4.5000E+06 5.9780E-04 4.6000E+06 8.2600E-04265610103    8
4.7000E+06 1.0180E-03 4.8000E+06 1.2000E-03 4.9000E+06 1.4269E-032656 3103    4
5.0000E+06 1.7300E-03 5.2000E+06 2.6468E-03 5.2500E+06 2.9400E-032656 3103    5
5.4000E+06 4.0158E-03 5.5000E+06 4.9328E-03 5.6000E+06 6.0416E-032656 3103    6
5.7500E+06 8.1297E-03 5.8000E+06 8.9545E-03 6.0000E+06 1.3000E-022656 3103    7
6.2000E+06 1.7877E-02 6.4000E+06 2.2895E-02 6.6000E+06 2.7798E-022656 3103    8
6.8000E+06 3.2482E-02 7.0000E+06 3.7000E-02 7.2000E+06 4.1576E-022656 3103    9
7.4000E+06 4.6189E-02 7.6000E+06 5.0585E-02 7.8000E+06 5.4484E-022656 3103   10
8.0000E+06 5.7600E-02 8.2000E+06 6.0256E-02 8.4000E+06 6.2928E-022656 3103   11
8.6000E+06 6.5572E-02 8.8000E+06 6.8144E-02 9.0000E+06 7.0600E-022656 3103   12
9.2000E+06 7.3019E-02 9.4000E+06 7.5477E-02 9.6000E+06 7.7926E-022656 3103   13
9.8000E+06 8.0316E-02 1.0000E+07 8.2600E-02 1.0500E+07 8.8006E-022656 3103   14
1.1000E+07 9.3200E-02 1.1500E+07 9.8161E-02 1.2000E+07 1.0300E-012656 3103   15
1.2500E+07 1.0783E-01 1.3000E+07 1.1100E-01 1.3500E+07 1.0957E-012656 3103   16
1.4000E+07 1.0600E-01 1.4500E+07 1.0359E-01 1.5000E+07 9.8900E-022656 3103   17
1.5500E+07 8.9411E-08 1.6000E+07 7.9200E-02 1.6500E+07 7.0254E-022656 3103   18
1.7000E+07 6.2700E-02 1.7500E+07 5.8870E-02 1.8000E+07 5.5500E-02265610103   23
1.8500E+07 5.0400E-02 1.9000E+07 4.5900E-02 1.9500E+07 4.2240E-02265610103   24
2.0000E+07 3.9100E-02 2.1000E+07 3.4390E-02 2.2000E+07 3.0500E-02265610103   25
2.3000E+07 2.6300E-02 2.4000E+07 2.3000E-02 2.5000E+07 2.0890E-02265610103   26
2.6000E+07 1.9200E-02 2.7000E+07 1.7730E-02 2.8000E+07 1.6500E-02265610103   27
2.9000E+07 1.5498E-02 3.0000E+07 1.4432E-02 3.1000E+07 1.3387E-02265610103   28
3.2000E+07 1.2475E-02 3.3000E+07 1.1654E-02 3.4000E+07 1.0861E-02265610103   29
3.5000E+07 1.0131E-02 3.6000E+07 9.4574E-03 3.7000E+07 8.8653E-03265610103   30
3.8000E+07 8.2685E-03 3.9000E+07 7.7751E-03 4.0000E+07 7.2988E-03265610103   31
                                                                 265610  0   32
2.6056E+04 5.5365E+01          0          0          1           0265610107    0
0.        -3.2610E+05          0          0          2         107265610107    1
       23           2        107          5                     265610107    2
1.0000E-05 0.          1.0000E+06 2.9010E-06 1.1000E+06 3.2384E-06265610107    3
1.2000E+06 3.5840E-06 1.3000E+06 3.9377E-06 1.4000E+06 4.2995E-06265610107    4
1.5000E+06 4.6692E-06 1.6000E+06 5.0468E-06 1.7000E+06 5.4322E-06265610107    5
1.8000E+06 5.8253E-06 1.9000E+06 6.2260E-06 2.0000E+06 6.6343E-06265610107    6
2.1000E+06 7.0499E-06 2.2000E+06 7.4729E-06 2.3000E+06 7.9031E-06265610107    7
2.4000E+06 8.3405E-06 2.5000E+06 8.7849E-06 2.6000E+06 9.2363E-06265610107    8
2.7000E+06 9.6947E-06 2.8000E+06 1.0160E-05 2.9000E+06 1.0632E-05265610107    9
3.0000E+06 1.1110E-05 3.1000E+06 1.1730E-05 3.2000E+06 1.2660E-05265610107   10
3.3000E+06 1.3790E-05 3.4000E+06 1.5000E-05 3.5000E+06 1.6380E-05265610107   11
3.6000E+06 1.8410E-05 3.7000E+06 2.1640E-05 3.8000E+06 2.7000E-05265610107   12
3.9000E+06 4.1850E-05 4.0000E+06 8.0780E-05 4.1000E+06 1.5920E-04265610107   13
4.2000E+06 2.7000E-04 4.3000E+06 4.0330E-04 4.4000E+06 5.8400E-04265610107   14
4.5000E+06 7.8850E-04 4.6000E+06 9.6000E-04 4.7000E+06 1.0920E-03265610107   15
```

```
4.8000E+06 1.2280E-03 4.9000E+06 1.3650E-03 5.0000E+06 1.5000E-03265610107   16
5.2000E+06 1.7830E-03 5.4000E+06 2.1000E-03 5.6000E+06 2.4330E-03265610107   17
5.8000E+06 2.7410E-03 6.0000E+06 3.1500E-03 6.2000E+06 3.8820E-03265610107   18
6.4000E+06 4.9210E-03 6.6000E+06 5.9970E-03 6.8000E+06 7.1810E-03265610107   19
7.0000E+06 8.4700E-03 7.2000E+06 9.8190E-03 7.4000E+06 1.1200E-02265610107   20
7.6000E+06 1.2590E-02 7.8000E+06 1.3970E-02 8.0000E+06 1.5300E-02265610107   21
8.2000E+06 1.6580E-02 8.4000E+06 1.7810E-02 8.6000E+06 1.8970E-02265610107   22
8.8000E+06 2.0080E-02 9.0000E+06 2.1100E-02 9.2000E+06 2.2030E-02265610107   23
9.4000E+06 2.2900E-02 9.6000E+06 2.3690E-02 9.8000E+06 2.4440E-02265610107   24
1.0000E+07 2.5100E-02 1.0500E+07 2.6500E-02 1.1000E+07 2.7700E-02265610107   25
1.1500E+07 2.8900E-02 1.2000E+07 2.9600E-02 1.2500E+07 3.1000E-02265610107   26
1.3000E+07 3.1600E-02 1.3500E+07 3.2500E-02 1.4000E+07 3.3500E-02265610107   27
1.4500E+07 3.4100E-02 1.5000E+07 3.4200E-02 1.5500E+07 3.3860E-02265610107   28
1.6000E+07 3.3000E-02 1.6500E+07 3.1370E-02 1.7000E+07 2.9100E-02265610107   29
1.7500E+07 2.8660E-02 1.8000E+07 2.4100E-02 1.8500E+07 2.1560E-02265610107   30
1.9000E+07 1.9100E-02 1.9500E+07 1.6800E-02 2.0000E+07 1.4800E-02265610107   31
2.1000E+07 1.1560E-02 2.2000E+07 9.1000E-03 2.3000E+07 6.7630E-03265610107   32
2.4000E+07 5.2000E-03 2.5000E+07 4.3710E-03 2.6000E+07 3.7000E-03265610107   33
2.7000E+07 3.1510E-03 2.8000E+07 2.7000E-03 2.9000E+07 2.3321E-03265610107   34
3.0000E+07 2.0106E-03 3.1000E+07 1.7396E-03 3.2000E+07 1.5237E-03265610107   35
3.3000E+07 1.3585E-03 3.4000E+07 1.2236E-03 3.5000E+07 1.1046E-03265610107   36
3.6000E+07 9.9077E-04 3.7000E+07 8.8547E-04 3.8000E+07 7.8472E-04265610107   37
3.9000E+07 6.9884E-04 4.0000E+07 6.1955E-04                     265610107   38
                                                                265610  0   39
                                                                2656 0  0
                                                                   0 0  0
                                                                  -1
```

REFERENCES


1. C. R. Head, "Nuclear Data Requirements of the Magnetic Fusion Power Program of the United States of America," presented at the IAEA Advisory Group Meeting on Nuclear Data for Fusion Reactor Technology, Vienna, Austria (Dec. 11-15, 1978).

2. C. Y. Fu and F. G. Perey, EDNF/B-V data file for natural Fe (MAT 1326), summarized in BNL-NCS-17541 (ENDF 201) compiled by R. Kinsey, National Nuclear Data Center, Brookhaven National Laboratory, Upton, NY (July 1979).

3. W. Hauser and H. Feshbach, "The Inelastic Scattering of Neutrons," Phys. Rev. 87, 366 (1952).

4. J. P. Delaroche, Ch. Lagrange, and J. Salvy, "The Optical Model with Particular Considerations of the Coupled-Channel Optical Model," IAEA-190, p. 251 (1976).

5. C. M. Perey and F. G. Perey, "Compilation of Phenomenological Optical Model Parameters, 1954-1975," Atomic Data and Nuclear Data Tables 17, 1 (1976).

6. F. G. Perey, T. A. Love, and W. E. Kinney, "A Test of Neutron Total Cross Section Evaluations from 0.2 to 20 MeV for C, O, Al, Si, Ca, Fe, and $SiO_2$," Oak Ridge National Laboratory report ORNL-4823 (1972).

7. L. A. Galloway, III, and E. F. Shrader, "Neutron Total Cross Section Measurements Using A White Neutron Source," COO-1573-6 (1966).

8. R. B. Schwartz, personal communication to R. J. Howerton, Lawrence Livermore Laboratory (1969).

9. A. D. Carlson and R. J. Cerbone, "High Resolution Measurements of the Total Neutron Cross Sections of Nitrogen and Iron," Nucl. Sci. Eng. 42, 28 (1970).

10. S. Cierjacks, P. Forti, D. Kopsch, L. Kropp, and J. Nebe, "Level Structure of $^{24}$Na Observed in the Total Neutron Cross Section of Sodium from 300 to 900 keV," Phys. Rev. Lett. B29, 417 (1969).

11. A. D. Carlson and H. H. Barschall, "Fluctutations in Neutron Total Cross Sections," Phys. Rev. 158, 1142 (1967).

12. D. G. Foster, Jr., and D. W. Glasgow, "Neutron Total Cross Sections, 2.5-15 MeV, Part 1 (Experimental), Phys. Rev. C3, 576 (1971).

13. D. C. Larson, J. A. Harvey, and N. W. Hill, "Neutron Total Cross Sections of Hydrogen, Carbon, Oxygen, and Iron from 500 keV to 60 MeV," Proc. Conf. on Nuclear Data for Technology, Knoxville, TN (1979).

14. F. P. Brady, personal communication (1979); C. I. Zanelli, F. P. Brady, J. L. Romero, C. M. Castaneda, and D. L. Johnson, "Neutron Total Cross Sections in Fe and Ca at 35.3, 40.3, and 50.4 MeV," Proc. Symposium on Neutron Cross Sections from 10-50 MeV, Brookhaven National Laboratory (May 1980).

15. G. Deconnick, A. Gonze, P. Macq, and J. P. Meulders, "Total Neutron Cross Sections for 28.4-MeV Neutrons," J. Phys. Radium 22, 652 (1961).

16. J. M. Peterson, A. Bratenahl, and J. P. Stoering, "Neutron Total Cross Sections in the 17- to 29-MeV Range," Phys. Rev. 120, 521 (1960).

17. G. J. McCallum, G. S. Mani, and A. T. G. Ferguson, "Neutron Total Cross Sections in the 12 to 21 MeV Region," Nucl. Phys. 16, 313 (1960).

18. I. Angeli, J. Csikai, and I. Hunyadi, "Correlation Between Nuclear Radii and Binding Energies for Light Nuclei," Acta Physica. Acad. Sci. Hungaricae 28, 87 (1970).

19. W. K. Robinson, J. L. Nagi, and J. L. Duggan, "A Time-of-Flight Neutron Experiment for the Undergraduate Laboratory," Amer. J. Phys. 37, 482 (1969).

20. Ch. Lagrange, personal communication (1979).

21. R. W. Hill, "Angular Distributions of Elastic Scattering of 5-MeV Neutrons," Phys. Rev. 109, 2105 (1958).

22. B. Holmqvist, S. G. Johansson, G. Lodin, and T. Wiedling, "Neutron Scattering from Iron at 1.5 to 8 MeV," Nucl. Phys. 146, 321 (1970).

23. W. E. Kinney and F. G. Perey, "Neutron Elastic and Inelastic Scattering Cross Sections for $^{56}Fe$ in the Energy Range 4.19 to 8.56 MeV," Oak Ridge National Laboratory report ORNL-4515 (1970).

24. B. Holmqvist and T. Wiedling, "Optical Model Analyses of Experimental Fast Neutron Elastic Scattering Data," AE-430 (1971).

25. R. M. Wilenzick, K. K. Seth, P. R. Bevington and H. W. Lewis, "Elastic and and Inelastic Scattering of 6-MeV Neutrons," Bull. Am. Phys. Soc. 6, 252 (1961).

26. R. M. Wilenzick, K. K. Seth, P. R. Bevington, and H. W. Lewis, "Elastic and Inelastic Scattering of 6-MeV Neutrons," Nucl. Phys. 63, 511 (1965).

27. W. P. Bucher, C. E. Hollandsworth, and R. Lamareaus, "On The Measurement of the Small-Angle Scattering of Fast Neutrons," Nucl. Instr. Meth. 111, 237 (1973); see also Ballistics Research Laboratory report BRL-R-1764 (1975).

28. J. C. Ferrer, J. D. Carlson, and J. Rapport, "Neutron Elastic Scattering at 11 MeV and the Isospin Dependence of the Neutron-Nucleus Optical Potential," Nucl Phys. A275, 325 (1977).

29. D. E. Velkley, D. W. Glasgow, J. D. Brandenberger, M. T. McEllistrem, J. C. Manthuruthil, and C. P. Poirier, "Scattering of 9.0-MeV Neutrons by Al, Si, Fe, Ni, and Co," Phys. Rev. C9, 2181 (1974).

30. T. P. Stuart, J. D. Anderson, and C. Wong, "Elastic Scattering of 24-MeV Neutrons by Al, Fe, Sn, and Bi," Phys. Rev. 125, 276 (1962).

31. J. D. Anderson, C. C. Gardner, M. P. Nakada, and C. Wong, "Back-Angle Elastic Scattering of 14.6-MeV Neutrons," Phys. Rev. 110, 160 (1958).

32. J. H. Coon, R. W. Davis, H. E. Felthauser, and D. B. Nicodemus, "Scattering of 14.5 MeV Neutrons by Complex Nuclei," Phys. Rev. 111, 250 (1958).

33. M. E. Gurtovoj, A. S. Kukhlenko, E. P. Kadkin, B. E. Leshchenko, and V. I. Strizhak, "Scattering of 14-MeV Neutrons by Iron," Atomnaya Energiya 30, 455 (1971).

34. M. Hyakutake, M. Matoba, T. Tonai, and J. Nidone, "Scattering of 14.1 MeV Neutrons from Fe," J. Phys. Soc. Japan 38, 606 (1975).

35. K. Yuasa, "Differential Elastic Scattering of 14-MeV Neutrons in Al, Fe, Pb, Bi, for Large Angles," J. Phys. Soc. Japan 13, 1248 (1958).

36. J. O. Elliot, "Differential Elastic Scattering of 14-MeV Neutrons in Bi, Ta, In, Fe, and S," Phys. Rev. 101, 684 (1956).

37. F. P. Brady, personal communication (1979); C. I. Zanelli, P. P. Urone, J. L. Romero, F. P. Brady, M. L. Johnson, G. A. Needham, J. L. Ullman, and D. L. Johnson, "Total Nonelastic Cross Section Measurements for Neutrons on C, O, Ca, and Fe at 40.3 and 50.4 MeV," Proc. Symposium on Neutron Cross Sections from 10-50 MeV, Brookhaven National Laboratory (May 1980).

38. M. H. MacGregor, W. P. Ball, and R. Booth, "Neutron Nonelastic Cross Sections at 21.0, 25.5, and 29.2 MeV," Phys. Rev. 111, 1155 (1955).

39. N. N. Flerov and V. M. Talyzin, "Cross Section for Inelastic Interactions of 14.5-MeV Neutrons with Various Elements," Atomnaya Energiya 1, 155 (1956).

40. Y. G. Degtyarev and V. G. Nadtochii, "Measurement of the Cross Sections For Inelastic Interaction of Neutrons with an Energy of 13 to 20 MeV Using Certain Isotopes," Atomnaya Energiya 11, 397 (1961).

41. M. H. MacGregor, W. P. Ball, and R. Booth, "Nonelastic Neutron Cross Sections at 14 MeV," Phys. Rev. 108, 726 (1957).

42. V. I. Strizhak, "Inelastic Interaction of 14-MeV Neutrons with Nuclei," Atomnaya Energiya 2, 68 (1957).

43. E. R. Graves and R. W. Davis, "Cross Sections of Nonelastic Interactions of 14-MeV Neutrons with Various Elements," Phys. Rev. 97, 1205 (1955).

44. P. P. Lebedev, Y. A. Zysin, I. S. Klintsov, and B. D. Stsiborskii, "Neutron Yield in Inelastic Collisions of 14-MeV Neutrons with Nuclei and Cross Sections for the (n,2n) Reactions," Atomnaya Energiya 5, 522 (1958).

45. M. Walt and J. R. Beyster, "Interaction of 4.1-MeV Neutrons with Nuclei," Phys. Rev. 98, 677 (1955).

46. J. R. Beyster, R. L. Henkel, R. A. Nobles, and J. M. Kister, "Inelastic Collision Cross Sections at 1.0, 4.0, 4.5 MeV," Phys. Rev. 98, 1216 (1955).

47. M. K. Machwe, D. W. Kent, and S. C. Snowdon, "Elastic Scattering of 3.7-MeV Neutrons from S, Fe, Co, Ni, Cu, and Zn," Phys. Rev. 114, 1563 (1959).

48. H. L. Taylor, O. Lonsjo, and T. W. Bonner, "Nonelastic Scattering Cross Sections for Fast Neutrons," Phys. Rev. 100, 174 (1955).

49. M. V. Pasechnik, "Inelastic Scattering of Fast Neutrons by Atomic Nuclei," Proc. Int. Conf. Peaceful Uses of Atomic Energy, Geneva (1955).

50. J. R. Beyster and M. Walt, "Interactions of 1.0 MeV to 7.0 MeV Neutrons With Nuclei," Phys. Rev. 104, 1319 (1956).

51. V. I. Strizhak, "Inelastic Scattering Cross Sections of Nuclei for 2.5 MeV Neutrons," J. Expt. Theoret. Phys. (USSR) 31, 907 (1956).

52. A. I. Abramov, "Measurement of the Inelastic Collision Cross Sections with Nuclei of Chromium, Iron, Nickel, Niobium, and Molybdenum at Energies up to 2.6 MeV," Atomnaya Energiya 12, 62 (1962).

53. G. C. Morrison, "Inelastic Neutron Scattering," Proc. Amsterdam Conf. on Nuclear Reactions, p. 1135 (1956).

54. F. G. Perey, "Optical Model Analysis of Proton Elastic Scattering in the Range of 9 to 22 MeV," Phys. Rev. 131, 745 (1962).

55. J. L. Jenkins and A. G. Wain, "Excitation Functions for the Bombardment of $^{56}$Fe with Protons," J. Inorg. Chem. 32, 1419 (1970).

56. F. Nemets, L. T. Slyusarenko, and V. V. Tokarevskii, "Total Reaction Cross Sections for Charged Particles up to 100 MeV," Sov. J. Particles and Nuclei 6, 335 (1975).

57. C. H. Johnson, A. Galonsky, and R. L. Kernell, "Anomalous Optical Model Potential for Sub-Coulomb Protons for 89 < A < 130," Phys. Rev. Lett. 39, 1604 (1977); and C. H. Johnson, R. L. Kernell, and S. Ramavataram, "The $^{89}$Y(p,n)$^{89}$Zr Cross Section Near the First Two Analogue Resonances," Nucl. Phys. A107, 21 (1968).

58. R. D. Albert, personal communication to F. K. McGowan, tabulated in ORNL-CPXI (1965).

59. C. H. Johnson, A. Galonsky, and C. N. Inskeep, "Cross Sections for (p,n) Reactions in Intermediate Weight Nuclei," Oak Ridge National Laboratory progress report ORNL-2910 (1960).

60. O. F. Lemos, "Diffusion Elastique de Particules Alpha de 21 a 29.6 MeV sur des Noyaux de la Region Ti-Zn," Orsay report, Series A, No. 136 (1972).

61. S. Tanaka, M. Furukawa, T. Mikumo, S. Iwata, M. Yagi, and H. Amano, "Excitation Functions for Alpha-Induced Reactions on Mananese-55," J. Phys. Soc. Japan 15, 545 (1960).

62. A. Iguchi, H. Amano, and S. Tanaka, "($\alpha$,n) Cross Sections for $^{48}$Ti and $^{51}$V," J. Atomic Energy Soc. Japan 2, 24 (1960).

63. D. G. Gardner and M. A. Gardner, "Gamma-Ray Strength Functions in the Mass 90 Region," Bull. Am. Phys. Soc. 22, 993 (1977).

64. E. D. Arthur, "Parameter Determination and Application to Nuclear Model Calculations of Neutron-Induced Reactions on Yttrium and Zirconium Isotopes," Nucl. Sci. & Eng. 76, 137 (1980).

65. B. J. Allen, A. R. L. Musgrove, J. W. Boldeman, and R. L. Macklin, "Valence Neutron Capture in $^{54}$Fe," Nucl. Phys. A283, 37 (1977).

66. B. J. Allen, A. R. L. Musgrove, J. W. Bolderman, M. J. Kenny, and R. L. Macklin, "Resonance Neutron Capture in $^{56}$Fe," Nucl. Phys. A269, 408 (1976).

67. C. M. Lederer and V. S. Shirley, Table of Isotopes, Seventh Edition (John Wiley and Sons, Inc., New York, 1978).

68. A. Gilbert and A. G. W. Cameron, "A Composite Nuclear-Level Density Formula with Shell Corrections," Can. J. Phys. 43, 1446 (1965).

69. J. L. Cook, H. Ferguson, and A. R. L. Musgrove, "Nuclear Level Densities in Intermediate and Heavy Nuclei," Aust. J. Phys. 20, 477 (1967).

70. C. Kalbach, "The Griffin Model, Complex Particles and Direct Nuclear Reactions," Z. Phys. A283, 401 (1978).

71. C. Kalbach, "Exciton Number Dependence of the Griffin Model Two-Body Matrix Element," Z. Phys. A287, 319 (1978).

72. C. Kalbach and F. M. Mann, "Phenomenology of Preequilibrium Angular Distributions," Proc. Symposium on Neutron Cross Sections from 10-50 MeV, Brookhaven National Laboratory (May 1980).

73. P. D. Kunz, "DWUCK - A Distorted Wave Born Approximation Program," unpublished.

74. G. S. Mani, "Spin Assignments to Excited States of $^{56}$Fe Using Inelastic Proton Scattering," Nucl. Phys. A165, 225 (1977).

75. O. Bersillon, "SCAT2 - A Spherical Optical Model Code," in "Progress Report of the Nuclear Physics Division, Bruyeres-le-Chatel 1977," CEA-N-2037, p. 111 (1978).

76. C. L. Dunford, "A Unified Model for Analysis of Compound Nucleus Reactions," Atomics International report AI-AEC-12931 (July 1970).

77. P. G. Young and E. D. Arthur, "GNASH: A Preequilbrium Statistical Nuclear-Model Code for Calculation of Cross Sections and Emission Spectra," Los Alamos Scientific Laboratory report LA-6947 (Nov. 1977).

78. W. E. Kinney and F. G. Perey, "$^{54}$Fe Neutron Elastic and Inelastic Scattering Cross Sections from 5.50 to 8.50 MeV," Oak Ridge National Laboratory report ORNL-4907 (1974).

79. P. P. Boschung, J. T. Lindow, and E. F. Shrader, "Scattering of Fast Neutrons by $^{12}$C, $^{54}$Fe, $^{56}$Fe, $^{58}$Ni, and $^{60}$Ni," Nucl. Phys. 161, 593 (1971).

80. V. C. Rogers, L. E. Beghian, and F. M. Clikeman, "Neutron Inelastic Scattering Cross Sections for Iron, Nickel, Niobium, and Tantalum from Threshold to 1.8 MeV," Nucl. Sci. Eng. 45, 297 (1971).

81. N. P. Glaskov, "Cross Sections of the Inelastic Scattering of Neutrons with Energies of 0.4-1.2 MeV on Medium and Light Nuclei," Atomnaya Energiya 15, 416 (1963).

82. Y. G. Degtyarev and A. N. Protopopov, "Excitation of Low-Lying Levels of $Al^{27}$, $Cr^{52}$, $Fe^{56}$, and $Bi^{209}$ in the Inelastic Scattering of 1-4 MeV Neutrons," Atomnaya Energiya 23, 568 (1967).

83. D. A. Kardashev, V. S. Stavinskii, D. L. Broder, A. I. Lashuk, and I. P. Sadokhin, "Analysis of Excitation Functions of Levels of the $Fe^{56}$ Nucleus in Inelastic Scattering of Neutrons in the Optical Model of the Nucleus," Atomnaya Energiya 13, 587 (1962).

84. E. Barnard, J. A. M. DeVilliers, C. A. Engelbrecht, D. Reitmann, and A. B. Smith, "High-Resolution Fast-Neutron Cross Sections of Iron," Nucl. Phys. 118, 321 (1968).

85. B. Antolkovic, B. Holmqvist, and T. Wiedling, "Fast Neutron Scattering Cross Sections Measurements on Fe and Co," EANDC(OR)-51L (1966).

86. J. C. Hopkins and M. G. Silbert, "Inelastic Scattering of 2- to 5-MeV Neutrons by Iron," Nucl. Sci. Eng. 19, 431 (1964).

87. W. B. Gilboy and J. H. Towle, "A Neutron Scattering Study of $Fe^{56}$," Nucl. Phys. 64, 130 (1965).

88. W. E. Meyerhof, personal communication (1962); A. B. Tucker, J. T. Wells, and W. E. Meyerhof, "Inelastic Neutron Scattering Near Threshold," Phys. Rev. 137, 1181 (1965).

89. W. E. Kinney, "Neutron Elastic and Inelastic Scattering from $^{56}Fe$ from 4.60 to 7.55 MeV," Oak Ridge National Laboratory report ORNL-TM-2052 (1968).

90. B. E. Leshchenko, M. E. Gurtovoi, A. S. Kukhlenko, and V. I. Strizhak, "Excitation of Collective States of Some Medium Nuclei by 14-MeV Neutrons," Sov. J. Nucl. Phys. 15, 5 (1972).

91. D. Hermsdorf, A. Meister, S. Sassonoff, D. Selliger, K. Seidel, and F. Shalin, "Differentielle Neutronenemissionsquerschnitte $\sigma_{nM}(E_0;E;\theta)$ bei 14.6 MeV Einschussenergie fur die Elemente Be, C, Na, Mg, Al, Si, P, S, Ca, Ti, V, Cr, Mn, Fe, Co, Ni, Cu, Zn, Ga, Se, Br, Zr, Nb, Cd, In, Sn, Sb, I, Ta, W, Au, Hg, Pb, und Bi," Zentralinstitut fur Kernforschung report ZKF-277(U) (1975).

92. A. H. Lukyanov, O. A. Salnikov, and E. M. Saprykin, "Analysis of the Spectra of Inelastically Scattered Neutrons with Account of Direct Interactions," Sov. J. Nucl. Phys. 21, 35 (1975).

93. H. Vonach, A. Chalupka, F. Wenninger, and G. Staffel, "Measurement of the Angle-Integrated Secondary Neutron Spectra from Interaction of 14-MeV Neutrons with Medium and Heavy Nuclei," Symp. on Neutron Cross Sections from 10-50 MeV, Brookhaven National Laboratory (May 1980).

94. G. Clayeux and J. Voignier, "Diffusion Non Elastique de Neutrons de 14 MeV sur Mg, Al, Si, S, Ca, Sc, Fe, Ni, Cu, Au, Pb et Bi," Commissariat a l'Energie Atomique report CEA-R-4279 (1972).

95. J. L. Kammerdiener, "Neutron Spectra Emitted by $^{239}Pu$, $^{238}U$, $^{235}U$, Pb, Nb, Ni, Al, and C Irradiated by 14-MeV Neutrons," University of California report UCRL-51232 (1972).

96. J. Frehaut and G. Mosinski, Nuclear Cross Sections and Technology Conference, NBS Special Publication 425, p. 855 (1975).

97. L. R. Veeser, personal communication (1979).

98. J. Terrell and D. M. Holm, "Excitation Functions for $Fe^{56}(n,p)Mn^{56}$," Phys. Rev. 109, 2031 (1958).

99. M. J. Depraz, G. Legros, and M. R. Salin, "Measurements of (n,p), (n,alpha), and (n,2n) Reactions," J. Phys. Radium 21, 377 (1960).

100. D. M. Chittenden, D. G. Gardner, and R. W. Fink, "New Isotope of Manganese; Cross Sections of the Iron Isotopes for 14.8-MeV Neutrons," Phys. Rev. 122, 860 (1961).

101. J. Csikai and S. Nagy, "Some (n,p) Reaction Cross Sections for 14.7-MeV Neutrons," Nucl. Phys. 91, 222 (1967).

102. W. G. Cross, unpublished report (1963).

103. L. A. Rayburn, "14-MeV (n,2n) Cross Sections of $^{14}N$, $^{31}P$, $^{39}K$, $^{46}Te$, $^{50}Cr$, and $^{54}Fe$," Phys. Rev. 122, 168 (1961).

104. C. Carles, "Mesures de Sections Efficaces de Reactions (n,2n) Produites par Neutrons de 14 MeV," Compt. Rend. 257, 659 (1963).

105. H. Pollehn and H. Neurt, "Bestimmung von Wirkungsquerschnitten Einiger Kernreaction durch 14-MeV Neutronen nach einer Aktivierungsmethode," Z. Naturforschg 16, 227 (1961).

106. S. R. Salisbury and R. A. Chalmers, "$Fe^{54}$(n,p), (n,$\alpha$), and (n,2n) Cross Sections," Phys. Rev. 140, 305 (1965).

107. D. L. Allan, "Protons from the Interaction of 14-MeV Neutrons with Medium Weight Nuclei," Proc. Phys. Soc. (London) 70, 195 (1957).

108. R. A. Sigg and P. K. Kuroda, "14.8 MeV Neutron-Induced (n,2n), (n,p), and (n,$\alpha$) Cross Sections for some Closed Shell Nuclides," J. Inorg. Nucl. Chem. 37, 631 (1975).

109. T. B. Ryves, P. Kolkowski, and K. J. Zieba, "Cross Section Measurements of $^{14}N(n,2n)^{13}N$, $^{19}F(n,2n)^{18}F$, $^{54}Fe(n,2n)^{53}Fe$, $^{27}Al(n,p)^{27}Mg$, and $^{27}Al(n,\alpha)^{24}Na$ between 14.7 and 19.0 MeV," J. Phys. G: Nucl.Phys., 4, 1783 (1978).

110. R. C. Barrall, M. Silbergeld, and D. G. Gardner, UCRL-71499 (1968).

111. R. C. Barrall, J. A. Holmes, and M. Silbergeld, "High-Energy Cross Section Validation and Neutron Flux Spectrum Using the Henre Source," Air Force Weapons Lab report AFWL-TR-68, 134 (1969).

112. J. J. Singh, "Neutron Reaction Cross Sections of Iron at 14.5 MeV," Trans. Am. Nucl. Soc. 15, 147 (1972).

113. R. S. Storey, W. Jack, and A. Ward, "Experiments Involving the Emission of Particles from Compound Nuclei," Proc. Phys. Soc. (London) 75, 526 (1960).

114. D. L. Allan, "An Experimental Test of the Statistical Theory of Nuclear Reactions," Nucl. Phys. 24, 274 (1961).

115. A. Paulsen, R. Widera, F. Arnotte, and H. Liskien, "Cross Sections for the Reactions $^{54}Fe(n,\alpha)^{54}Fe$, and $^{56}Fe(n,p)^{56}Mn$," Nucl. Sci. Eng. 72,

116. A. Lauber and S. G. Malmskog, "Measurements of the $^{54}Fe(n,p)^{54}Mn$ Reaction Cross Section in the Neutron Energy Range 2.3-3.8 MeV," Nucl. Phys. 73, 234 (1965).

117. D. L. Smith and J. W. Meadows, "Measurement of Several (n,p) Reaction Cross Sections Using Activation Methods," Trans. Am. Nucl. Soc. 16, 312 (1973).

118. P. V. Rao and R. W. Fink, "Neutron Reaction Cross Sections of Selenium and Iron at 14.4 MeV," Phys. Rev. 154, 1023 (1967).

119. E. E. Carroll, G. G. Smith, and R. W. Stooksberry, "Zirconium and Iron-54 (n,p) Cross Section Measurements," Trans. Am. Nucl. Soc. 7, 268 (1964).

120. E. E. Carroll and G. G. Smith, "Iron-54 (n,p) Cross-Section Measurement," Nucl. Sci. Eng. 22, 411 (1965).

121. J. J. VanLoef, "Activation Cross Sections for (n,p) Reactions in Some Medium-Weight Nuclei with D + D Neutrons," Nucl. Phys. 24, 340 (1961).

122. W. G. Cross and R. L. Clarke, "Cross-Section Measurements," AECL-1542, p. 7 (1962).

123. H. K. Vonach, W. G. Vonach, H. Munzer, and P. Schramel, "Precision Measurements of Excitation Functions of (n,p), (n,α), and (n,2n) Reactions Induced by 13.5-14.7 MeV Neutrons," Proc. Conf. on Neutron Cross Section Tech., Washington D.C., p. 885 (1968).

124. F. Gabbard and B. D. Kern, "Cross Sections for Charged Particle Reactions Induced in Medium Weight Nuclei by Neutrons in the Energy Range 12-18 MeV," Phys. Rev. 128, 1276 (1962).

125. S. G. Forbes, "Activation Cross Sections for 14-MeV Neutrons," Phys. Rev. 88, 1309 (1952).

126. H. Liskien and A. Paulsen, "Cross-Section Measurement for the Threshold Reactions $^{56}Fe(n,p)^{56}Mn$, $^{59}Co(n,\alpha)^{56}Mn$, and $^{63}Cu(n,2n)^{62}Cu$ Between 12.6 and 19.6 MeV Neutron Energy," J. Nucl. Eng. A/B 19, 73 (1965).

127. H. Liskien and A. Paulsen, "Cross Sections for the $^{63}Cu(n,\alpha)^{60}Co$, $^{60}Ni(n,p)^{60}Co$ and Some Other Threshold Reactions Using Neutrons from the $^{9}Be(\alpha,n)^{12}C$ Reaction," Nukleonik 8, 315 (1966).

128. B. D. Kern, W. E. Thompson, and J. M. Ferguson, "Cross Sections for Some (n,p) and (n,α) Reactions," Nucl. Phys. 10, 226 (1959).

129. M. Bormann, E. Fretwurst, P. Schehka, G. Wrege, H. Buttner, A. Lindner, and H. Meldner, "Some Excitation Functions of Neutron Induced Reactions in the Energy Range 12.6-19.6 MeV," Nucl. Phys. 63, 438 (1965).

130. G. C. Bonazzola, P. Brovetto, E. Chiavassa, R. Spinoglio, and A. Pasquarelli, "The Measurement by Activation of Cross Sections for 14.7 MeV Neutrons," Nucl. Phys. 51, 337 (1964).

131. E. B. Paul and R. L. Clarke, "Cross-Section Measurements of Reactions Induced by Neutrons of 14.5 MeV Energy," Can. J. Phys. 31, 267 (1953).

132 N. C. Dyer and J. H. Hamilton, "$^{56}$Fe and $^{58}$Fe(n,p) Cross Sections for 14.4 MeV Neutrons," J. Inorg. Nucl. Chem. 34, 1119 (1972).

133. S. Yasumi, "Nuclear Reactions Induced by 14-MeV Neutrons," J. Phys. Soc. Japan 12, 443 (1957).

134. G. W. McClure, D. W. Kent, and J. Franklin, "Inelastic Scattering of 14-MeV Neutrons," J. Franklin Inst. 260, 238 (1955).

135. D. C. Santry and J. P. Butler, "Excitation Curves for the Reactions $Fe^{56}(n,p)Mn^{56}$ and $Co^{59}(n,\alpha)Mn^{56}$," Can. J. Phys. 42, 1030 (1964).

136. J. A. Grundl, "A Study of Fission-Neutron Spectra with High Energy Activation Detectors, Part 1. Detector Development and Excitation Measurements," Nucl. Sci. Eng. 30, 39 (1967).

137. B. Joensson, K. Nyberg-Pennert, and I. Bergqvist, "High Resolution Measurements of Gamma Rays Produced by 15-MeV Neutrons," Arkiv Fysik 39, 295 (1969).

138. S. M. Grimes and R. C. Haight, "Charged-Particle Emission in Reactions of 15-MeV Neutrons with Isotopes of Chromium, Iron, Nickel, and Copper," Phys. Rev. C19, 2127 (1979).

139. G. N. Maslov, F. Nasyrov, and N. F. Pashkin, Yaderna Konstanty Obninst report USSR YK-9, 50 (1972).

140. G. T. Chapman, G. L. Morgan, and F. G. Perey, "A Re-Measurement of the Neutron Induced Gamma-Ray Production Cross Sections for Iron in the Energy Range 850 keV $\leq$ E $\leq$ 20.0 MeV," Oak Ridge National Laboratory report ORNL/TM-5416 (1976).

141. D. M. Van Patter and R. W. Jackiev, "The $Fe^{56}(n,n'\gamma)$ Reaction and Comparison to Theory," Proc. Int. Conf. on Nucl. Structure, Kingston, p. 244 (1960).

142. K. Nishimura, K. Okahno, and S. Kikuchi, "Studies of Excitation Cross Sections of $(n,n'\gamma)$ Reactions," Nucl. Phys. 70, 421 (1965).

143. J. Lachkar, J. Sigaud, Y. Patin, and G. Haouat, "Gamma-Ray Production Cross Sections for the $^{56}$Fe$(n,n'\gamma)$ Reaction from 2.5- to 14.1-MeV Neutron Energies," Nucl. Sci. Eng. 55, 168 (1974).

144. V. G. Orphan, C. G. Hoot, and V. C. Rogers, "Gamma-Ray Production Cross Sections for Iron from 0.86 to 16.7 MeV," Nucl. Sci. Eng. 57, 309 (1975).

145. R. W. Benjamin, P. S. Buchanan, and I. L. Morgan, "Gamma Rays Produced in the $^{56}Fe(n,n\gamma)^{56}Fe$ Reaction," Nucl. Phys. 79, 241 (1966).

146. D. L. Broder, A. F. Gamalii, A. I. Lashuk, and I. P. Sadokhin, Nucl. Data For Reactors 2, 295 (1970).

147. J. K. Dickens, G. L. Morgan, and F.G. Perey, "Gamma-Ray Production Due to Neutron Interactions with Iron for Incident Neutron Energies Between 0.8 and 20 MeV: Tabulated Differential Cross Sections," Oak Ridge National Laboratory report ORNL-4798 (1972).

148. D.M. Drake, E. D. Arthur, and M. G. Silbert, "Cross Sections for Gamma-Ray Production by 14-MeV Neutrons," Nucl. Sci. Eng. 65, 49 (1978).

149. G. Clayeux and G. Grenier, "Recoil Spectra Produced by 14.1 MeV Neutrons," CEA-R-3807 (1969).

150. G. Grenier, Second Nat. Soviet Conf. on Neutron Physics, Kiev, 28 May - 1 June, 1973.

151. B. I. Sukhanov and N. P. Trach, "Gamma Rays in Inelastic Interactions of 14-MeV Neutrons with N, O, Al, and Fe Nuclei," Sov. J. Nucl. Phys. 11, 17 (1970).

152. U. Abbondanno, R. Giacomich, M. Lagonegro, and G. Pauli, "Gamma Rays Resulting from Nonelastic Processes of 14.2-MeV Neutrons with Sodium, Magnesium, Silicon, Sulphur, Titanium, Chromium, and Iron," J. Nucl. Energy 27, 227 (1973).

153. D. L. Broder, A. G. Dovbenko, V. E. Kolesov, A. I. Lashuk, and I. P. Sadokhin, INDSWG-126E, 7 (1966).

154. V. Corcalciuc, B. Holmqvist, A. Marcinkowski, and G. A. Prokopets, "A Study of the Neutron Induced Reactions for $^{19}F$, $^{56}Fe$, and $^{59}Co$ in the Energy Interval 16 to 22 MeV, Nucl. Phys. A307, 445 (1978).

155. R. Michel, G. Brinkmann, H. Weigel, and W. Herr, "Measurement and Hybrid-Model Analysis of Proton-Induced Reactions with V, Fe, and Co," Nucl. Phys. A322, 40 (1979).

156. L. E. Beghian, D. A. Hicks, and B. Milman, "Inelastic Scattering of 2.5-MeV Neutrons by $^{54}Fe$ and $^{56}Fe$," Phil. Mag. 46, 963 (1955).

157. J. Barrows, personal communication to N.N.C.S.C. (1965).

158. D. B. Thomson, "Nuclear Level Densities and Reaction Mechanisms from Inelastic Neutron Scattering," Phys. Rev. 129, 1649 (1963).

159. G. A. Prokopesc and V. I. Strizhak, Ukr. Fiz. Zh. 14, 330 (1969).

160. H. H. Landon, A. J. Elwyn, G. N. Glasoe, and S. Oleksa, "Neutron Scattering at 2.2 MeV by Time of Flight," Phys. Rev. 112, 1192 (1958).

161. A. Jacquot and C. Rousseau, "Fast Neutron Scattering Cross Sections of Iron," Nucl. Phys. 84, 239 (1966).

162. F. Cvelbar, A. Hudoklin-Bozic, M. V. Milhailovic, M. Najzer, and V. Ramsak, "Radiative Neutron Capture in the Region of the Dipole Giant Resonance," Nucl. Phys. 130, 401 (1969).

163. B. C. Diven, J. Terrell, and A. Hemmendinger, "Radiative Capture Cross Sections for Fast Neutrons," Phys. Rev. 120, 556 (1960).

164. A. V. Malyshev, Y. Y. Stavisskii, and A. V. Shapar, "Radiative Capture Cross Sections for Fast Neutrons in Iron," Atomnaya Energiya 17, 508 (1964).

165. R. Wenusch and H. K. Vonach, Anz. Oesterr. Akad. Wiss Math 99, 1 (1962).

166. V. J. Ashby, H. C. Catron, L. L. Newkirk, and C. J. Taylor, "Absolute Measurement of (n,2n) Cross Sections at 14.1 MeV," Phys. Rev. 111, 616 (1958).

167. S. M. Qaim, "A Systematic Investigation of (n,$^{3}$He) Reactions at 14.6 MeV and an Analysis of the Gross Trend in the Cross Section Data," Radiochimica Acta 25, 13 (1978).

168. F. D. Becchetti, Jr. and G. W. Greenlees, "Nucleon-Nucleus Optical-Model Parameters, A > 40, E < 50 MeV," Phys. Rev. 182, 1190 (1969).

169. M. R. Bhat and S. Pearlstein, Eds., Proc. of Symposium on Neutron Cross Sections from 10 to 40 MeV, Brookhaven National Laboratory report BNL-NCS-50681 (May 1977).



☆U.S. GOVERNMENT PRINTING OFFICE: 1980—777-022/227

Printed in the United States of America
Available from
National Technical Information Service
US Department of Commerce
5285 Port Royal Road
Springfield, VA 22161

Microfiche $3.50 (A01)

| Page Range | Domestic Price | NTIS Price Code | Page Range | Domestic Price | NTIS Price Code | Page Range | Domestic Price | NTIS Price Code | Page Range | Domestic Price | NTIS Price Code |
|---|---|---|---|---|---|---|---|---|---|---|---|
| 001-025 | $ 5.00 | A02 | 151-175 | $11.00 | A08 | 301-325 | $17.00 | A14 | 451-475 | $23.00 | A20 |
| 026-050 | 6.00 | A03 | 176-200 | 12.00 | A09 | 326-350 | 18.00 | A15 | 476-500 | 24.00 | A21 |
| 051-075 | 7.00 | A04 | 201-225 | 13.00 | A10 | 351-375 | 19.00 | A16 | 501-525 | 25.00 | A22 |
| 076-100 | 8.00 | A05 | 226-250 | 14.00 | A11 | 376-400 | 20.00 | A17 | 526-550 | 26.00 | A23 |
| 101-125 | 9.00 | A06 | 251-275 | 15.00 | A12 | 401-425 | 21.00 | A18 | 551-575 | 27.00 | A24 |
| 126-150 | 10.00 | A07 | 276-300 | 16.00 | A13 | 426-450 | 22.00 | A19 | 576-600 | 28.00 | A25 |
| | | | | | | | | | 601-up | † | A99 |

†Add $1.00 for each additional 25-page increment or portion thereof from 601 pages up.